Supplementary Information for

Guest Inclusion Modulates Concentration and Persistence of Photo-generated Radicals in Assembled Triphenylamine Macrocycles.

Ammon J. Sindt,[†] Baillie A. DeHaven,[†] Dustin W. Goodlett,[†] Johannes O. Hartel,[†] Pooja J. Ayare,[†] Yong Du,[‡] Mark D. Smith,[†] Anil K. Mehta,[§] Alexander M. Brugh,[∥] Malcolm D. E. Forbes,[∥] Clifford R. Bowers,[‡] Aaron K. Vannucci,[†] and Linda S. Shimizu*[,†]

[†]Department of Chemistry and Biochemistry, University of South Carolina, Columbia, South Carolina 29208, United States

[‡]Department of Chemistry, University of Florida, Gainesville, Florida 32611, United States

[§]National High Magnetic Field Laboratory and McKnight Brain Institute, University of Florida, Gainesville, Florida 32610, United States

[§]Department of Chemistry and Center for Photochemical Sciences, Bowling Green State University, Bowling Green, Ohio 43403, United States

Fax: 803-777-9521; *Tel:* 803-777-2066

E-mail: SHIMIZLS@mailbox.sc.edu

Contents

General Experimental

NMR spectra were recorded on Bruker Avance 300 or 400 MHz spectrometers. Chemical shifts are reported in ppm (δ) and were internally referenced with the solvent peak. All chemicals were purchased from chemical suppliers and were used as received unless otherwise noted. High-resolution mass spectrum data were recorded using a direct exposure probe (DEP) in electron ionization mode on a Waters QTOF-I quadrupole time-of-flight mass spectrometer. UV-irradiation of all materials were carried out with Waveform Lighting realUV LED strips (365 nm, 4.5 W/ft, 3.2 ft). Samples were purged with argon before irradiation. Hosts **1** and **1a** were activated by placing them under vacuum at 90°C either for 2.5 hours (**1a**) or overnight (**1**). Higher temperatures were found to degrade these materials. The host-guest complexes of **1a** with lower volatility guests (**1a**·C_6H_5Cl, **1a**·C_6H_5Br, and **1a**·DMF) were allowed to air dry on the balance until no more weight loss was detected (~1-2 hours). In addition, TGAs were also measured on samples upon completion of the radical studies (Figures S33-S35) for comparison. PXRDs (Figures S27-S31) were measured to monitor the phase purity of the samples. Figures S36 and S38-S45 compare the solid-state absorption spectra. All other instrument protocols and sample preparations are described in their own sections hereafter.

Synthesis and Characterization of Compounds

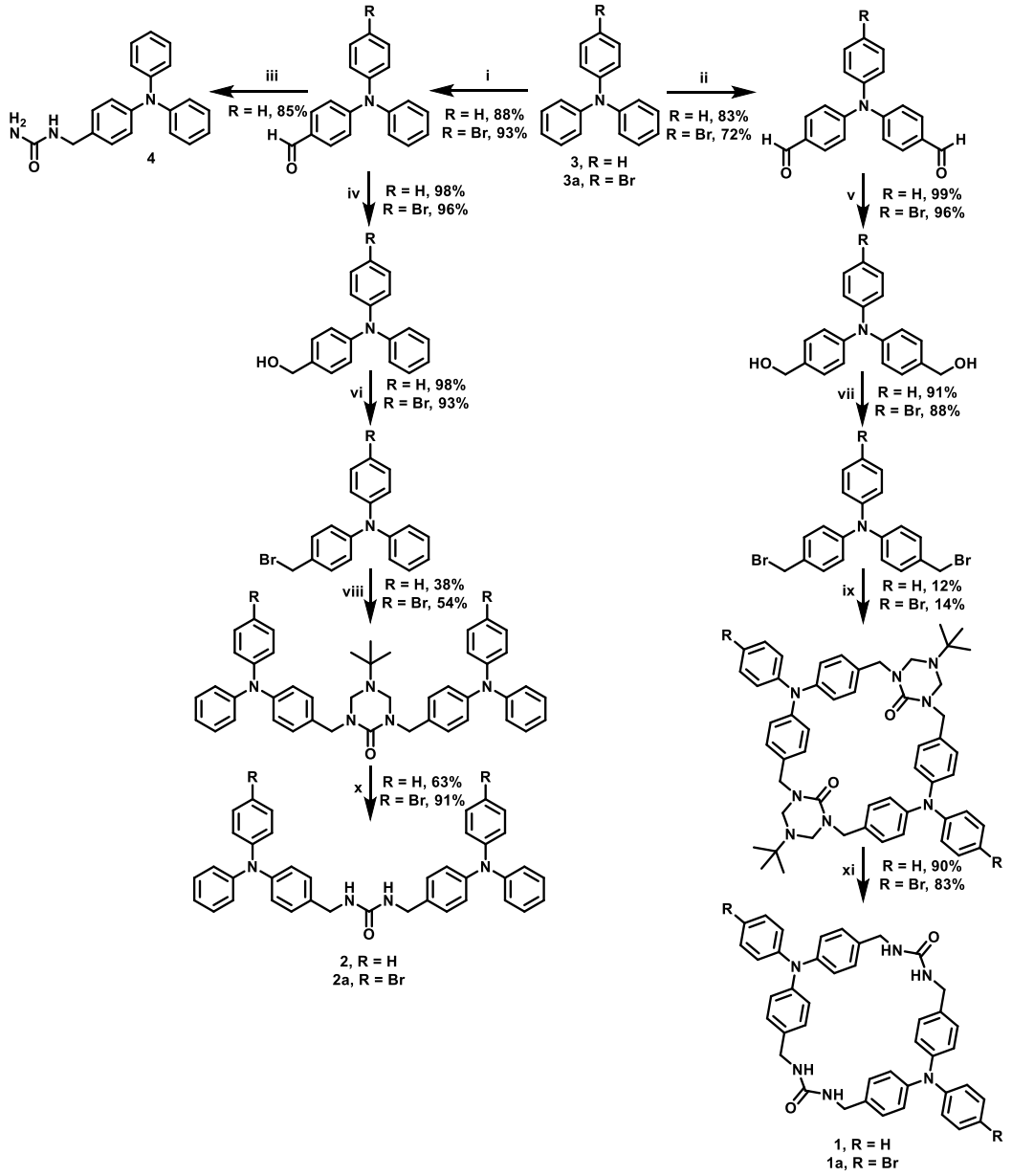

Scheme S1. Synthesis of compounds. i) $POCl_3$, DMF, 40 °C (R = H) or 60 °C (R = Br), 12h (R = H) or 2h (R = Br). ii) $POCl_3$, DMF, 105 °C, 4 h. iii) 1) Urea, TMSCl, CH_3CO_2H 2) $NaBH_4$. iv) $NaBH_4$, DCM/EtOH. v) $NaBH_4$, THF/EtOH. vi) PBr_3 (0.7 eq.), Et_2O vii) PBr_3 (1.2 eq.), Et_2O. viii) NaH, triazinone (0.5 eq.), THF, Δ, 12 h. ix) NaH, triazinone (1 eq.), THF, Δ, 48 h. x) 9:1 DMF/DEA (0.5 mL/mg), pH~2, 90 °C, 48 h. xi) 9:1 DMF/DEA (1 mL/mg), pH~2, 90 °C, 48 h.

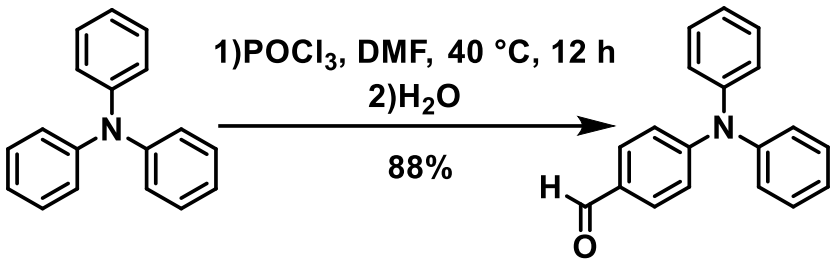

4-(Diphenylamino)benzaldehyde: Compound was made according to previous procedures.[1] Phosphoryl chloride (1.0 mL, 11.4 mmol) was added dropwise to dry *N, N*-dimethylformamide (875 µL, 11.4 mmol) and the mixture was stirred at room temperature for 20 min. Then a solution of triphenylamine (1.000 g, 4.1 mmol) in 10 mL of *N, N*-dimethylformamide was added, and this mixture was heated at 40 ˚ C overnight. After cooling to room temperature, 35 mL of ice-cold water was added to the mixture and the solution was filtered. The resulting residue was recrystallized in ethanol giving a yellow crystalline product (0.980 g, 88%). Spectra matched that as previously reported.[1] ^{1}H NMR (300 MHz, $CDCl_3$): δ (ppm) 9.83 (s, 1H), 7.70 (d, *J* = 8.7 Hz, 2H), 7.37 (t, *J* = 7.7 Hz, 4H), 7.24-7.15 (m, 6H), 7.04 (d, *J* = 8.7 Hz, 2H).

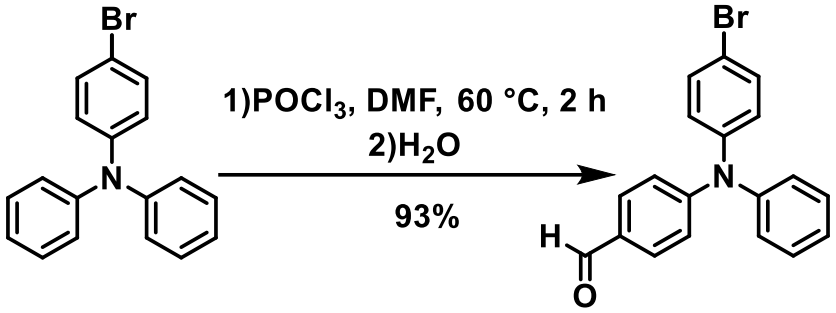

4-((4-Bromophenyl)(phenyl)amino)benzaldehyde: Compound was made according to previous procedures.[2] Phosphoryl chloride (840 µL, 9.0 mmol) was added dropwise to dry *N, N*-dimethylformamide (830 µL, 10.8 mmol) in an ice bath and the mixture was stirred for 20 min. Then 4-bromo-*N, N*-diphenylaniline (2.590 g, 8.0 mmol) was added, and this mixture was heated to 110 ˚C for 5 min then cooled to 60 ˚C for 2 h with stirring. After cooling to room temperature, 50 mL of ice water was added, and the solution was neutralized with saturated aqueous $NaHCO_3$. Then the mixture was extracted with chloroform (3 x 50 mL) and washed with water (1 x 50 mL), then brine (1 x 50 mL), and dried with $MgSO_4$. The solvent was removed under reduced pressure and the crude material was further purified by column chromatography (Hexanes/Ethyl Acetate = 3:1) to yield the product as a yellow solid (2.616 g, 93%). Spectra matched that as previously reported.[2] ^{1}H NMR (300 MHz, $CDCl_3$): δ (ppm) 9.82 (s, 1H), 7.69 (d, *J* = 8.7 Hz, 2H), 7.44 (t, *J* = 8.7 Hz, 2H), 7.35 (t, *J* = 7.7 Hz, 2H), 7.22-7.11 (m, 3H), 7.08-6.99 (m, 4H).

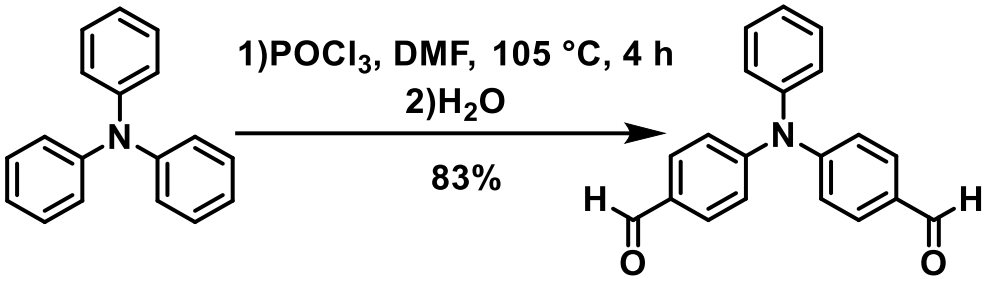

4,4'-(Phenylazanediyl)dibenzaldehyde: Compound was made by modifying previous procedures.[3] Phosphoryl chloride (7.17 mL, 76.9 mmol) was added dropwise to dry *N, N*-dimethylformamide (7.71 mL, 100.0 mmol) under nitrogen at 0 ˚C and the mixture was stirred at room temperature for one hour. Then triphenylamine (1.890 g, 7.7 mmol) was added, and this mixture stirred for 4 h at 105 ˚C. After the mixture cooled to room temperature, 80 mL of ice-cold H_2O was added to the mixture and it was neutralized with sodium bicarbonate. This mixture was extracted with chloroform (3 x 80 mL) and the organics were washed with water (3 x 80 mL) and brine (1 x 80). After drying with $MgSO_4$, the solvent was removed with rotary evaporation. The crude product was purified by column chromatography (Hexanes/Diethyl Ether = 3:1) to yield the product as a yellow solid (1.926 g, 83%). Spectra matched that as previously reported.[4] ^{1}H NMR (300 MHz, $CDCl_3$): δ (ppm) 9.90 (s, 2H), 7.78 (d, *J* = 8.7 Hz, 4H), 7.40 (t, *J* = 7.2 Hz, 2H), 7.29 (t, *J* = 7.3 Hz, 1H), 7.18 (m, 6H).

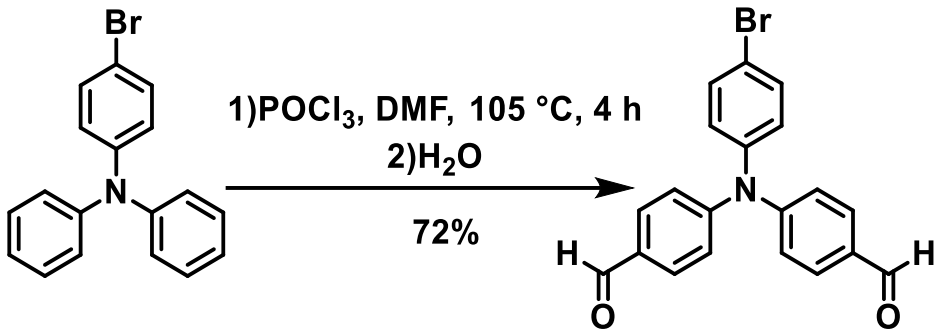

4,4'-((4-Bromophenyl)azanediyl)dibenzaldehyde: Compound was made according to previous procedures.[5] Phosphoryl chloride (9.12 mL, 97.8 mmol) was added dropwise to dry *N, N*-dimethylformamide (10.00 mL, 129.7 mmol) under nitrogen and the mixture was stirred at room temperature for one hour. Then 4-bromo-*N, N*-diphenylaniline (3.17 g, 9.78 mmol) was added, and this mixture stirred for 4 h at 105 ˚C. After the mixture cooled to room temperature, 100 mL of ice-cold water was added followed by further dilution to 1 L with water. Then the suspension was filtered, and the crude product was purified by column chromatography (Hexanes/Diethyl Ether = 3:1) to yield the product as a yellow solid (2.677 g, 72%). Spectra matched that as previously reported.[6] ^{1}H NMR (300 MHz, $CDCl_3$): δ (ppm) 10.03 (s, 2H), 7.79 (d, *J* = 8.6 Hz, 4H), 7.50 (d, *J* = 8.7 Hz, 2H), 7.18 (d, *J* = 8.4 Hz, 4H), 7.05 (d, *J* = 8.8 Hz, 2H).

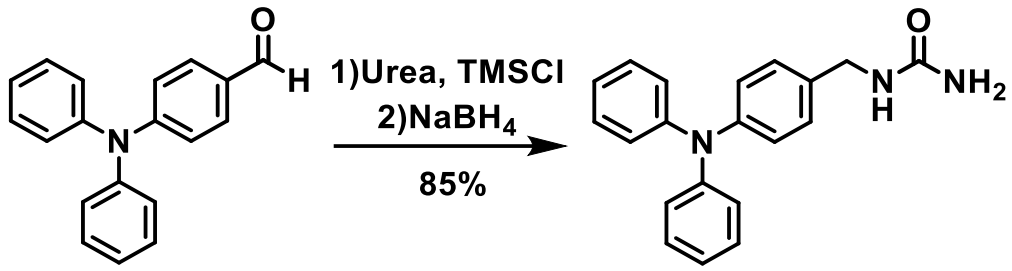

1-(4-(diphenylamino)benzyl)urea: The previous aldehyde (0.460 g, 1.7 mmol), urea (1.000 g, 16.8 mmol), and trimethylsilyl chloride (0.315 mL, 2.52 mmol) were dissolved in 30 mL of acetic acid and stirred at room temperature overnight. Then sodium borohydride (0.095 g, 2.52 mmol) was added and the mixture stirred for an additional 2 h. After reaction completion, 500 mL of water was added, and the precipitate was filtered and washed with plenty of water. Then column chromatography (Dichloromethane/Ethyl Acetate = 1:1) was used to purify the product as a beige solid (0.454 g, 85%). ^{1}H NMR (300 MHz, CD_3OD): δ (ppm) 7.28-7.15 (m, 6H), 7.04-6.94 (m, 8H), 4.25 (s, 2H). HRMS (DEP): [M+] calculated, 317.1528; found, 317.1524.

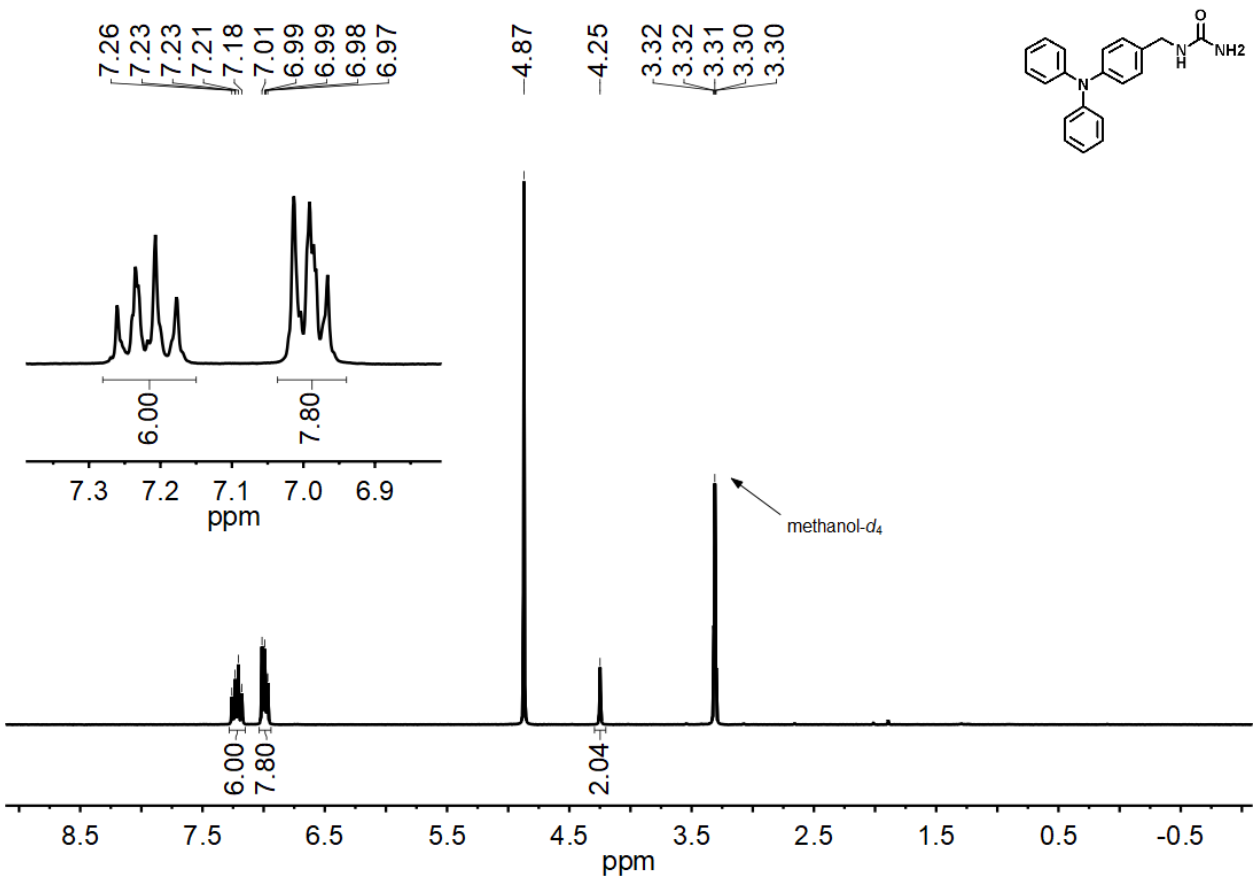

Figure S1. ^{1}H NMR of TPA **4** ($(CD_3OD$, 300 MHz).

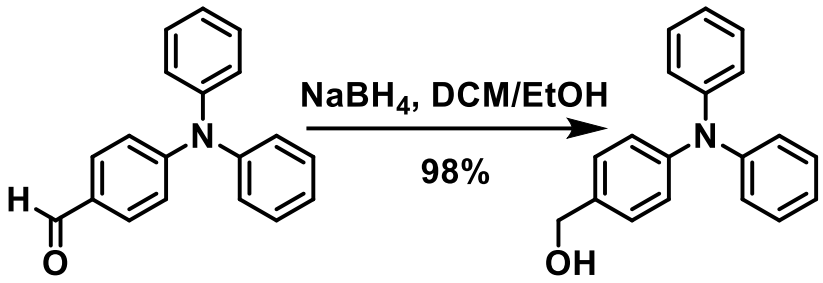

(4-(Diphenylamino)phenyl)methanol: Compound was made according to previous procedures.[7] The previous aldehyde (0.4885 g, 1.8 mmol) was dissolved in 28 mL of a 3:1 mixture of dry dichloromethane and ethanol. Sodium borohydride (0.074 g, 2.0 mmol) was added after and the mixture stirred at room temperature for 2 h in the dark. Then 40 mL of water was added, and the mixture was extracted with dichloromethane (3 x 15 mL) and dried with $MgSO_4$. Solvent was removed *via* rotary evaporation leaving behind the alcohol as a sticky solid (0.482 g, 98%). Spectra matched that as previously reported.[3] ^{1}H NMR (300 MHz, $(CD_3)_2SO$): δ (ppm) 7.33-7.21 (m, 6H), 7.06-6.92 (m, 8H), 5.12 (t, *J* = 5.7 Hz, 1H), 4.44 (d, *J* = 5.6 Hz, 2H).

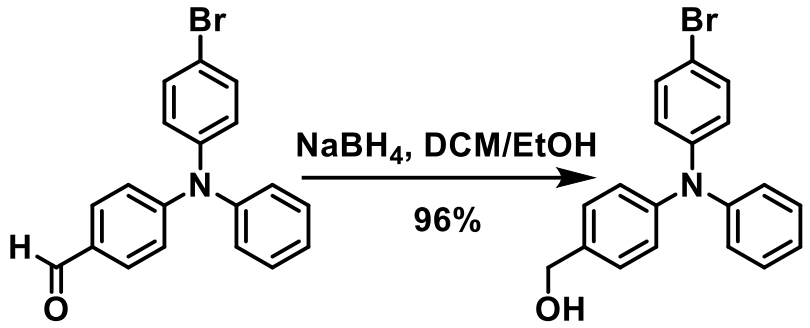

(4-((4-Bromophenyl)(phenyl)amino)phenyl)methanol: Compound was made according to previous procedures.[8] The previous aldehyde (1.0466 g, 3.0 mmol) was dissolved in 50 mL of a 3:1 mixture of dry dichloromethane and ethanol. Sodium borohydride (0.124 g, 3.3 mmol) was added after and the mixture stirred at room temperature for 12 h in the dark. Then 70 mL of water was added, and the mixture was extracted with dichloromethane (3 x 70 mL) and dried with $MgSO_4$. Solvent was removed *via* rotary evaporation leaving behind the alcohol as a sticky solid (1.011 g, 96%). Spectra matched that as previously reported.[8] ^{1}H NMR (300 MHz, $(CD_3)_2SO$): δ (ppm) 7.41 (d, *J* = 8.8 Hz, 2H), 7.35-7.23 (m, 4H), 7.09-6.96 (m, 5H), 6.86 (d, *J* = 8.9 Hz, 2H), 5.14 (t, *J* = 5.7 Hz, 1H), 4.45 (d, *J* = 5.7 Hz, 2H).

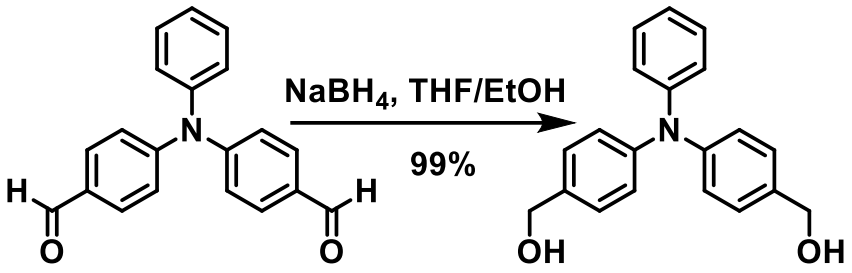

((Phenylazanediyl)*bis*(4,1-phenylene))dimethanol: Compound was made according to previous procedures.[9] The previous aldehyde (2.439 g, 8.1 mmol) and sodium borohydride (0.674 g, 17.8 mmol) were suspended in 180 mL of a 2:1 mixture of dry tetrahydrofuran and ethanol and heated at 40 ˚C overnight in the dark. Then the reaction was cooled to room temperature and 180 mL of water was added to quench the reaction. The mixture was extracted with chloroform (3 x 180 mL) and dried with $MgSO_4$. Then the solvent was removed under rotary evaporation to yield the alcohol as a white solid (2.446 g, 99%). Spectra matched that as previously reported.[9] ^{1}H NMR (300 MHz, $CDCl_3$): δ (ppm) 7.24-7.20 (m, 5H), 7.11-6.98 (m, 8H), 4.64 (s, 4H).

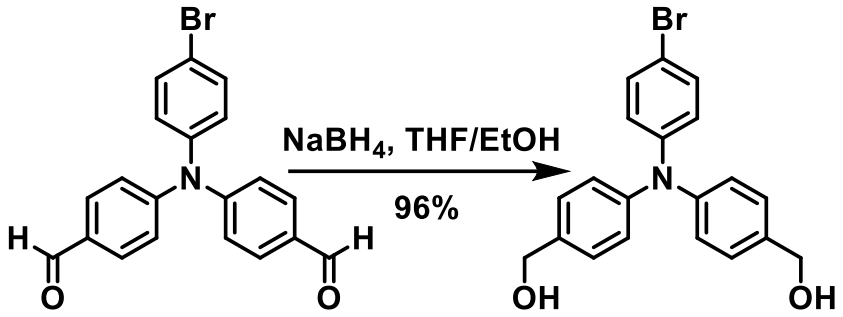

(((4-Bromophenyl)azanediyl)*bis*(4,1-phenylene))dimethanol: Compound was made according to previous procedures.[5] The previous aldehyde (2.6574 g, 7.0 mmol) and sodium borohydride (0.582 g, 15.4 mmol) were suspended in 180 mL of a 2:1 mixture of dry tetrahydrofuran and ethanol and was heated at 40 ˚C overnight in the dark. Then the reaction was cooled to room temperature and 180 mL of water was added to quench the reaction. The mixture was extracted with chloroform (3 x 180 mL) and dried with $NaSO_4$. The solvent was removed under rotary evaporation yielding the product as a white solid (2.579 g, 96%). Spectra was similar to that as previously recorded.[5] ^{1}H NMR (300 MHz, $CDCl_3$): δ (ppm) 7.32 (d, *J* = 8.7 Hz, 2H), 7.26 (d, *J* = 8.3 Hz, 4H), 7.05 (d, *J* = 8.4 Hz, 4H), 6.93 (d, *J* = 8.8 Hz, 2H), 4.65 (s, 4H), 1.64 (s, 2H).

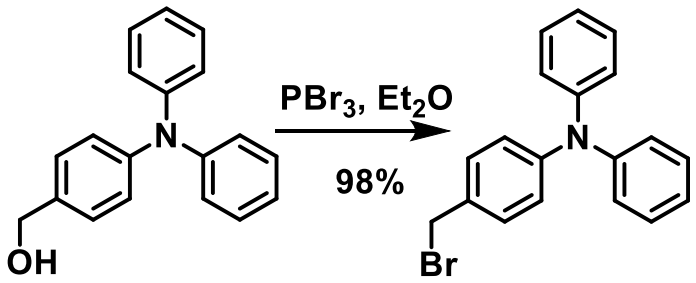

4-(Bromomethyl)-N,N-diphenylaniline: Compound was made according to previous procedures.[10] The previous alcohol (0.482 g, 1.8 mmol) was suspended in 20 mL of dry diethyl ether and was cooled to 0 ˚C. Then a solution of phosphorus tribromide (120 µL, 1.2 mmol) in 10 mL dry diethyl ether was added dropwise over 5 minutes. The reaction stirred at room temperature overnight in the dark. In the morning, ice cold water (20 mL) and saturated aqueous $NaHCO_3$ (10 mL) was added to quench the reaction. The mixture was extracted with (1 x 20 mL) of dichloromethane and the organics were washed with brine (3 x 20 mL) and dried with $MgSO_4$. The solvent was removed under rotary evaporation to yield the bromide as a sticky solid (0.580 g, 98%). Spectra was similar to that as previously recorded.[10] ^{1}H NMR (300 MHz, CD_2Cl_2): δ (ppm) 7.31-7.22 (m, 6H), 7.12-6.95 (m, 8H), 4.52 (s, 2H).

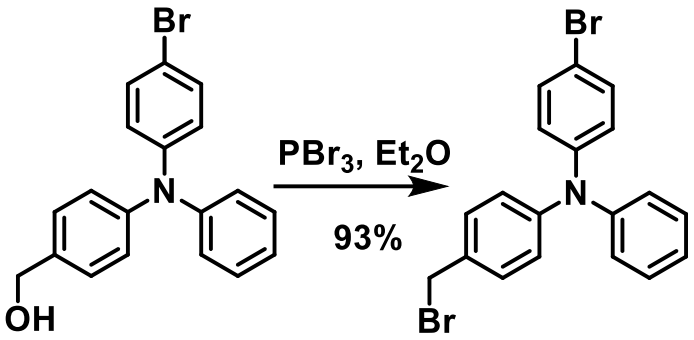

4-Bromo-*N*-(4-(bromomethyl)phenyl)-*N*-phenylaniline: Compound was made according to previous procedures.[8] The previous alcohol (1.013 g, 2.9 mmol) was suspended in 35 mL of dry diethyl ether and was cooled to 0 ˚C. Then a solution of phosphorus tribromide (163 µL, 1.7 mmol) in 10 mL dry diethyl ether was added dropwise over 5 minutes. The reaction stirred at room temperature overnight in the dark. In the morning, ice cold water (45 mL) and saturated aqueous $NaHCO_3$ (22.5 mL) was added to quench the reaction. The mixture was extracted with (1 x 45 mL) of dichloromethane and the organics were washed with brine (3 x 22.5 mL) and dried with $MgSO_4$. The solvent was removed under rotary evaporation to yield the bromide as a sticky solid (1.110 g, 93%). Spectra was similar to that as previously recorded.[8] ^{1}H NMR (300 MHz, CD_3Cl): δ (ppm) 7.30-7.14 (m, 6H), 7.04-6.95 (m, 3H), 6.95-6.84 (m, 4H), 4.41 (s, 2H).

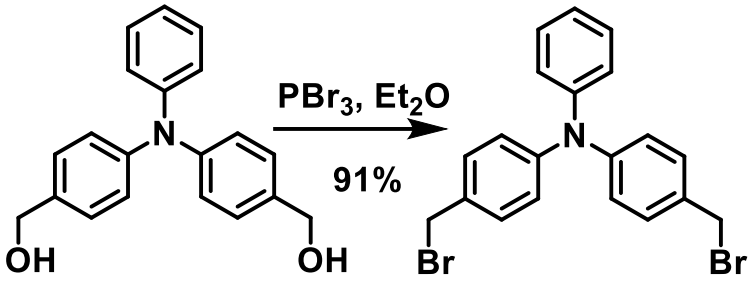

4-(Bromomethyl)-*N*-(4-(bromomethyl)phenyl)-*N*-phenylaniline: The previous alcohol (1.828 g, 6.0 mmol) was suspended in 62 mL of dry diethyl ether and was cooled to 0 ˚C. Then a solution of phosphorus tribromide (682 µL, 7.2 mmol) in 10 mL dry diethyl ether was added dropwise over 5 minutes. The reaction stirred at room temperature overnight in the dark. In the morning, ice cold water (72 mL) and saturated aqueous $NaHCO_3$ (36 mL) was added to quench the reaction. The mixture was extracted with 72 mL of dichloromethane and the organics were washed with brine (3 x 72 mL) and dried with $MgSO_4$. The solvent was removed under rotary evaporation to yield the bromide as colorless plates which were suitable for SC-XRD (2.349 g, 91%). ^{1}H NMR (300 MHz, CD_2Cl_2): δ (ppm) 7.34-7.23 (m, 6H), 7.13-7.05 (m, 3H), 7.01 (d, *J* = 8.4 Hz, 4H), 4.52 (s, 4H). ^{13}C NMR (75 MHz, CD_2Cl_2): δ (ppm) 148.03, 147.41, 132.40, 130.55, 129.88, 125.72, 124.34, 124.00, 34.49.

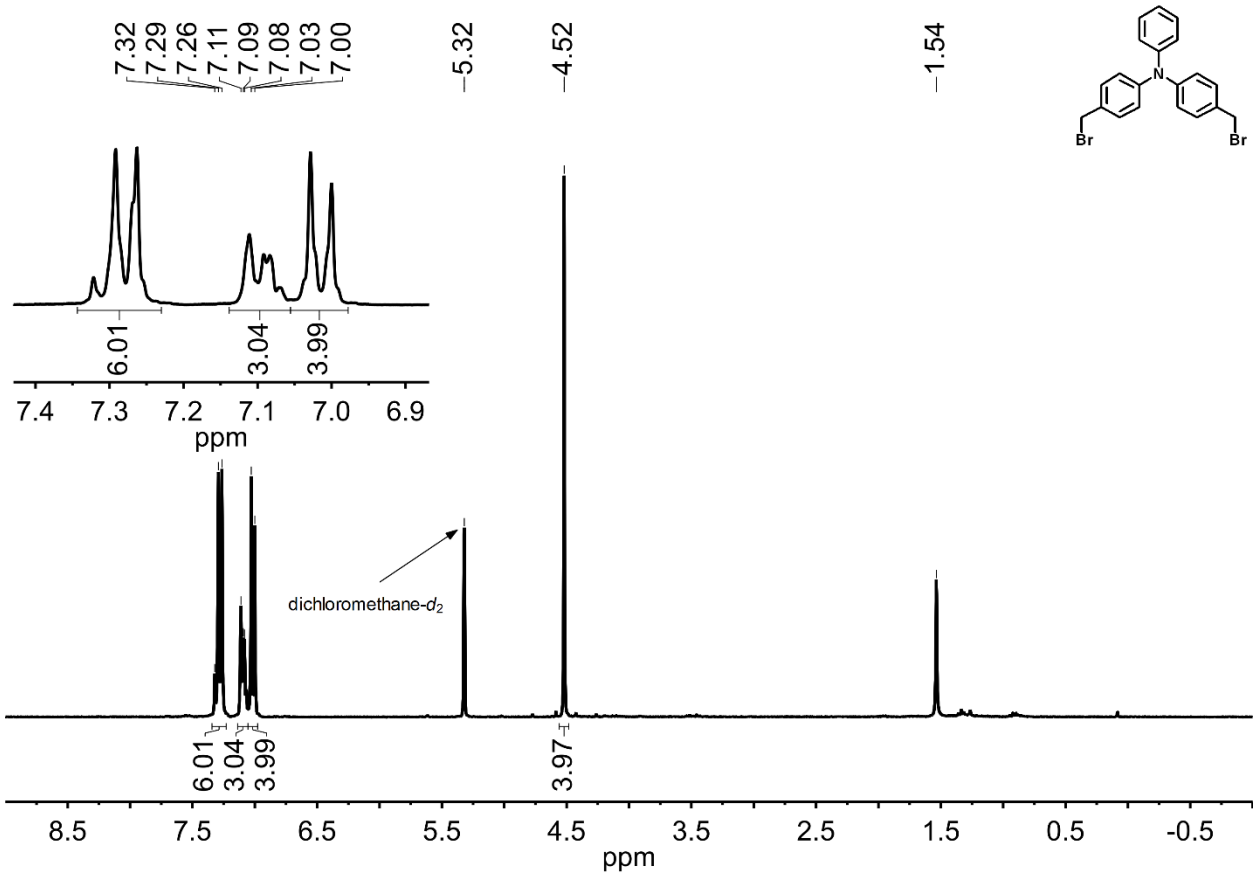

Figure S2. ^{1}H NMR of dibromide **1** (CD_2Cl_2, 300 MHz).

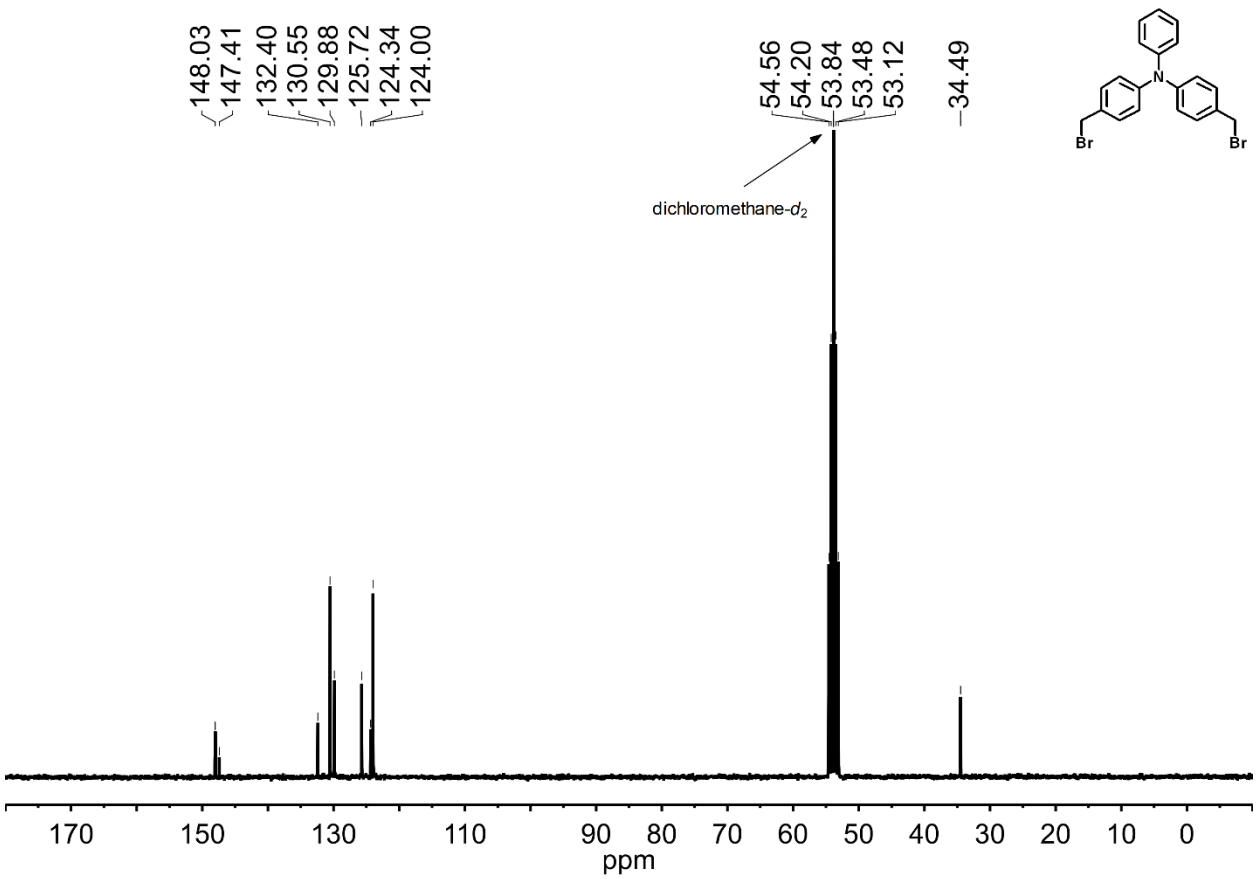

Figure S3. ^{13}C NMR of dibromide **1** (CD_2Cl_2, 75 MHz).

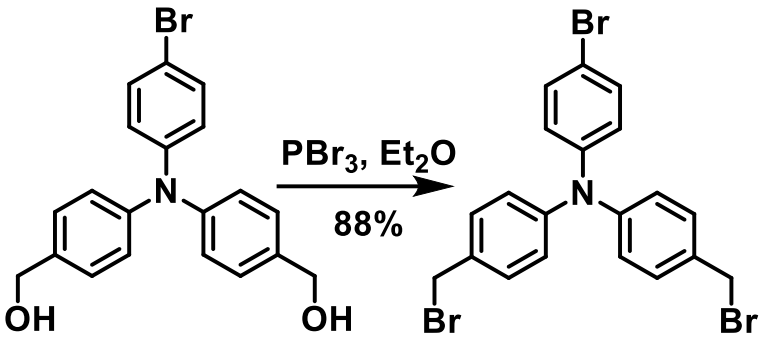

4-Bromo-*N*,*N*-*bis*(4-(bromomethyl)phenyl)aniline: Compound was made according to previous procedures.[5] The previous alcohol (2.568 g, 6.7 mmol) was suspended in 70 mL of dry diethyl ether and was cooled to 0 ˚C. Then a solution of phosphorus tribromide (761 µL, 8.0 mmol) in 10 mL dry diethyl ether was added dropwise over 5 minutes. The reaction stirred at room temperature overnight in the dark. In the morning, 80 mL ice cold water and 40 mL saturated aqueous $NaHCO_3$ were added to quench the reaction. The mixture was extracted with 80 mL of dichloromethane and the organics were washed with brine (3 x 40 mL) and dried with $MgSO_4$. The solvent was removed under rotary evaporation to yield the bromide as a sticky solid (2.999 g, 88%). Spectra matched that as previously recorded.[5] ^{1}H NMR (300 MHz, CD_2Cl_2): δ (ppm) 7.38 (d, *J* = 8.7 Hz, 2H), 7.29 (d, *J* = 8.5 Hz, 4H), 7.02 (d, *J* = 8.5 Hz, 4H), 6.97 (d, *J* = 8.7 Hz, 2H), 4.51 (s, 4H).

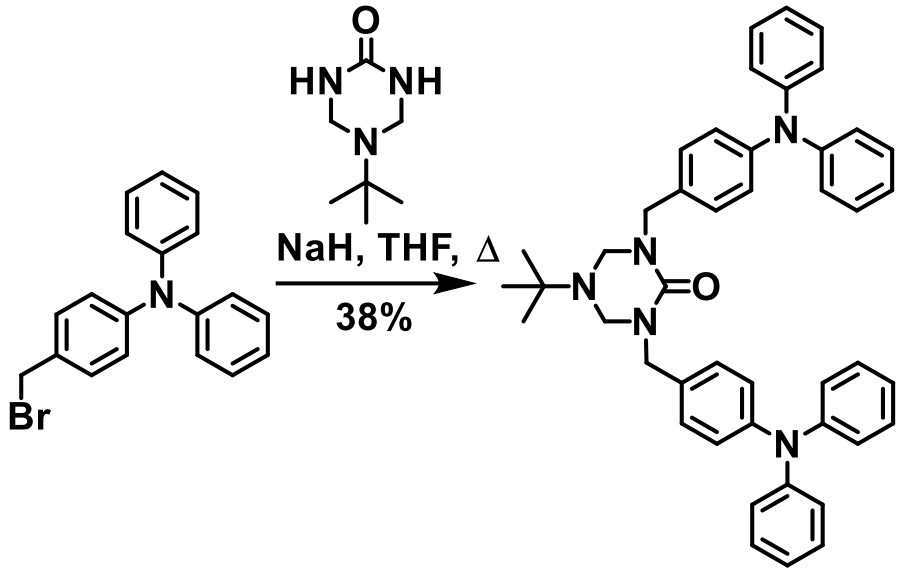

5-(*tert*-butyl)-1,3-*bis*(4-(diphenylamino)benzyl)-1,3,5-triazinan-2-one: *tert*-Butyl triazinanone (0.135 g, 0.9 mmol) and sodium hydride (60% suspension in paraffin oil, 0.103 g, 2.6 mmol) were suspended in 12 mL of dry tetrahydrofuran and was stirred for 5 minutes. Then the previous bromide (0.5778 g, 1.7 mmol) was added as a solution in 12 mL of dry tetrahydrofuran. The reaction stirred at reflux in the dark overnight. After cooling to room temperature, 4 mL of 1 N aqueous HCl and 4 mL of water were added to quench the reaction. This solution was extracted with dichloromethane (3 x 40 mL). The organics were washed with brine (1 x 40 mL) and dried with $MgSO_4$. The solvents were removed under rotary evaporation, and the product was isolated using column chromatography (Hexanes/Ethyl Acetate = 1:1) to yield the product as a sticky solid (0.218 g, 38%). ^{1}H NMR (300 MHz, $(CD_3)_2CO$): δ (ppm) 7.38-7.22 (m, 12H), 7.07-6.97 (m, 16H), 4.50 (s, 4H), 4.34 (s, 4H), 1.02 (s, 9H). ^{13}C NMR (75 MHz, $(CD_3)_2CO$): δ (ppm) 156.68, 148.83, 147.73, 134.77, 130.48, 130.16, 125.19, 124.63, 123.56, 62.34, 54.86, 48.37, 28.75. HRMS (DEP): [M+] calculated, 672.3697; found, 672.3699.

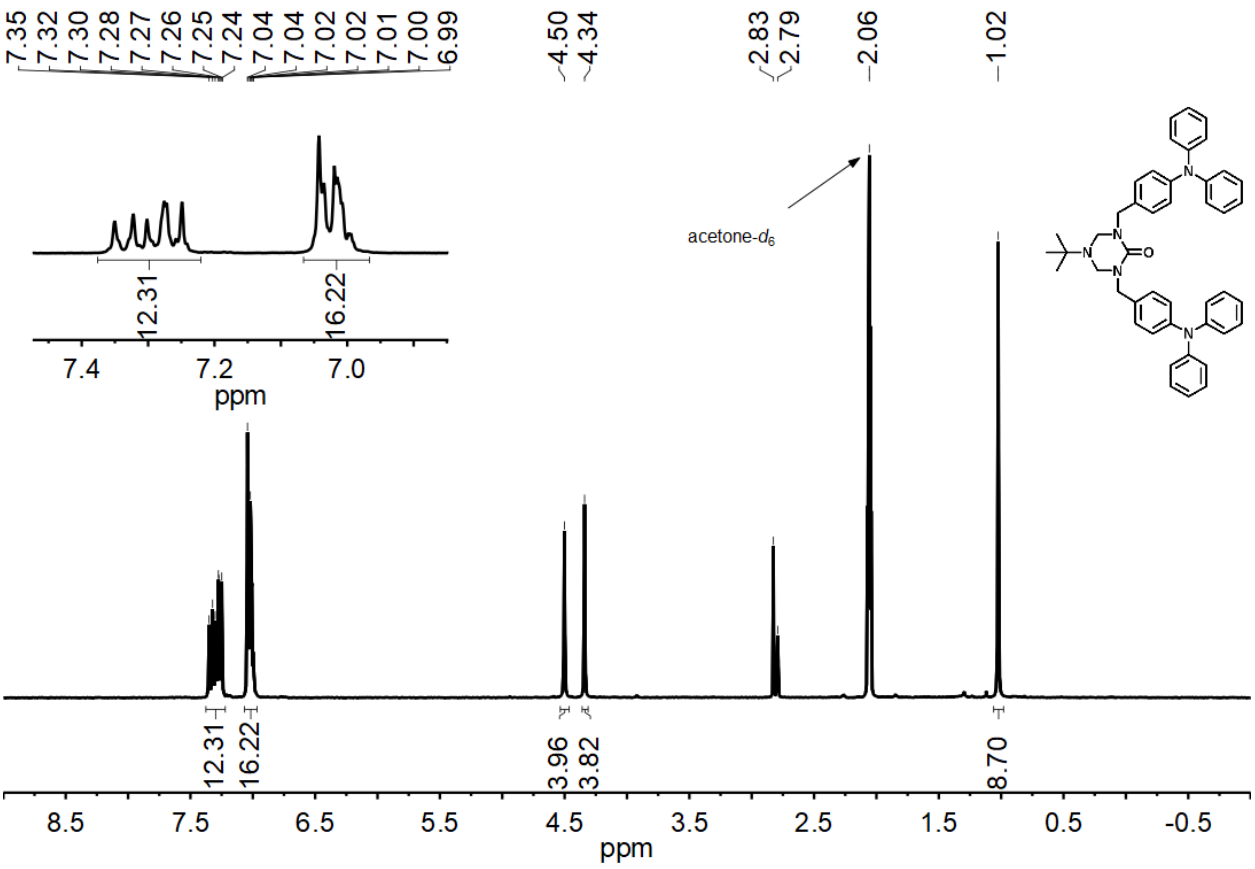

Figure S4. ^{1}H NMR protected **2** ($(CD_3)_2CO$, 300 MHz).

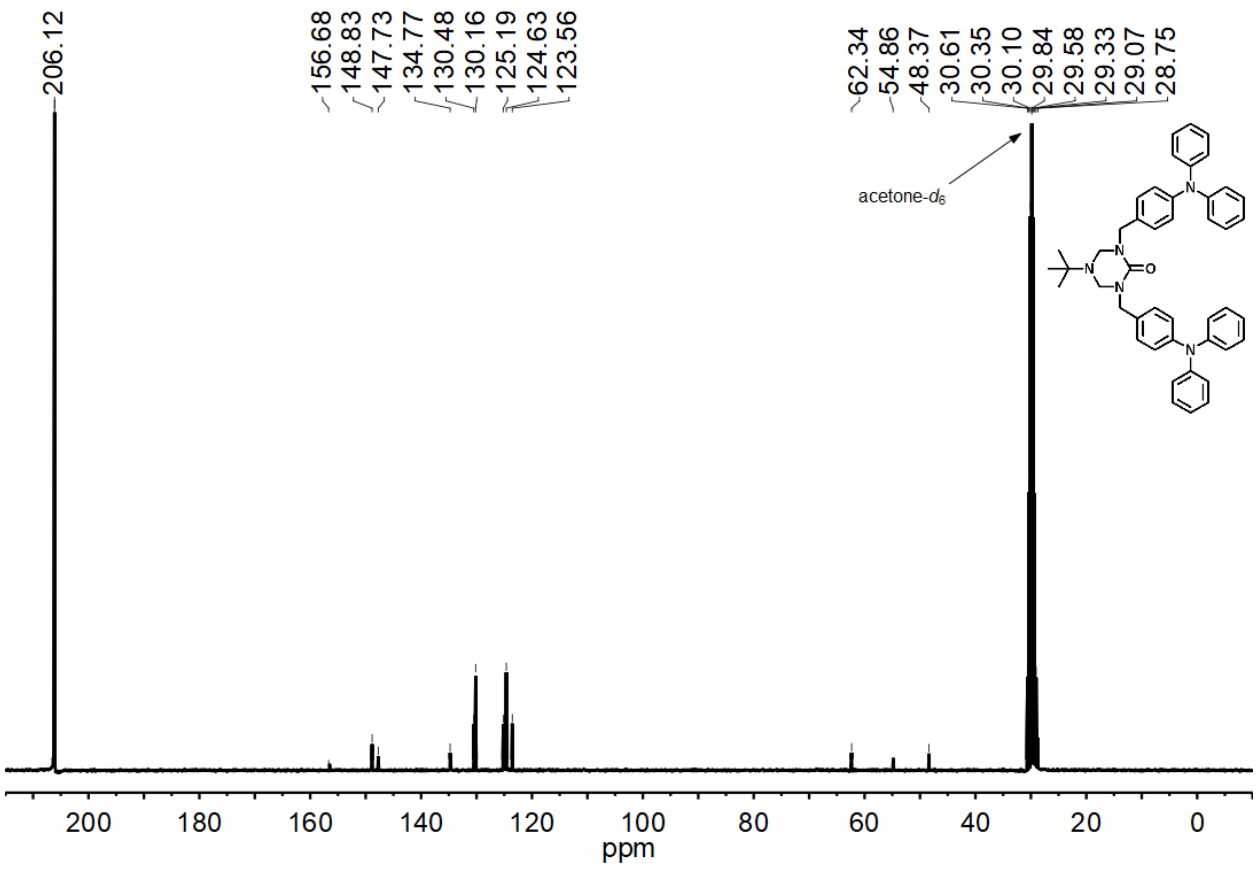

Figure S5. ^{13}C NMR protected **2** ($(CD_3)_2CO$, 75 MHz).

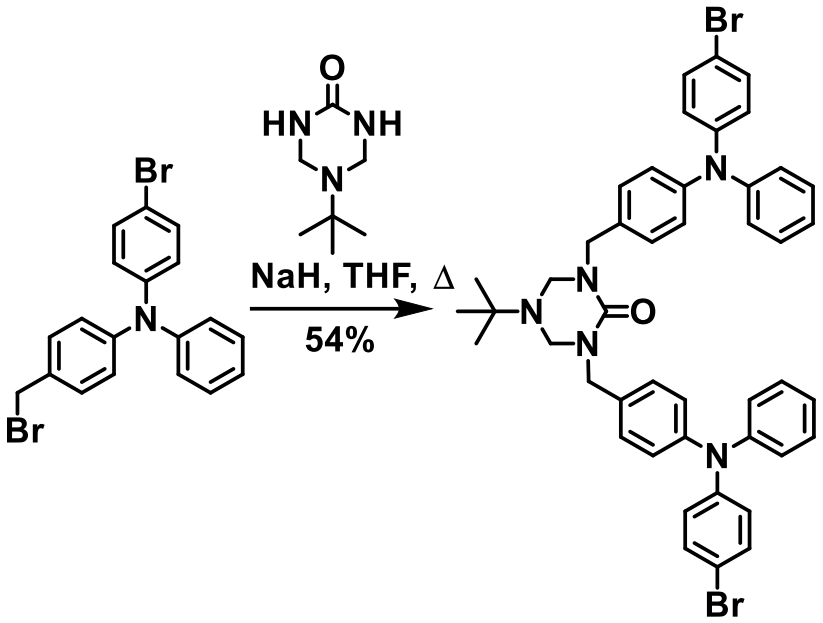

1,3-*bis*(4-((4-bromophenyl)(phenyl)amino)benzyl)-5-(*tert*-butyl)-1,3,5-triazinan-2-one:

Compound was made according to previous procedures.[8] *tert*-Butyl triazinanone (0.209 g, 1.3 mmol) and sodium hydride (60% suspension in paraffin oil, 0.160 g, 4.0 mmol) were suspended in 20 mL of dry tetrahydrofuran and was stirred for 10 minutes. Then the previous bromide (1.111 g, 2.7 mmol) was added as a solution in 20 mL of dry tetrahydrofuran. The reaction stirred at reflux in the dark overnight. After cooling to room temperature, 6 mL of 1 N aqueous HCl and 6 mL of water were added to quench the reaction. This solution was extracted with dichloromethane (3 x 60 mL). The organics were washed with brine (1 x 60 mL) and dried with $MgSO_4$. The solvents were removed under rotary evaporation, and the product was isolated using column chromatography (Hexanes/Ethyl Acetate = 2:1) to yield the product as a sticky solid (0.596 g, 54%). Spectra was similar to that as previously recorded.[8] ^{1}H NMR (300 MHz, $CDCl_3$): δ (ppm) 7.35-7.19 (m, 12H), 7.09-6.99 (m, 10H), 6.92 (d, *J* = 8.9 Hz, 4H), 4.50 (s, 4H), 4.26 (s, 4H), 1.03 (s, 9H).

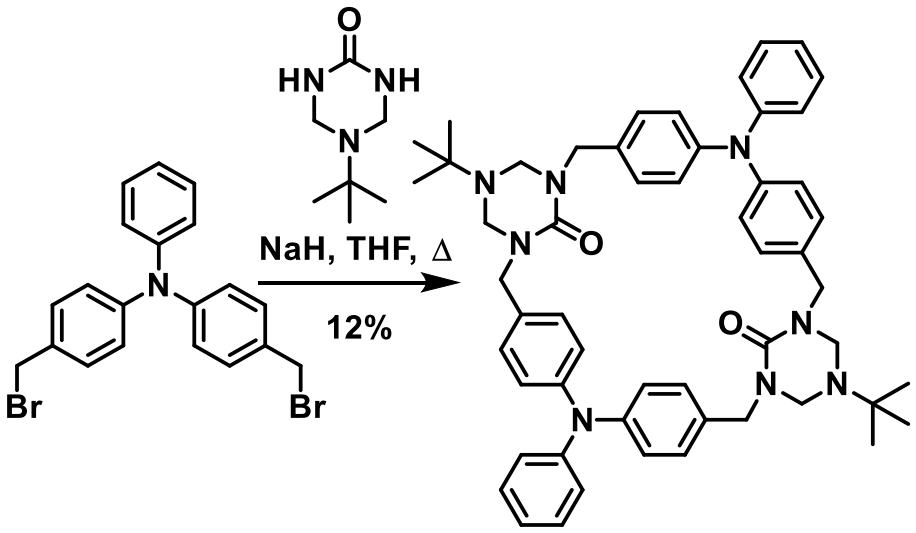

1^5,7^5-Di-*tert*-butyl-4,10-diphenyl-4,10-diaza-1,7(1,3)-ditriazinana-3,5,9,11(1,4)tetrabenzenacy-c-lododecaphane-1^2,7^2-dione: *tert*-Butyl triazinanone (1.148 g, 7.3 mmol) and sodium hydride (60% suspension in paraffin oil, 1.168 g, 7.3 mmol) were suspended in 285 mL of dry tetrahydrofuran and was stirred for 2 h at reflux. After cooling to room temperature, the previous bromide (3.149 g, 7.3 mmol) was added as a solution in 285 mL of dry tetrahydrofuran. The reaction stirred at reflux in the dark for 2 days. Upon completion, the reaction was quenched with 13 and 53 mL of 1N aqueous HCl and water then reduced *in vacuo* to 285 mL. An additional 40 mL 1N $HCl_{(aq)}$ and 173 mL of and water were added to the solution before it was extracted with dichloromethane (3 x 370 mL). The combined organic layers were washed with brine (1 x 370 mL) and dried with $MgSO_4$. The solvent was removed via rotary evaporation, and the material was recrystallized from chloroform. Vacuum drying the crystals yielded the product as a white powder (0.374 g, 12%). ^{1}H NMR (400 MHz, TCE-d_2, 90 ˚C): δ (ppm) 7.29 (t, *J* = 7.5 Hz, 4H), 7.23 (d, *J* = 8.0 Hz), 7.16 (d, *J* = 8.0 Hz, 4H), 7.06 (t, *J* = 7.1 Hz, 2H), 7.01 (d, *J* = 8.0 Hz, 8H) 4.47 (br, 8H), 4.29 (s, 8H), 0.85 (s, 18H). ^{13}C NMR (100 MHz, TCE-d_2, 90 ˚C): δ (ppm) 155.33, 147.34, 147.18, 132.41, 129.68, 129.03, 124.15, 123.74, 122.75, 60.53, 54.07, 47.19, 27.99. HRMS (DEP): [M+] calculated, 853.4912; found, 853.4935.

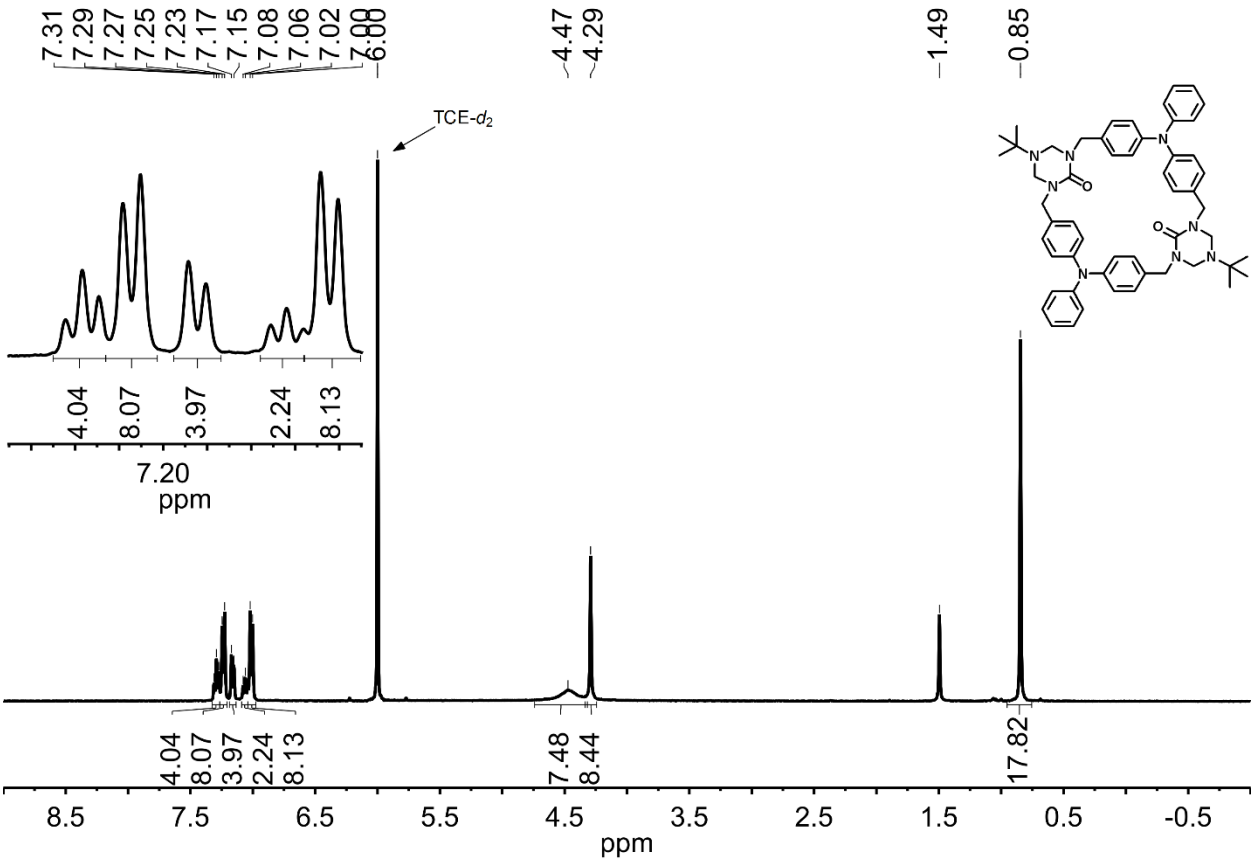

Figure S6. ^{1}H NMR of protected **1** (TCE-d_2, 90 ˚C, 400 MHz).

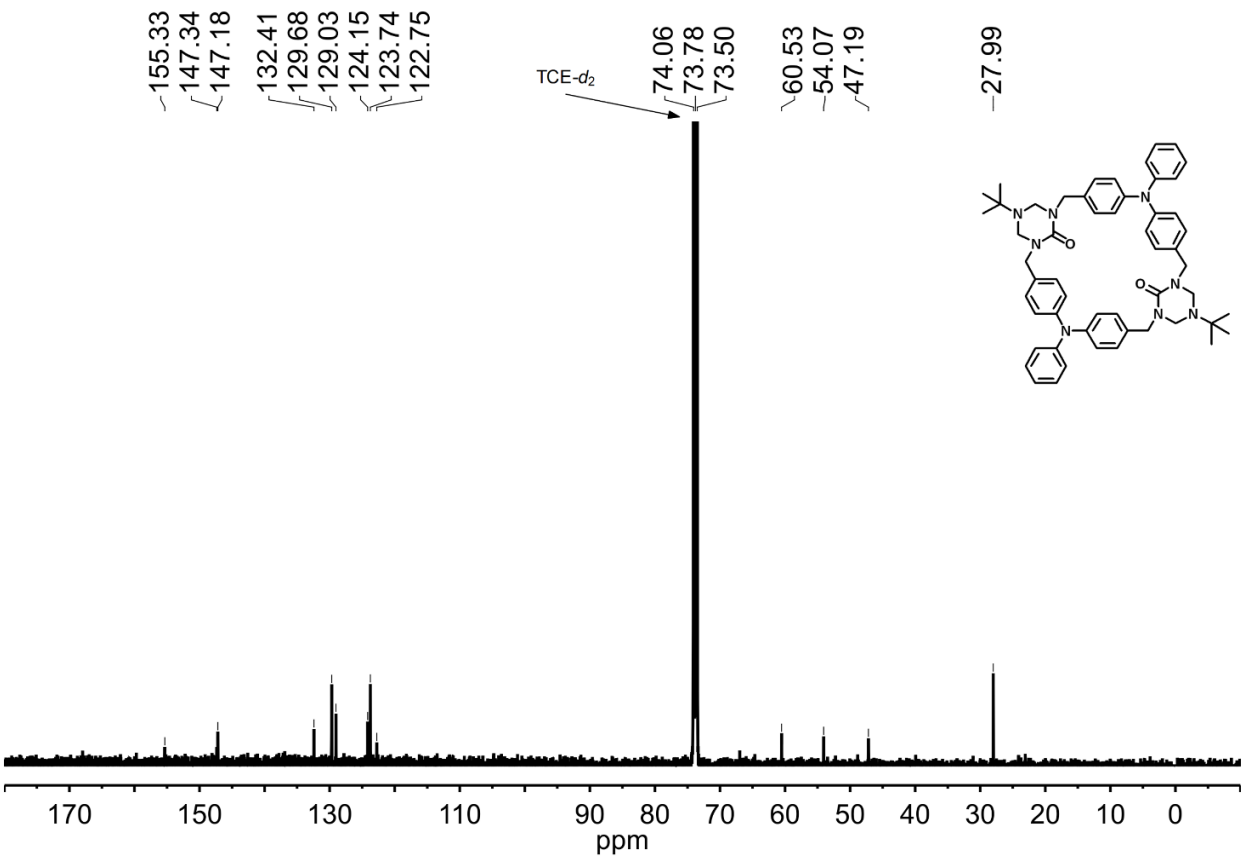

Figure S7. ^{13}C NMR of protected **1** (TCE-d_2, 90 ˚C, 100 MHz).

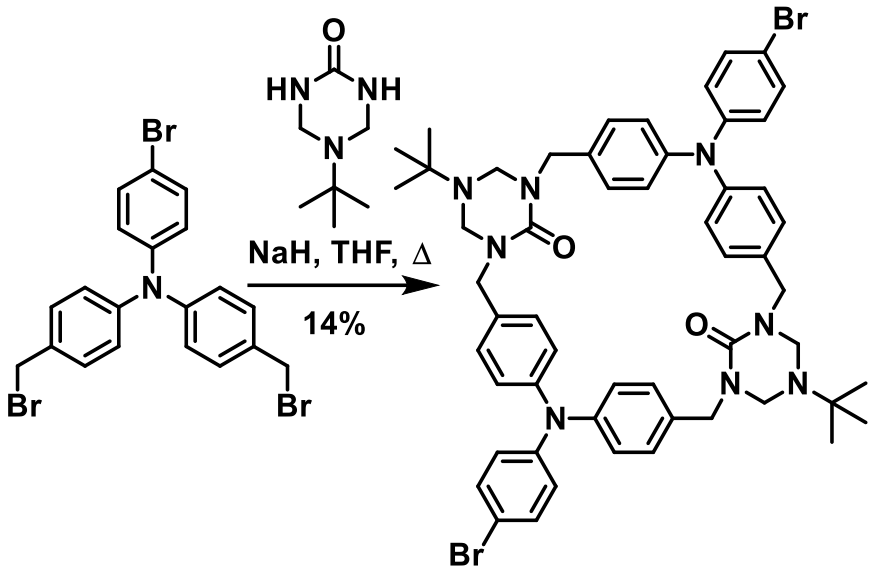

4,10-*bis*(4-Bromophenyl)-1^5,7^5-di-*tert*-butyl-4,10-diaza-1,7(1,3)-ditriazinana-3,5,9,11(1,4)-tetrabenzenacyclododecaphane-1^2,7^2-dione: Compound was made according to previous procedure.[5] *tert*-Butyl triazinanone (3.13 g, 6.1 mmol) and sodium hydride (60% suspension in paraffin oil, 0.983 g, 24.6 mmol) were suspended in 250 mL of dry tetrahydrofuran and was stirred for 2 h at reflux. After cooling to room temperature, the previous bromide (3.134 g, 6.1 mmol) was added as a solution in 250 mL of dry tetrahydrofuran. The reaction stirred at reflux in the dark for 2 days. Upon completion, the reaction was quenched with 12 mL of 1N aqueous HCl and 45 mL of water and was then reduced *in vacuo* to 330 mL. An additional 30 mL of 1N aqueous HCl and 140 mL of water were added to the solution before it was extracted with dichloromethane (3 x 300 mL). The combined organic layers were washed with brine (1 x 300 mL) and dried with $MgSO_4$. The solvent was removed via rotary evaporation, and then the material was recrystallized from chloroform. Vacuum drying the crystals yielded the product as a white powder (0.435 g, 14%). Spectra was similar to that as previously recorded.[5] ^{1}H NMR (300 MHz, CD_2Cl_2): δ (ppm) 7.33 (d, *J* = 8.7 Hz, 4H), 7.22 (d, 8.2 Hz, 8H), 7.02-6.91 (m, 12H), 4.44 (br, 8H), 4.22 (s, 8H), 0.73 (s, 18H).

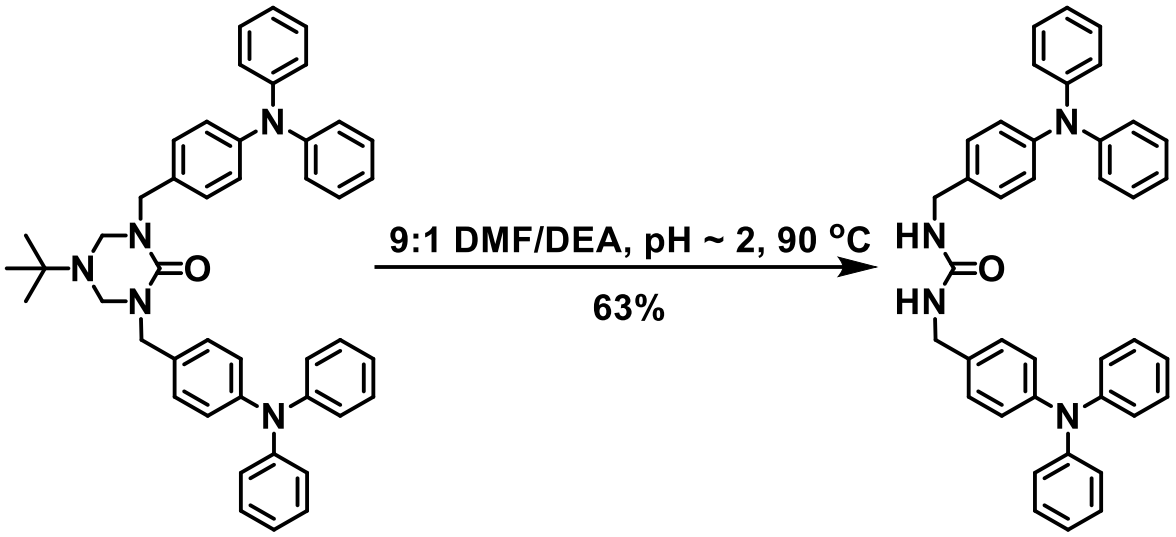

1,3-*bis*(4-(Diphenylamino)benzyl)urea: The previous protected urea (0.211 g, 0.4 mmol) was suspended in 100 mL of a 9:1 solution of *N, N*-dimethylformamide and diethanol amine and the pH was adjusted to 2 using 12 M aqueous HCl. This mixture was heated at 90 ˚C for 2 days in the dark. The pH was readjusted to 2 using 12 M aqueous HCl every 12 h until completion. After cooling to room temperature, 400 mL of water was added and the reaction was filtered. The residue was washed with 50 mL of water leaving behind the product as a beige solid (0.114 g, 63%). ^{1}H NMR (300 MHz, CD_2Cl_2): δ (ppm) 7.26-7.13 (m, 12H), 7.06-6.96 (m, 16H), 4.69 (t, *J* = 5.6 Hz, 2H), 4.31 (d, *J* = 5.8 Hz, 4H). ^{13}C NMR (75 MHz, $CDCl_3$): δ (ppm) 158.04, 147.85, 147.29, 133.19, 129.38, 128.54, 124.32, 124.24, 122.94, 44.48. HRMS (DEP): [M+] calculated, 575.2805 found, 575.2801.

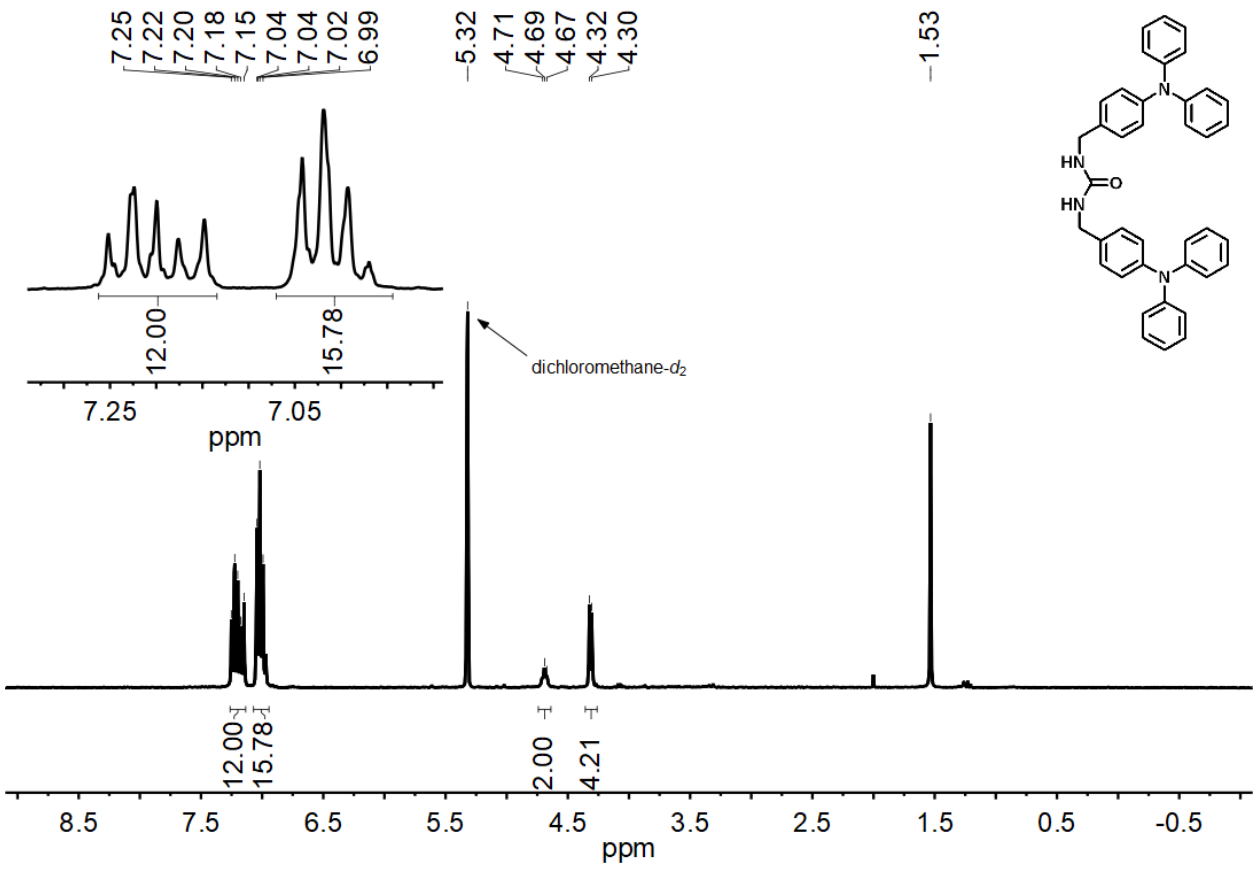

Figure S8. ^{1}H NMR linear analog **2** (CD_2Cl_2, 300 MHz).

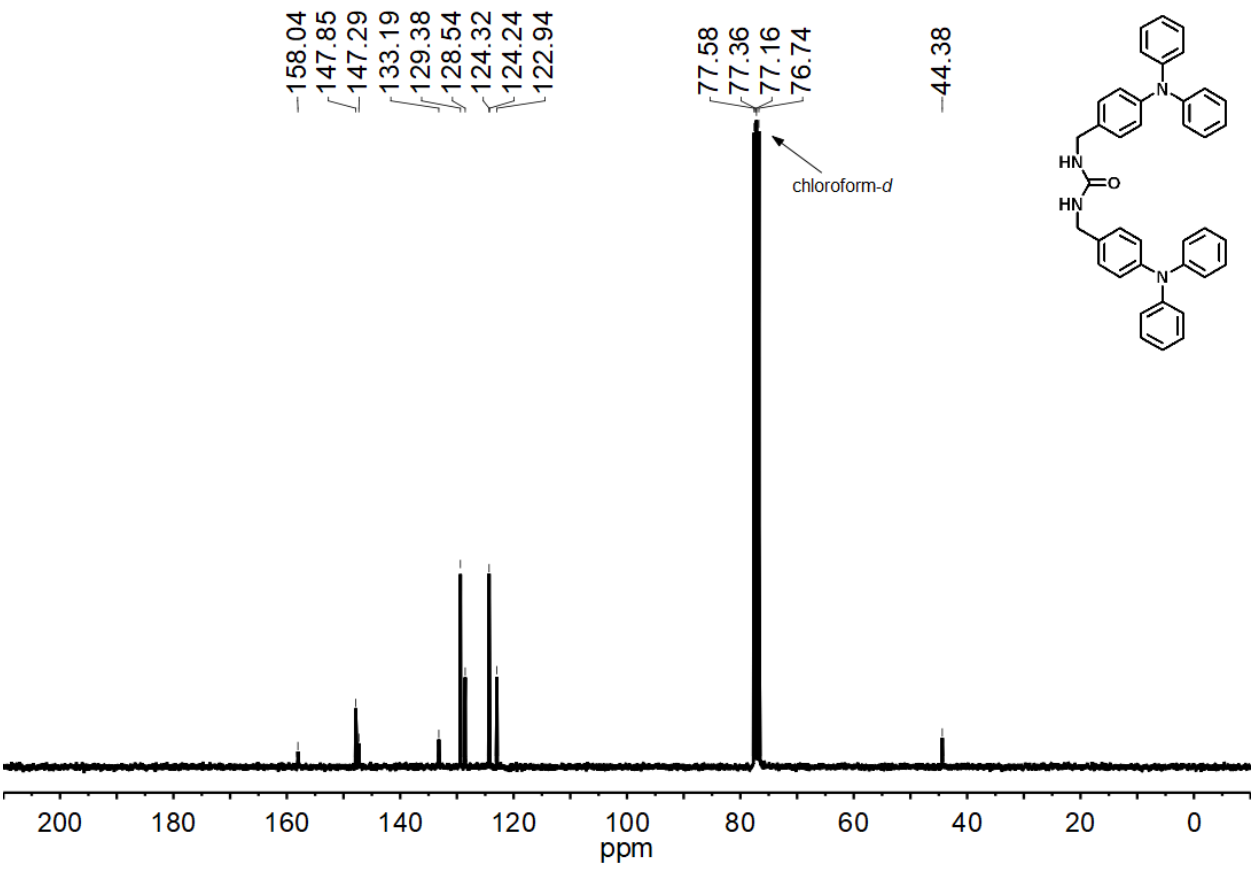

Figure S9. ^{13}C NMR linear analog **2** ($CDCl_3$, 75 MHz).

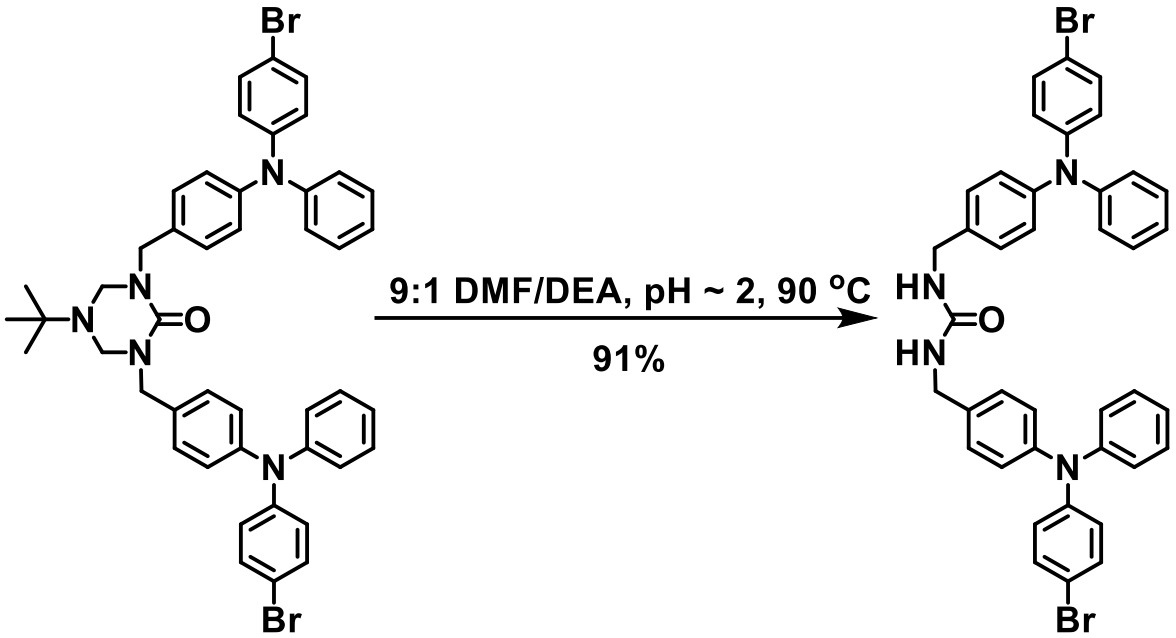

1,3-*bis*(4-((4-bromophenyl)(phenyl)amino)benzyl)urea: Compound was made according to previous procedure.[8] The previous protected urea (0.100 g, 0.1 mmol) was suspended in 50 mL of a 9:1 solution of *N, N*-dimethylformamide and diethanol amine and the pH was adjusted to 2 using 12 M aqueous HCl. This mixture was heated at 90 ˚C for 2 days in the dark. The pH was readjusted to 2 using 12 M aqueous HCl every 12 h until completion. After cooling to room temperature, the solution was neutralized with aqueous $NaHCO_3$, and was diluted to 500 mL with water. The resulting suspension was filtered, and the residue was washed with 50 mL of water leaving behind the product as a beige solid (0.080 g, 91%). The spectra was similar to that as previously recorded.[8] ^{1}H NMR (300 MHz, $(CD_3)SO_2$): δ (ppm) 7.40 (d, *J* = 8.8 Hz, 4H), 7.29 (t, *J* = 7.8 Hz, 4H), 7.20 (d, *J* = 8.4 Hz, 4H), 7.09-6.95 (m, 10H), 6.85 (d, 8.8 Hz, 4H), 6.43 (t, *J* = 5.9 Hz, 2H), 4.19 (d, *J* = 5.8 Hz, 4H).

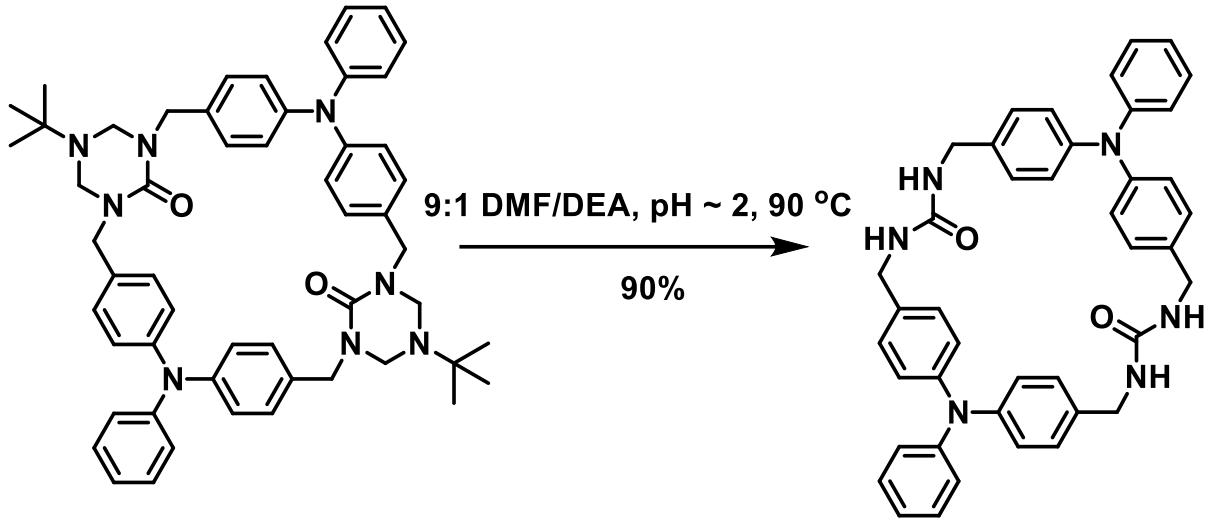

2,10-Diphenyl-2,5,7,10,13,15-hexaaza-1,3,9,11(1,4)-tetrabenzenacyclohexadecaphane-6,14-dione: The previous protected urea (0.026 g, 0.03 mmol) was dissolved in 30 mL of a 9:1 solution of DMF and diethanol amine the pH was adjusted to 2 using 12 M aqueous HCl. This mixture was heated at reflux for three days in the dark. During this time the pH was recalibrated to 2 every 12 h. After cooling to room temperature, the reaction was neutralized with saturated aqueous $NaHCO_3$ and diluted to 210 mL using water. The solution was filtered washed with 50 mL of water then acetonitrile leaving behind the product as a beige solid (0.018 g, 90%). ^{1}H NMR (300 MHz, $(CD_3)_2SO$): δ (ppm) 7.25 (t, *J* = 7.7 Hz, 4H), 7.13 (d, *J* = 8.4 Hz, 8H), 7.03-6.86 (m, 14H) 6.50 (t, *J* = 6.2 Hz, 4H), 4.18 (d, *J* = 6.1 Hz, 8H). ^{13}C NMR (75 MHz, $(CD_3)_2SO$): δ (ppm) 157.83, 147.48, 145.79, 135.90, 129.39, 127.95, 123.50, 123.37, 122.52, 42.08.

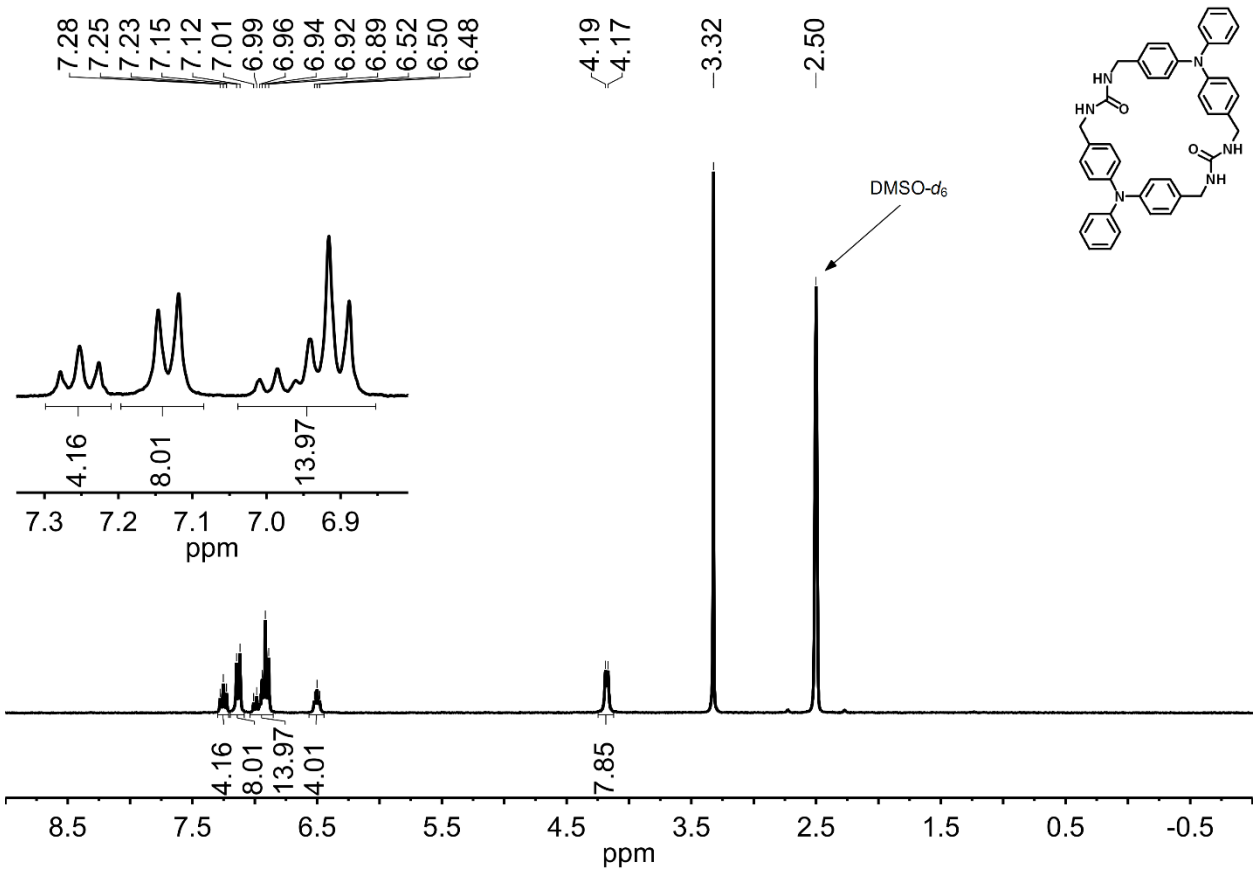

Figure S10. ^{1}H NMR of macrocycle **1** ($(CD_3)_2SO$, 300 MHz).

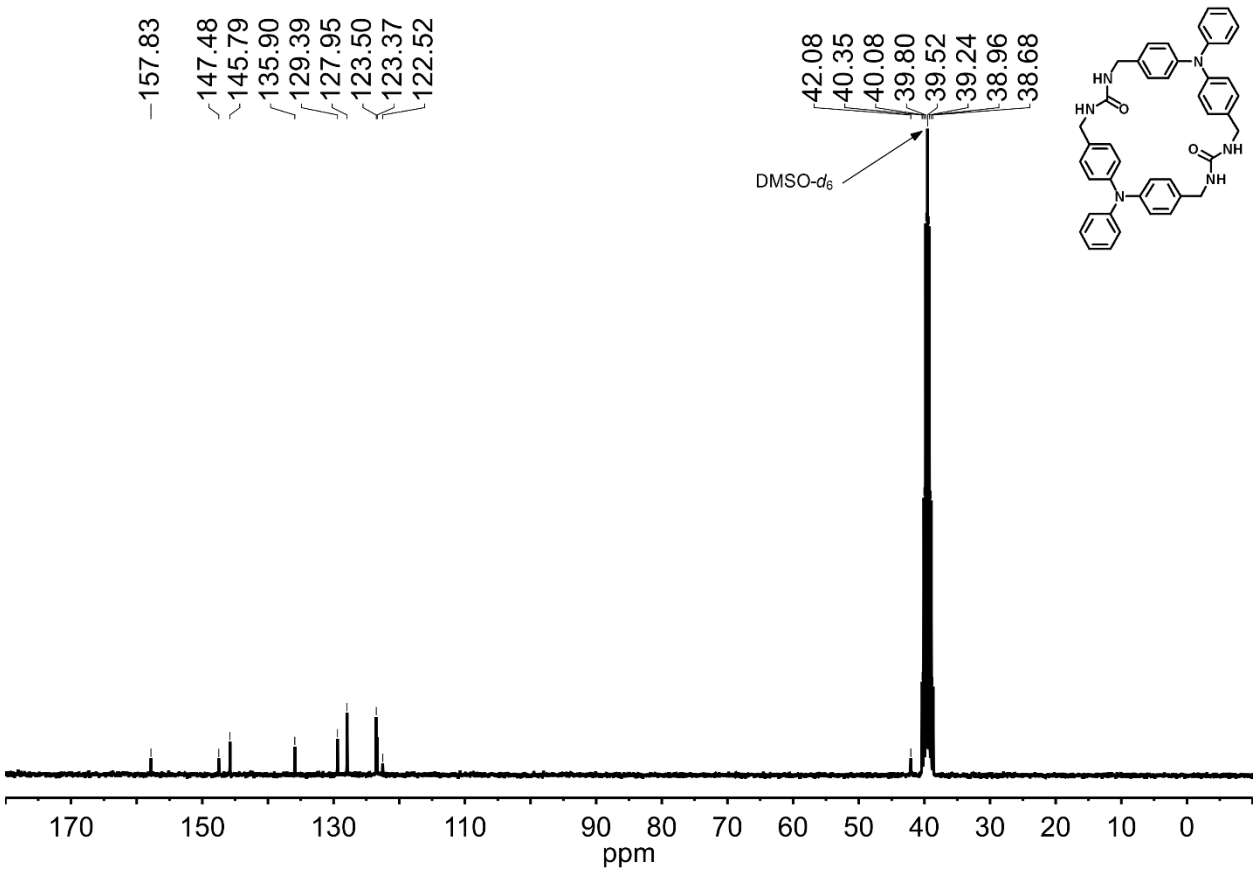

Figure S11. ^{13}C NMR of macrocycle **1** ($(CD_3)_2SO$, 75 MHz).

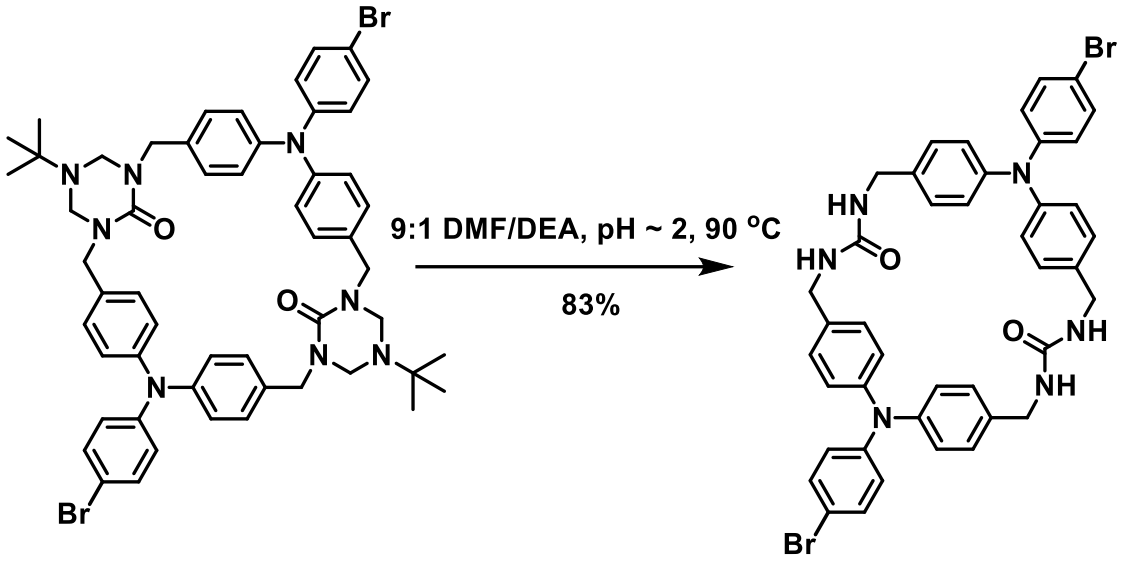

2,10-*bis*(4-Bromophenyl)-2,5,7,10,13,15-hexaaza-1,3,9,11(1,4)-tetrabenzenacyclohexadecaphane-6,14-dione: The previous protected urea (0.225 g, 0.22 mmol) was dissolved in 225 mL of a 9:1 solution of DMF and diethanol amine the pH was adjusted to 2 using 12 M aqueous HCl. This mixture was heated at reflux for three days in the dark. During this time the pH was recalibrated to 2 every 12 h. After cooling to room temperature, the reaction was neutralized with saturated aqueous $NaHCO_3$ and diluted to 1 L using water. The solution was filtered washed with water leaving behind the product as a beige solid (0.151 g, 83%). Spectra matched that as previously recorded.[5] ^{1}H NMR (300 MHz, $(CD_3)_2SO$): δ (ppm) 7.38 (d, *J* = 8.8 Hz, 4H), 7.15 (d, *J* = 8.3 Hz, 8H), 6.93 (d, *J* = 8.4 Hz, 8H), 6.82 (d, *J* = 8.7 Hz, 4H), 6.53 (t, *J* = 6.2 Hz, 4H), 4.18 (d, *J* = 5.9 Hz, 8H).

Crystal data and structure refinement

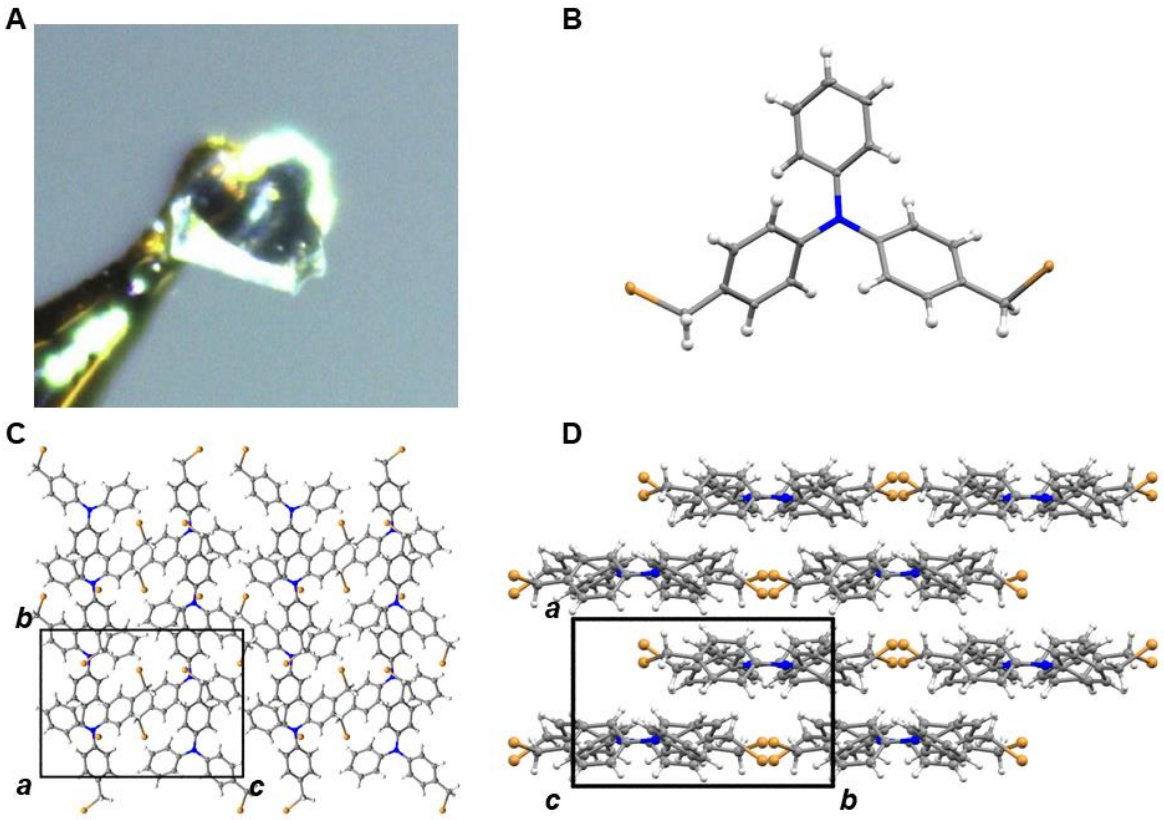

Figure S12. Crystal views of dibromide **1**. (A) Data crystal. (B) Molecular structure of the dibromide **1**. Thermal ellipsoids were drawn at the 30% probability level. (C) Crystal packing along the *a* axis. (E) Crystal packing along the *c* axis.

X-ray intensity data from a colorless plate were collected at 100(2) K using a Bruker D8 QUEST diffractometer equipped with a PHOTON-100 CMOS area detector and an Incoatec microfocus source (Mo Kα radiation, λ = 0.71073 Å). The raw area detector data frames were reduced and corrected for absorption effects using the Bruker APEX3, SAINT+ and SADABS programs.[11,12] Final unit cell parameters were determined by least-squares refinement of 9959 reflections taken from the data set. The structure was solved with SHELXT.[13,14] Subsequent difference Fourier calculations and full-matrix least-squares refinement against F^2 were performed with SHELXL-2017[13,14] using OLEX2.[15]

The compound crystallizes in the monoclinic system. The pattern of systematic absences in the intensity data was consistent with the space group $P2_1/c$, which was confirmed by structure solution. The asymmetric unit consists of one molecule. All non-hydrogen atoms were refined with anisotropic displacement parameters. Hydrogen atoms bonded to carbon were located in Fourier difference maps before being placed in geometrically idealized positions and included as riding atoms with *d*(C-H) = 0.95 Å and *U*iso(H) = 1.2*U*eq(C) for arene hydrogen atoms and *d*(C-H) = 0.99 Å and *U*iso(H) = 1.2*U*eq(C) for methylene hydrogen atoms. The largest residual electron density peak in the final difference map is +2.45 $e^-/Å^3$, located 2.13 Å from H4.

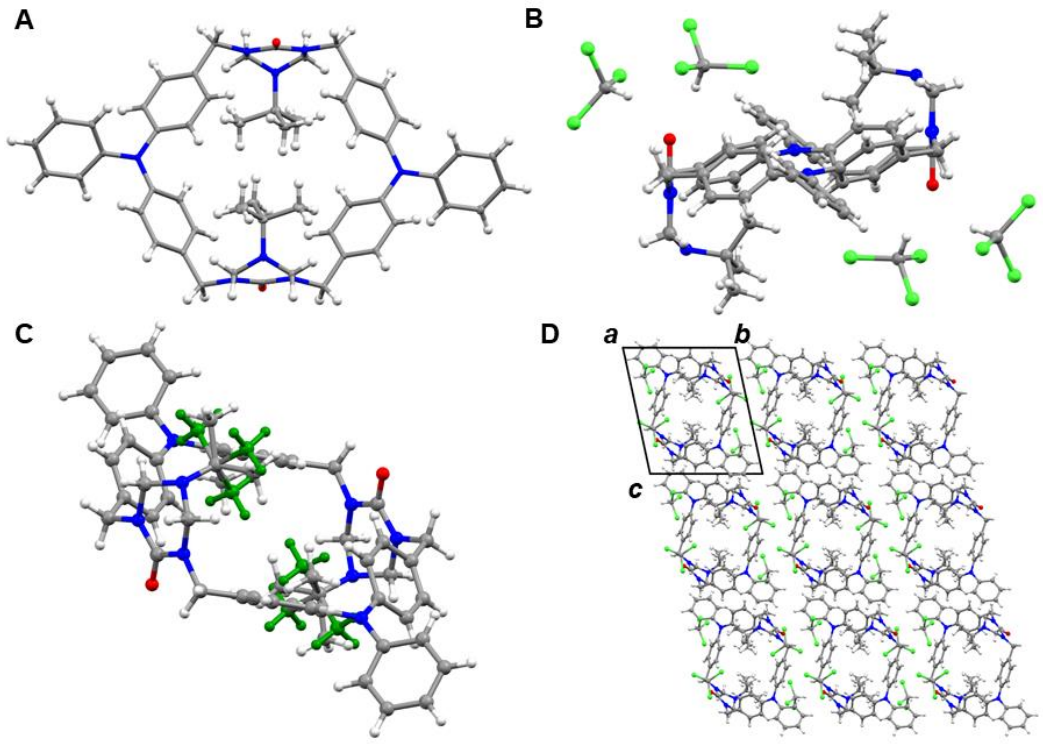

Figure S13. Crystal views of (protected macrocycle **1**)·$(CHCl_3)_4$. (A) Molecular structure of protected macrocycle **1** (disorder omitted for clarity). Thermal ellipsoids were drawn at the 30% probability level. (B) One unit cell (disorder omitted for clarity). (C) View showing disorder in the *tert*-butyl groups. The major component population fraction (non-green) was 0.697(6). (D) Crystal packing along the *a* axis.

X-ray intensity data from a colorless block were collected at 100(2) K using a Bruker D8 QUEST diffractometer equipped with a PHOTON-100 CMOS area detector and an Incoatec microfocus source (Mo Kα radiation, λ = 0.71073 Å). The raw area detector data frames were reduced and corrected for absorption effects using the Bruker APEX3, SAINT+ and SADABS programs.[11,12] Final unit cell parameters were determined by least-squares refinement of 9923 reflections taken from the data set. The structure was solved with SHELXT.[13,14] Subsequent difference Fourier calculations and full-matrix least-squares refinement against F^2 were performed with SHELXL-2018[13,14] using OLEX2.[15]

The compound crystallizes in the triclinic system. The space group *P*-1 (No. 2) was confirmed by structure solution. The asymmetric unit consists of half of one $C_{54}H_{60}N_8O_2$ molecule located on a crystallographic inversion center and two independent chloroform molecules. The unique *tert*-butyl

substituent of the $C_{54}H_{60}N_8O_2$ molecule is rotationally disordered over two orientations. The major component population fraction is 0.697(6). C-C distances in the disordered *t*-butyl groups were restrained to be similar to one another (SHELX SADI). All non-hydrogen atoms were refined with anisotropic displacement parameters. Hydrogen atoms bonded to carbon were before being placed in geometrically idealized positions and included as riding atoms with *d*(C-H) = 1.00 Å and *U*iso(H) = 1.2*U*eq(C) for methine hydrogen atoms, *d*(C-H) = 0.95 Å and *U*iso(H) = 1.2*U*eq(C) for aromatic hydrogen atoms, *d*(C-H) = 0.99 Å and *U*iso(H) = 1.2*U*eq(C) for methylene hydrogen atoms, and *d*(C-H) = 0.98 Å and *U*iso(H) = 1.5*U*eq(C) for methyl hydrogens. The methyl hydrogens were allowed to rotate as a rigid group to the orientation of maximum observed electron density. The largest residual electron density peak in the final difference map is 1.06 $e^-/Å^3$, located 0.99 Å from Cl6.

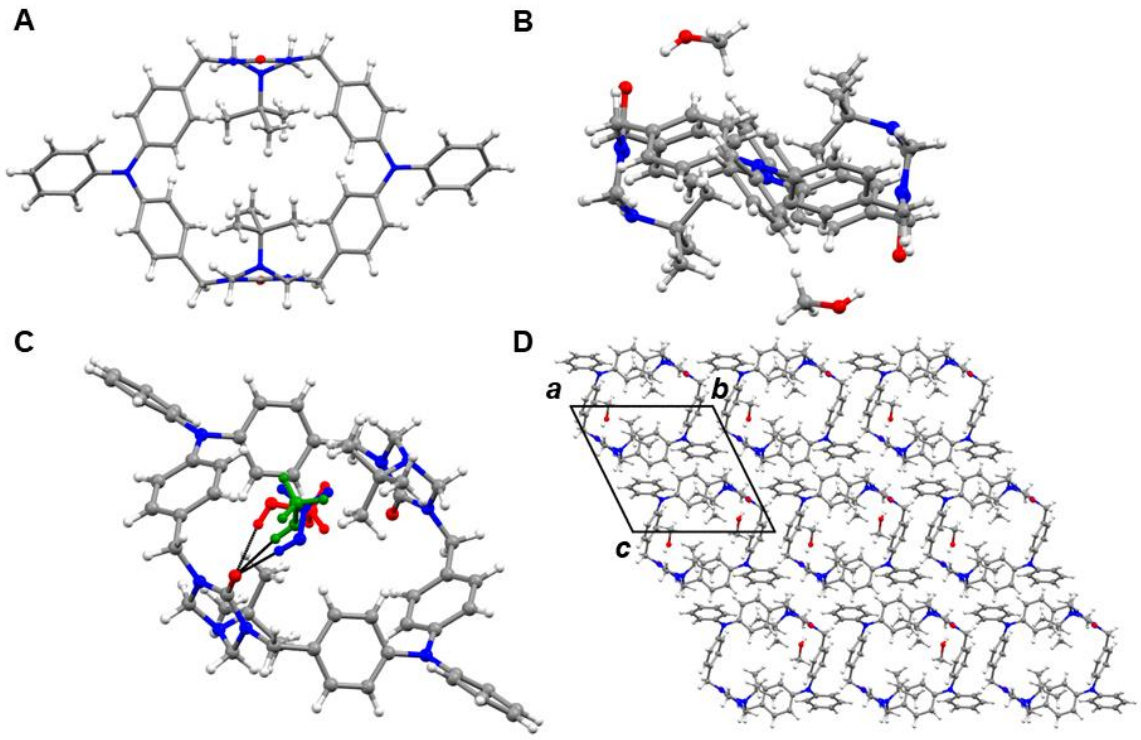

Figure S14. Crystal views of (protected macrocycle **1**)·$(MeOH)_2$. (A) Molecular structure of protected macrocycle **1**. Thermal ellipsoids were drawn at the 30% probability level. (B) One formula unit (disorder omitted for clarity). (C) View showing disorder in the methanol solvate. Hydrogen bonds are shown in black. (D) Crystal packing along the *a* axis (disorder omitted for clarity).

X-ray intensity data from an irregular colorless block were collected at 100(2) K using a Bruker D8 QUEST diffractometer equipped with a PHOTON-100 CMOS area detector and an Incoatec microfocus source (Mo Kα radiation, λ = 0.71073 Å). The raw area detector data frames were reduced and corrected for absorption effects using the Bruker APEX3, SAINT+ and SADABS programs.[11,12] Final unit cell parameters were determined by least-squares refinement of 9916 reflections taken from the data set. The structure was solved with SHELXT.[13,14] Subsequent difference Fourier calculations and full-matrix least-squares refinement against F^2 were performed with SHELXL-2018[13,14] using OLEX2.[15]

The compound crystallizes in the triclinic system. The space group *P*-1 (No. 2) was confirmed by structure solution. The asymmetric unit consists of half of one $C_{54}H_{60}N_8O_2$ molecule and one methanol molecule. The $C_{54}H_{60}N_8O_2$ molecule is located on a crystallographic inversion center. The methanol

molecule is positionally disordered and was modeled using three components. Total component occupancy was constrained to sum to one, and refined to O1S/O2S/O3S = 0.577(2)/0.346(2)/0.077(2). Methanol C-O distances were restrained to 1.45(2) Å. All non-hydrogen atoms were refined with anisotropic displacement parameters. Hydrogen atoms were placed in geometrically idealized positions and included as riding atoms with *d*(O-H) = 0.84 Å and *U*iso(H) = 1.5*U*eq(O) for hydrogen atoms bonded to oxygen, *d*(C-H) = 0.95 Å and *U*iso(H) = 1.2*U*eq(C) for aromatic hydrogen atoms, *d*(C-H) = 0.99 Å and *U*iso(H) = 1.2*U*eq(C) for methylene hydrogen atoms, and *d*(C-H) = 0.98 Å and *U*iso(H) = 1.5*U*eq(C) for methyl hydrogens. The methyl hydrogens were allowed to rotate as a rigid group to the orientation of maximum observed electron density. The largest residual electron density peak in the final difference map is 0.27 $e^{-}/Å^{3}$, located 0.70 Å from N4.

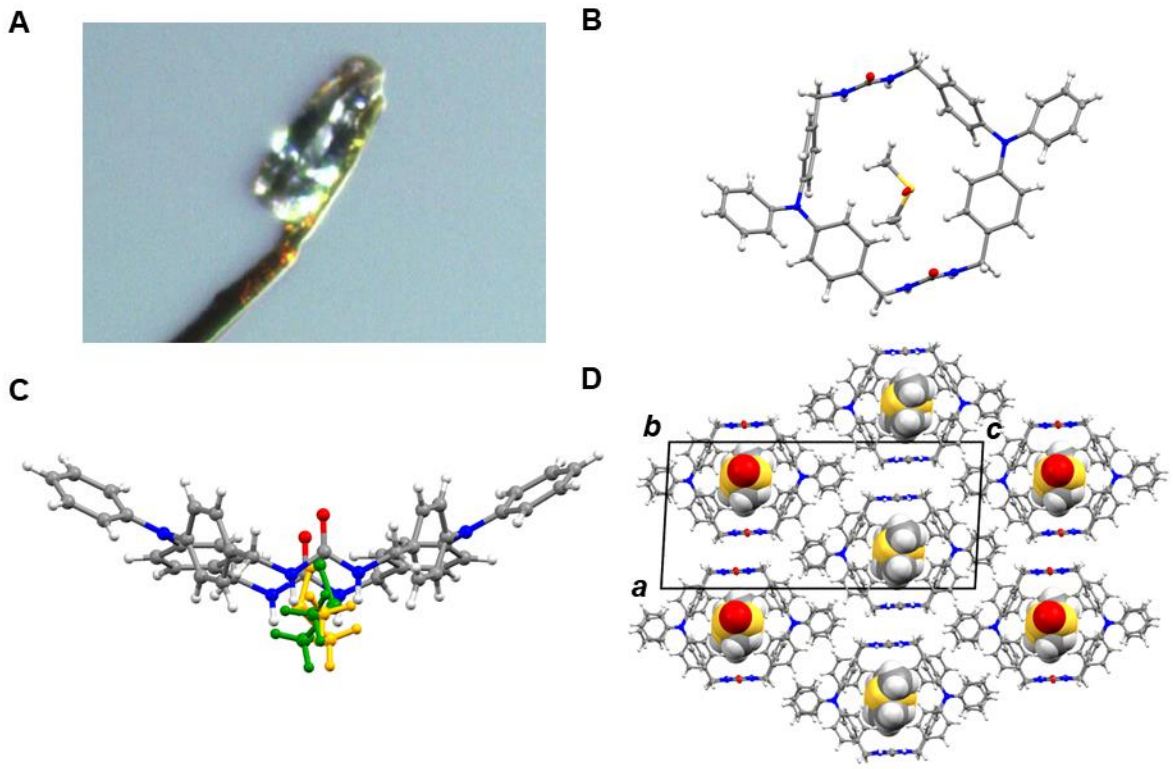

Figure S15. Crystal views of **1**·DMSO. (A) Data crystal. (B) Components of structure. Thermal ellipsoids were drawn at the 30% probability level. (C) View of DMSO disorder inside macrocycle **1**. (D) Crystal packing along the *b* axis (disorder omitted for clarity).

Crystals formed as colorless multifaceted rods. Several crystals examined, intact or cleaved and of various sizes, persistently gave doubled or split diffraction spots, along with difficulty in indexing the diffraction pattern to a reasonable unit cell. Eventually crystals of the material were determined to be twinned by non-merohedry. Using the Bruker Cell_Now program,[16] reflections from a set of 199 from the data crystal could be indexed entirely to two domains with the reported primitive monoclinic unit cell parameters. The derived twin law, relating indices of one domain to those of the other, is (-1 0 0 / 0 -1 0 / -0.24 0 -1). The twin law corresponds to a 180° rotation about the real-space [100] axis. X-ray intensity data were collected at 100(2) K using a Bruker D8 QUEST diffractometer equipped with a PHOTON 100 CMOS area detector and an Incoatec microfocus source (Mo Kα radiation, λ = 0.71073 Å). The raw area detector data frames were reduced and corrected for absorption effects using the SAINT+

and TWINABS programs.[16] TWINABS also constructed SHELX HKLF-4 and HKLF-5 format reflection files for solution and refinement, respectively. Final unit cell parameters were determined by least-squares refinement of 9957 reflections in the range 5.136° < 2θ < 48.445° taken from both twin domains of the crystal. The structure was solved by dual-space methods with SHELXT.[13,14] Subsequent difference Fourier calculations and full-matrix least-squares refinement against F^2 were done with SHELXL-2018[13,14] using OLEX2.[15] The major twin domain volume fraction refined to 0.520(1).

The compound crystallizes in the space group $P2_1/n$ of the monoclinic system. The asymmetric unit consists of one $C_{42}H_{38}N_6O_2$ molecular cycle and one DMSO molecule. The DMSO molecule is disordered over two closely spaced orientations with a major component occupancy of 0.516(4). The total DMSO occupancy was constrained to sum to one. Appropriate S-O and S-C distance restraints were applied. All non-hydrogen atoms were refined with anisotropic displacement parameters. Hydrogen atoms were located in Fourier difference maps before being placed in geometrically idealized positions and included as riding atoms with *d*(C-H) = 0.95 Å and *U*iso(H) = 1.2*U*eq(C) for aromatic hydrogen atoms, *d*(C-H) = 0.99 Å and *U*iso(H) = 1.2*U*eq(C) for methylene hydrogens and *d*(C-H) = 0.98 Å and *U*iso(H) = 1.5*U*eq(C) for methyl hydrogens. The methyl hydrogens were allowed to rotate as a rigid group to the orientation of maximum observed electron density. Hydrogen atoms bonded to urea nitrogen atoms were included with *d*(N-H) = 0.90 Å and *U*iso(H) = 1.2*U*eq(N). The largest residual electron density peak in the final difference map is 0.31 $e^-/Å^3$, located 1.11 Å from N4.

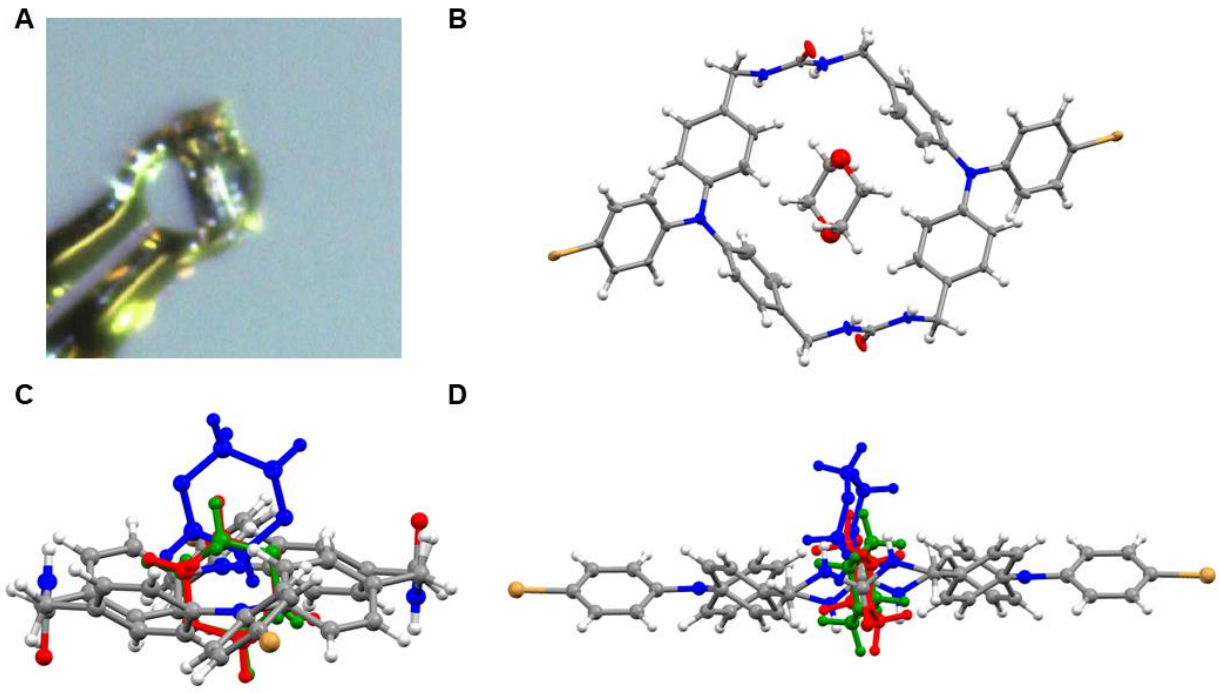

Figure S16. Crystal views of **1a**·1,4-dioxanes. (A) Data crystal. (B) Components of structure. Thermal ellipsoids were drawn at the 30% probability level. (C) View of 1,4-dioxanes disorder inside macrocycle **1a**. (D) Another view of the disorder.

X-ray intensity data from a colorless needle were collected at 100(2) K using a Bruker D8 QUEST diffractometer equipped with a PHOTON-100 CMOS area detector and an Incoatec microfocus source (Mo Kα radiation, λ = 0.71073 Å). The raw area detector data frames were reduced and corrected for absorption effects using the Bruker APEX3, SAINT+ and SADABS programs.[17,12] The structure was solved with SHELXT.[13,14] Subsequent difference Fourier calculations and full-matrix least-squares refinement against F^2 were performed with SHELXL-2018[13,14] using OLEX2.[15]

The compound crystallizes in the space group $P2_1/c$ of the monoclinic system. The asymmetric unit consists of half of one $C_{42}H_{36}Br_2N_6O_2$ cycle located on a crystallographic inversion center and several electron density peaks inside the tubular channels created by the cycle columns. The residual difference electron density in the channel region is disordered but arranged in a tapelike fashion along the crystallographic *b* axis direction. If assigned as carbon atoms, all peaks refined to significantly less than

full occupancy. The peaks could be reasonably fitted to half each (two carbon atoms and one oxygen atom) of three crystallographically independent dioxane molecules, all located on crystallographic inversion centers. For the disorder model, all 1,2- and 1,3- and 1,4- C-C and C-O distances in the dioxane guests were restrained to appropriate values. Occupancies of the three components refined to O1S-C2S = 0.22(1), O2S-C4S = 0. 23(1) and O3S-C6S = 0.13(1), generating a dioxane composition per cycle of 0.58(2). All non-hydrogen atoms were refined with anisotropic displacement parameters except for atoms of the disordered dioxane guests, which were refined isotropically. Components O2S-C4S and O3S-C6S were each assigned a separate common isotropic displacement parameter. Hydrogen atoms bonded to carbon were placed in geometrically idealized positions and included as riding atoms with *d*(C-H) = 0.95 Å and *U*iso(H) = 1.2*U*eq(C) for aromatic hydrogen atoms and *d*(C-H) = 0.99 Å and *U*iso(H) = 1.2*U*eq(C) for methylene hydrogen atoms. The two urea hydrogen atoms were located and refined with *d*(N-H) = 0.85(2) Å distance restraints and a common isotropic displacement parameter. The largest residual electron density peak in the final difference map is 0.53 $e^-/Å^3$, located 0.85 Å from C5S.

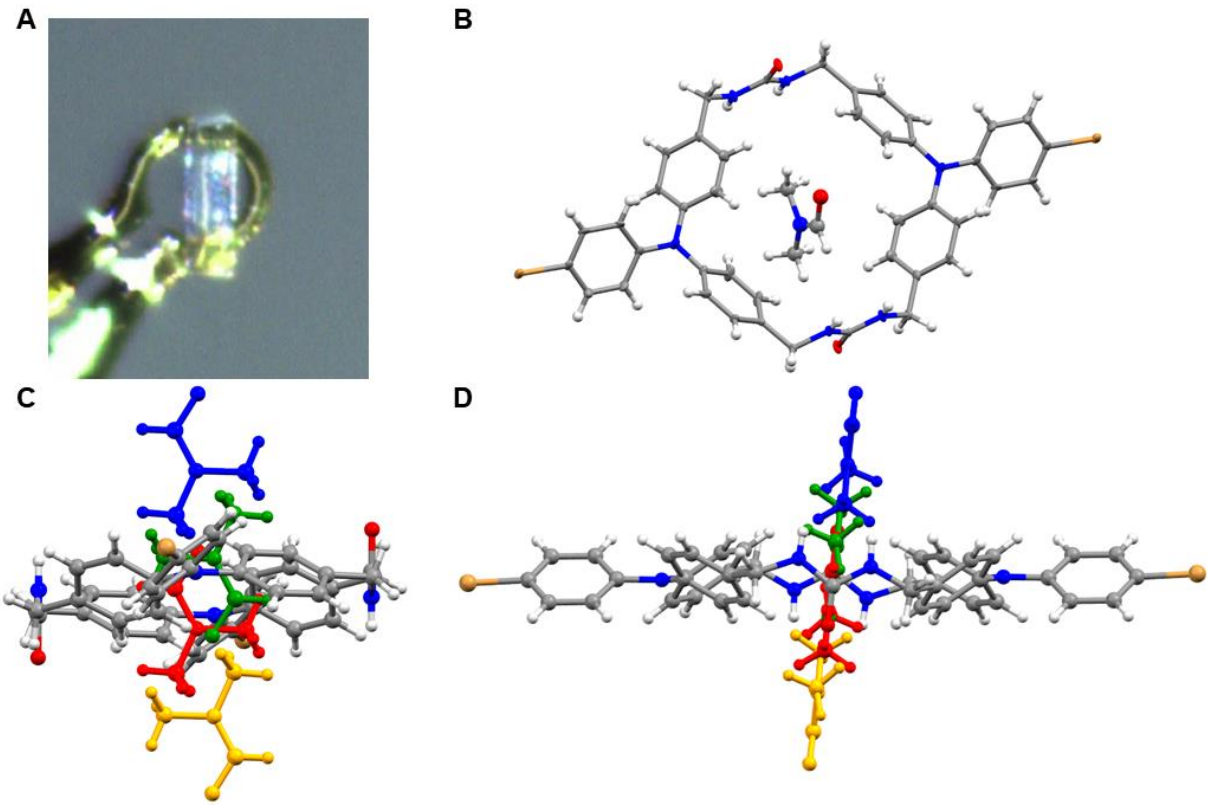

Figure S17. Crystal views of **1a**·$(DMF)_{0.65}$. (A) Data crystal. (B) Components of structure. Thermal ellipsoids were drawn at the 30% probability level. (C) View of DMF disorder inside macrocycle **1a**. (D) Another view of the disorder.

X-ray intensity data from colorless needle were collected at 100(2) K using a Bruker D8 QUEST diffractometer equipped with a PHOTON-100 CMOS area detector and an Incoatec microfocus source (Mo Kα radiation, λ = 0.71073 Å). The raw area detector data frames were reduced and corrected for absorption effects using the Bruker APEX3, SAINT+ and SADABS programs.[17,12] The structure was solved with SHELXT.[13,14] Subsequent difference Fourier calculations and full-matrix least-squares refinement against F^2 were performed with SHELXL-2018[13,14] using OLEX2.[15]

The compound crystallizes in the monoclinic system. The pattern of systematic absences in the intensity data was consistent with the space group $P2_1/c$, which was confirmed by structure solution. The asymmetric unit consists of half of one $C_{42}H_{36}Br_2N_6O_2$ cycle located on a crystallographic inversion center and several electron density peaks inside the tubular channels created by the cycle columns. The

residual difference electron density in the channel region is disordered, but arranged in a planar, tapelike fashion along the crystallographic *b* axis direction. If assigned as carbon atoms, all peaks refined to significantly less than full occupancy. The peaks could be reasonably fitted to one partially occupied, crystallographically independent DMF molecule, disordered across nearby crystallographic inversion centers. For the disorder model, 1,2-, 1,3- and 1,4- C-C, C-N and C-O distances of the DMF guest were restrained to appropriate values. The guest occupancy refined to 0.325(4), generating a DMF composition per cycle of 0.65(1). All non-hydrogen atoms were refined with anisotropic displacement parameters except for atoms of the disordered DMF guest, which were refined with a common isotropic displacement parameter. Hydrogen atoms bonded to carbon were placed in geometrically idealized positions and included as riding atoms with *d*(C-H) = 0.95 Å and *U*iso(H) = 1.2*U*eq(C) for aromatic hydrogen atoms, *d*(C-H) = 0.99 Å and *U*iso(H) = 1.2*U*eq(C) for methylene hydrogen atoms and *d*(C-H) = 0.98 Å and *U*iso(H) = 1.5*U*eq(C) for methyl hydrogen atoms. The two urea hydrogen atoms were located and refined with *d*(N-H) = 0.85(2) Å distance restraints and a common isotropic displacement parameter. The largest residual electron density peak in the final difference map is 0.76 $e^-/Å^3$, located 0.72 Å from N1S.

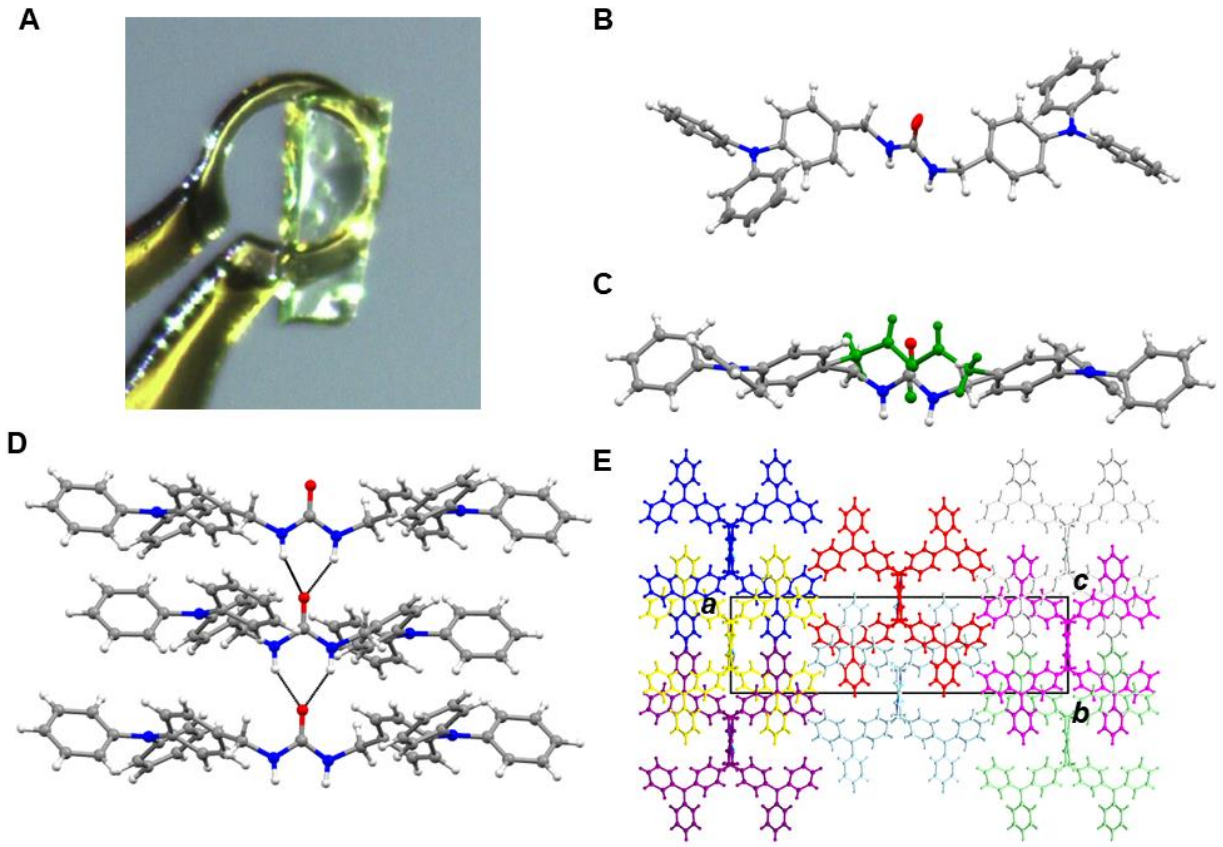

Figure S18. Crystal views of linear analog **2**. (A) Data crystal. (B) Molecular structure of linear analog **2**. Thermal ellipsoids were drawn at the 30% probability level. (C) View showing disorder in the methylene urea unit. Both units were found in equal populations resulting in (D) chains of hydrogen bonds going along either direction of the *c* axis. (E) Color coded crystal packing along the *c* axis.

X-ray intensity data from a pale-yellow needle were collected at 100(2) K using a Bruker D8 QUEST diffractometer equipped with a PHOTON-100 CMOS area detector and an Incoatec microfocus source (Mo Kα radiation, λ = 0.71073 Å). The raw area detector data frames were reduced and corrected for absorption effects using the Bruker APEX3, SAINT+ and SADABS programs.[17,12] The structure was solved with SHELXT.[13,14] Subsequent difference Fourier calculations and full-matrix least-squares refinement against F^2 were performed with SHELXL-2018[13,14] using OLEX2.[15]

The compound crystallizes in the orthorhombic system. The best solution was obtained in the centrosymmetric space group *Pbcn*. This space group was also indicated by the pattern of systematic

absences in the intensity data, which were uniquely consistent with *Pbcn*. The structure is disordered and required several distance and displacement parameter restraints to achieve a reasonable and stable refinement. In *Pbcn* there is half of one molecule in the asymmetric unit, located on a crystallographic inversion center. The central urea group (atoms O1, N1, N2, C1) is inconsistent with inversion symmetry and is thus disordered across the center. The disorder extends to the -CH_2- group (C2A/C2B) bonded to the urea. Occupancies of disordered atoms were fixed at 50%. The carbonyl C=O distance was restrained to 1.20(2) Å. Like C-C and C-N distances were restrained to similar values (SHELX SADI). A rigid-bond restraint (RIGU) was applied to atoms C1 and O1 for stability; these atoms are nearly superimposed with symmetry-equivalents. All non-hydrogen atoms were refined with anisotropic displacement parameters. Hydrogen atoms bonded to carbon were placed in geometrically idealized positions and included as riding atoms with *d*(C-H) = 0.95 Å and *U*iso(H) = 1.2*U*eq(C) for aromatic hydrogen atoms and *d*(C-H) = 0.99 Å and *U*iso(H) = 1.2*U*eq(C) for methylene hydrogen atoms. Hydrogen atoms bonded to the urea nitrogen atoms were also idealized with *d*(N-H) = 0.90 Å and *U*iso(H) = 1.2*U*eq(N). The largest residual electron density peak in the final difference map is 0.21 $e^-/Å^3$, located 1.49 Å from H12.

Similar disorder issues were observed in the acentric space group *Pca*2_1. In *Pca*2_1, the central -CH_2N(H)CON(H)CH_2- grouping is still disordered, though now over two pseudo-inversion related orientations. In addition, refinement instability was encountered because of strong correlations between inversion-related atoms of the triphenylamine substituent. Solution in monoclinic space groups gave similar results; *i.e*. the disorder is not resolved by lowering crystal symmetry. For these reasons, *Pbcn* was retained as the best description of the structure. The disorder encountered upon solution and refinement was foretold during the crystal screening process. Despite showing excellent extinctions in polarized light, all of several crystals examined from two separate crystallizations showed diffuse scattering, appearing as relatively faint streaks between strong Bragg diffraction peaks in the area

detector frames. This persisted regardless of crystal size and data collection temperature. Several trial specimens were cleaved as thin as mechanically possible to eliminate misaligned crystal domains (twinning) or other defects, and data frames were collected at room temperature and after flash-cooling to 100 K, but the diffuse streaking was still observed in all cases.

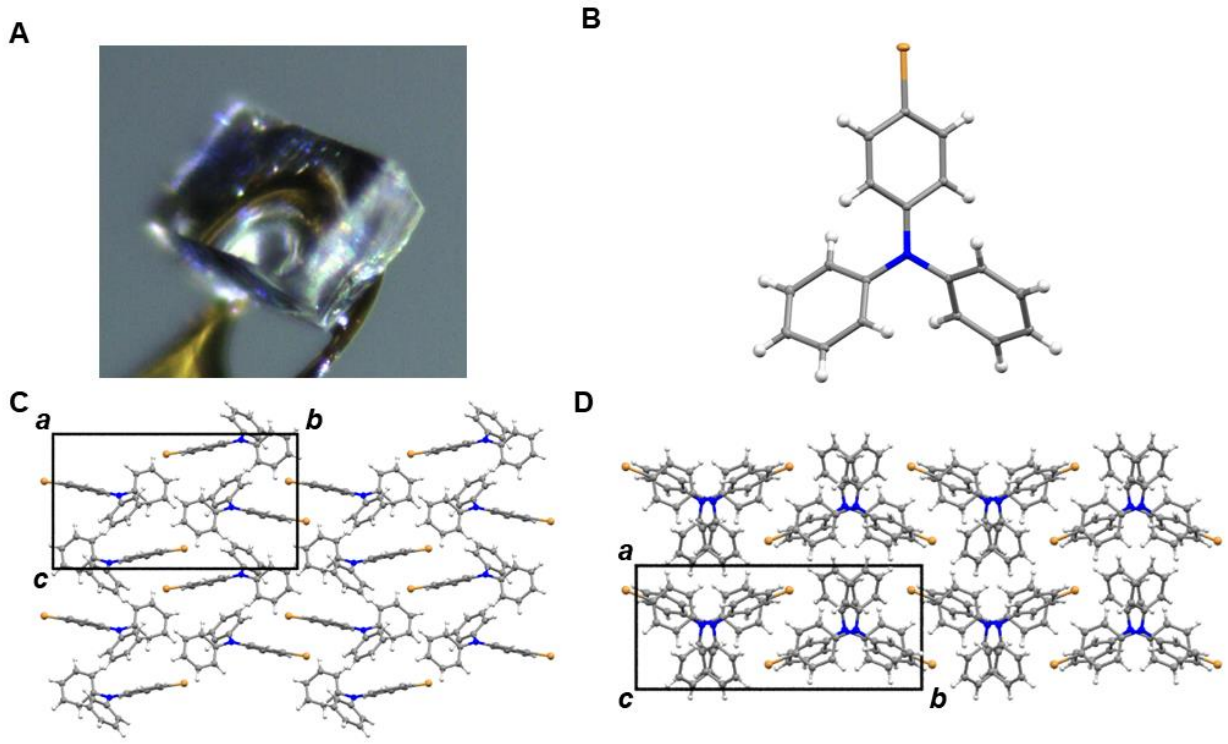

Figure S19. Crystal views of the monoclinic polymorph of TPA **3a**. (A) Data crystal. (B) Molecular structure of TPA **3a**. Thermal ellipsoids were drawn at the 30% probability level. (C) Crystal packing along the *a* axis. (D) Crystal packing along the *c* axis.

X-ray intensity data from a colorless block were collected at 100(2) K using a Bruker D8 QUEST diffractometer equipped with a PHOTON-100 CMOS area detector and an Incoatec microfocus source (Mo Kα radiation, λ = 0.71073 Å). The raw area detector data frames were reduced and corrected for absorption effects using the Bruker APEX3, SAINT+ and SADABS programs.[17,12] The structure was solved with SHELXT.[13,14] Subsequent difference Fourier calculations and full-matrix least-squares refinement against F^2 were performed with SHELXL-2018[13,14] using OLEX2.[15]

The compound crystallizes in the monoclinic system. The pattern of systematic absences in the intensity data was consistent with the space group $P2_1/c$, which was confirmed by structure solution. The asymmetric unit consists of one molecule. All non-hydrogen atoms were refined with anisotropic displacement parameters. Hydrogen atoms bonded to carbon were located in difference Fourier maps

before being placed in geometrically idealized positions and included as riding atoms with *d*(C-H) = 0.95 Å and *U*iso(H) = 1.2*U*eq(C). The largest residual electron density peak in the final difference map is 0.47 $e^-/Å^3$, located 0.68 Å from C18.

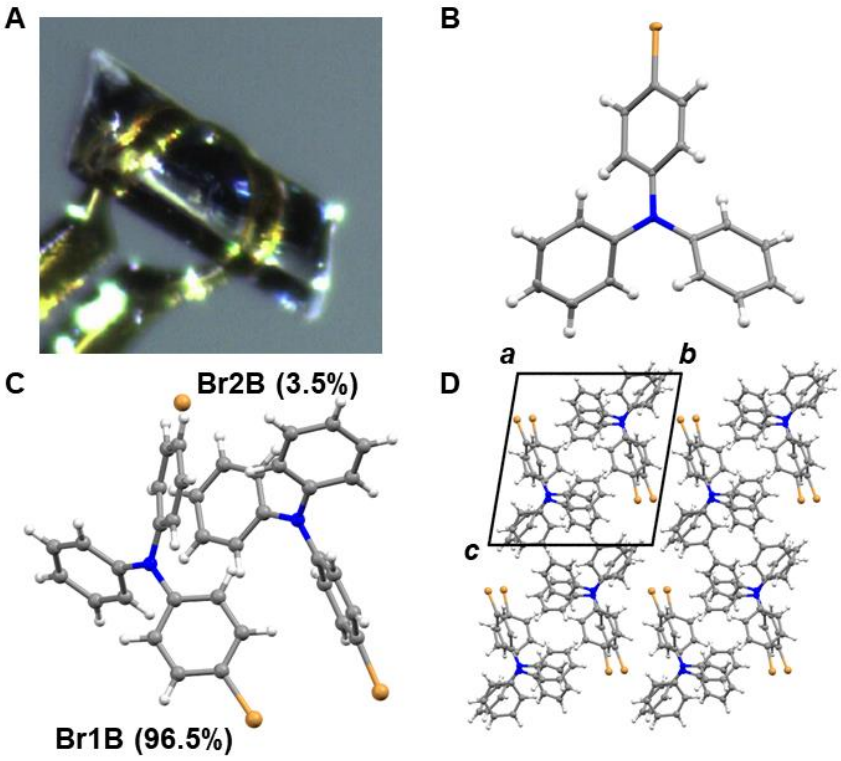

Figure S20. Crystal views of the triclinic polymorph of TPA **3a**. (A) Data crystal. (B) Molecular structure of TPA **3a**. Thermal ellipsoids were drawn at the 30% probability level. (C) Asymmetric unit of the crystal. Two crystallographically independent molecules were found. Br2B is a minor disorder component of molecule "B", with an occupancy of 3.5%. Only the Br atom of the minor component was modeled. (D) Crystal packing along the *a* axis (disorder omitted for clarity).

X-ray intensity data from a colorless needle were collected at 100(2) K using a Bruker D8 QUEST diffractometer equipped with a PHOTON-100 CMOS area detector and an Incoatec microfocus source (Mo Kα radiation, λ = 0.71073 Å). The raw area detector data frames were reduced and corrected for absorption effects using the Bruker APEX3, SAINT+ and SADABS programs.[17,12] The structure was solved with SHELXT.[13,14] Subsequent difference Fourier calculations and full-matrix least-squares refinement against F^2 were performed with SHELXL-2018[13,14] using OLEX2.[15]

The compound crystallizes in the triclinic system. The space group *P*-1 (No. 2) was confirmed by structure solution. The asymmetric unit consists of two crystallographically independent but chemically identical molecules, labeled identically except for atom label suffixes A or B. All non-hydrogen atoms

were refined with anisotropic displacement parameters. After normal location and anisotropic refinement of the two independent molecules, a single large residual electron density peak of magnitude +3.78 e-/Å was observed *ca*. 1.7 Å from C16B of molecule "B". The next largest peak was +1.35 e-/Å. The highest peak was interpreted as arising from the bromine atom of a minor disorder component of this molecule. Trial refinements of site occupancy parameters supported this assumption, as free refinement of the occupancies of the major bromine (Br1B) and the likely minor bromine peak (Br2B) resulted in occupancies of 0.965(1) and 0.035(1), respectively, summing to one bromine per molecule. Inspection of the packing shows this minor peak Br2B in the vicinity of a symmetry-equivalent Br1B, *i.e.* they are disordered together in a physically reasonable assembly (Br1B present, Br2B absent and *vice versa*). Omitting this single peak gave *R*1 = 0.044 / *wR*2 = 0.118 and the offending difference map. Instead of a whole-molecule model to account for 3% of one Br atom, Br2B was left isolated (with no minor component triphenylamine), and a fully occupied H atom refined on C16B. Additonally, no H atom was added to C4B, which would have an occupancy of 3% H. Hydrogen atoms were located in difference Fourier maps before being placed in geometrically idealized positions and included as riding atoms with *d*(C-H) = 0.95 Å and *U*iso(H) = 1.2*U*eq(C). The largest residual electron density peak in the final difference map is 1.38 $e^-/Å^3$, located 0.77 Å from Br1B.

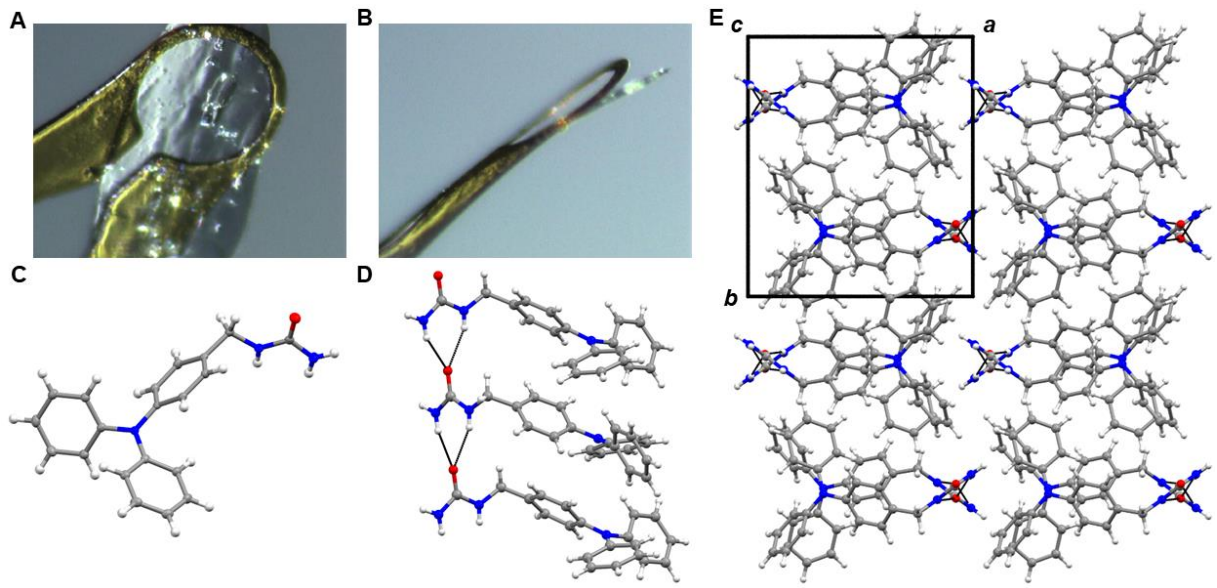

Figure S21. Crystal views of TPA **4**. (A) Data crystal. (B) Another view of the crystal. (C) Molecular structure of TPA **4**. Thermal ellipsoids were drawn at the 30% probability level. (D) Hydrogen bonding through the urea groups. Hydrogen bonds are shown in black. (E) Crystal packing along the *c* axis.

Crystals formed as thin colorless flakes with an irregular shape. Because of their extreme brittleness, several attempts were necessary to mount a suitably-sized plate without bending or breaking the crystal. It was necessary to use a crystal much larger than the X-ray beam in order to observe sufficient diffraction intensity and also to provide mechanical stability of the thin plate in the flowing cold stream. X-ray intensity data were collected at 100(2) K using a Bruker D8 QUEST diffractometer equipped with a PHOTON-100 CMOS area detector and an Incoatec microfocus source (Mo Kα radiation, λ = 0.71073 Å). The raw area detector data frames were reduced and corrected for absorption effects using the Bruker APEX3, SAINT+ and SADABS programs.[11,12] Final unit cell parameters were determined by least-squares refinement of 5698 reflections taken from the data set. The structure was solved with SHELXT.[13,14] Subsequent difference Fourier calculations and full-matrix least-squares refinement against F^2 were performed with SHELXL-2017[13,14] using OLEX2.[15]

The compound crystallizes in the monoclinic system. The pattern of systematic absences in the intensity data was consistent with the space group $P2_1/c$, which was verified by structure solution. The

asymmetric unit consists of one molecule. All non-hydrogen atoms were refined with anisotropic displacement parameters. Hydrogen atoms bonded to carbon were located in Fourier difference maps before being placed in geometrically idealized positions and included as riding atoms with *d*(C-H) = 0.95 Å and *U*iso(H) = 1.2*U*eq(C) for aromatic hydrogen atoms and *d*(C-H) = 0.99 Å and *U*iso(H) = 1.2*U*eq(C) for methylene hydrogen atoms. Hydrogen atoms bonded to nitrogen were located in difference maps and refined freely. The largest residual electron density peak in the final difference map is 0.29 $e^-/Å^3$, located 0.86 Å from C5.

Table S1. Data Collection and Refinement for Macrocycle **1** Related Compounds.

Identification Code	Dibromide 1	Protected 1·$(CHCl_3)_4$	Protected 1·$(MeOH)_2$	1·DMSO
CCDC	1961251	1961244	1961245	1961246
Empirical formula	$C_{20}H_{17}NBr_2$	$C_{58}H_{64}Cl_{12}N_8O_2$	$C_{56}H_{68}N_8O_4$	$C_{44}H_{44}N_6O_3S$
Formula weight	431.17	1330.57	917.18	736.91
Temperature/K	100(2)	100(2)	100(2)	100(2)
Crystal system	monoclinic	triclinic	triclinic	monoclinic
Space group	$P2_1/c$	P-1	P-1	$P2_1/n$
a/Å	8.1537(4)	10.0428(5)	9.4489(11)	13.2794(5)
b/Å	12.3944(6)	12.0048(7)	12.1817(13)	9.6773(4)
c/Å	17.4953(8)	13.6585(8)	12.3451(14)	28.5236(11)
α/deg	90	76.855(2)	63.821(4)	90
β/deg	102.0490(10)	83.018(2)	76.099(5)	93.197(2)
γ/deg	90	79.682(2)	87.623(5)	90
Volume/$Å^3$	1729.13(14)	1571.99(15)	1234.5(2)	3659.8(2)
Z	4	1	1	4
$\rho_{calc}g/cm^3$	1.656	1.406	1.234	1.337
μ/mm^{-1}	4.687	0.577	0.079	0.140
F(000)	856.0	688.0	492.0	1560.0
Crystal size/mm^3	0.18 × 0.16 × 0.06	0.52 × 0.46 × 0.36	0.56 × 0.48 × 0.42	0.2 × 0.08 × 0.06
Radiation	MoKα (λ = 0.71073)	MoKα (λ = 0.71073)	MoKα (λ = 0.71073)	MoKα (λ = 0.71073)
2Θ range for data collection/deg	4.762 to 52.324	4.942 to 56.63	4.454 to 56.718	4.446 to 48.592
Index ranges	-10 ≤ h ≤ 10, -15 ≤ k ≤ 15, -21 ≤ l ≤ 21	-13 ≤ h ≤ 13, -15 ≤ k ≤ 15, -18 ≤ l ≤ 18	-12 ≤ h ≤ 12, -16 ≤ k ≤ 16, -16 ≤ l ≤ 16	-15 ≤ h ≤ 15, 0 ≤ k ≤ 11, 0 ≤ l ≤ 33
Reflections collected	41775	61229	34422	9387
Independent reflections	3442 [R_{int} = 0.0481, R_{sigma} = 0.0251]	7782 [R_{int} = 0.0366, R_{sigma} = 0.0250]	6165 [R_{int} = 0.0432, R_{sigma} = 0.0373]	9387 [R_{int} = 0.0466, R_{sigma} = 0.0827]
Data/restraints/parameters	3442/0/208	7782/15/389	6165/4/343	9387/6/512
Goodness-of-fit on F^2	1.058	1.033	1.026	1.046
Final R indexes [I ≥ 2σ (I)]	R_1 = 0.0441, wR_2 = 0.1086	R_1 = 0.0460, wR_2 = 0.1227	R_1 = 0.0419, wR_2 = 0.0926	R_1 = 0.0629, wR_2 = 0.1259
Final R indexes [all data]	R_1 = 0.0579, wR_2 = 0.1146	R_1 = 0.0613, wR_2 = 0.1319	R_1 = 0.0664, wR_2 = 0.1026	R_1 = 0.1213, wR_2 = 0.1456
Largest diff. peak/hole / e $Å^{-3}$	2.45/-0.85	1.06/-0.68	0.27/-0.22	0.31/-0.30

Table S2. Data Collection and Refinement for Macrocycle **2** Related Compounds.

Identification Code	**1a·(1,4-dioxanes)$_{0.58}$**	**1a·(DMF)$_{0.65}$**
CCDC	1961243	1961242
Empirical formula	$C_{44.34}H_{40.66}Br_2N_6O_{3.17}$	$C_{43.95}H_{40.56}Br_2N_6.65O_{2.65}$
Formula weight	867.97	864.16
Temperature/K	100(2)	100(2)
Crystal system	monoclinic	monoclinic
Space group	$P2_1/c$	$P2_1/c$
a/Å	15.838(2)	15.8837(16)
b/Å	4.6056(6)	4.6117(5)
c/Å	26.637(3)	26.786(3)
α/deg	90	90
β/deg	99.746(3)	100.216(2)
γ/deg	90	90
Volume/Å^3	1915.0(4)	1931.0(3)
Z	2	2
ρ_{calc}g/cm^3	1.505	1.486
μ/mm^{-1}	2.168	2.149
F(000)	888.0	884.0
Crystal size/mm^3	0.12 × 0.05 × 0.02	0.16 × 0.06 × 0.04
Radiation	MoKα (λ = 0.71073)	MoKα (λ = 0.71073)
2Θ range for data collection/deg	4.38 to 50.364	4.382 to 50.082
Index ranges	-18 ≤ h ≤ 18, -5 ≤ k ≤ 5, -31 ≤ l ≤ 31	-18 ≤ h ≤ 18, -5 ≤ k ≤ 5, -31 ≤ l ≤ 31
Reflections collected	19443	17340
Independent reflections	3429 [R_{int} = 0.0470, R_{sigma} = 0.0291]	3413 [R_{int} = 0.0617, R_{sigma} = 0.0405]
Data/restraints/parameters	3429/35/277	3413/11/261
Goodness-of-fit on F^2	1.102	1.045
Final R indexes [I ≥ 2σ (I)]	R_1 = 0.0467, wR_2 = 0.0995	R_1 = 0.0470, wR_2 = 0.0971
Final R indexes [all data]	R_1 = 0.0617, wR_2 = 0.1079	R_1 = 0.0666, wR_2 = 0.1051
Largest diff. peak/hole / e Å^{-3}	0.53/-0.68	0.76/-0.56

Table S3. Data Collection and Refinement for Non-Macrocycle Related Compounds.

Identification Code	2	Triclinic Polymorph of 3a	Monoclinic Polymorph of 3a	4
CCDC	1961250	1961247	1961248	1961249
Empirical formula	$C_{39}H_{34}N_4O$	$C_{18}H_{14}BrN$	$C_{18}H_{14}NBr$	$C_{20}H_{19}N_3O$
Formula weight	574.70	324.21	324.21	317.38
Temperature/K	100(2)	100(2)	100(2)	100(2)
Crystal system	orthorhombic	triclinic	monoclinic	monoclinic
Space group	Pbcn	P-1	$P2_1/c$	$P2_1/c$
a/Å	35.075(2)	9.9285(5)	7.8591(5)	12.9146(18)
b/Å	9.9908(6)	12.2758(6)	18.1807(11)	13.9280(19)
c/Å	8.8263(6)	12.5370(6)	10.0050(6)	9.4512(13)
α/deg	90	98.954(2)	90	90
β/deg	90	90.731(2)	91.477(2)	110.841(4)
γ/deg	90	106.446(2)	90	90
Volume/Å^3	3093.0(3)	1445.03(12)	1429.08(15)	1588.8(4)
Z	4	4	4	4
ρ_{calc}g/cm^3	1.234	1.490	1.507	1.327
μ/mm^{-1}	0.075	2.833	2.865	0.084
F(000)	1216.0	656.0	656.0	672.0
Crystal size/mm^3	0.28 × 0.14 × 0.05	0.4 × 0.16 × 0.08	0.5 × 0.32 × 0.22	0.8 × 0.46 × 0.01
Radiation	MoKα (λ = 0.71073)	MoKα (λ = 0.71073)	MoKα (λ = 0.71073)	MoKα (λ = 0.71073)
2Θ range for data collection/deg	4.646 to 48.956	4.286 to 63.35	4.48 to 63.094	4.466 to 50.462
Index ranges	-40 ≤ h ≤ 40, -11 ≤ k ≤ 11, -10 ≤ l ≤ 10	-14 ≤ h ≤ 14, -18 ≤ k ≤ 18, -18 ≤ l ≤ 18	-11 ≤ h ≤ 11, -26 ≤ k ≤ 26, -14 ≤ l ≤ 14	-15 ≤ h ≤ 15, -15 ≤ k ≤ 16, -11 ≤ l ≤ 11
Reflections collected	41755	72155	36454	28771
Independent reflections	2541 [R_{int} = 0.0772, R_{sigma} = 0.0401]	9692 [R_{int} = 0.0341, R_{sigma} = 0.0200]	4785 [R_{int} = 0.0323, R_{sigma} = 0.0181]	2851 [R_{int} = 0.0786, R_{sigma} = 0.0433]
Data/restraints/parameters	2541/7/227	9692/0/367	4785/0/182	2851/0/230
Goodness-of-fit on F^2	1.125	1.086	1.018	1.017
Final R indexes [I ≥ 2σ (I)]	R_1 = 0.0639, wR_2 = 0.1422	R_1 = 0.0362, wR_2 = 0.0893	R_1 = 0.0245, wR_2 = 0.0604	R_1 = 0.0438, wR_2 = 0.0984
Final R indexes [all data]	R_1 = 0.0881, wR_2 = 0.1524	R_1 = 0.0430, wR_2 = 0.0922	R_1 = 0.0293, wR_2 = 0.0626	R_1 = 0.0761, wR_2 = 0.1120
Largest diff. peak/hole / e Å^{-3}	0.21/-0.17	1.38/-1.29	0.47/-0.51	0.29/-0.20

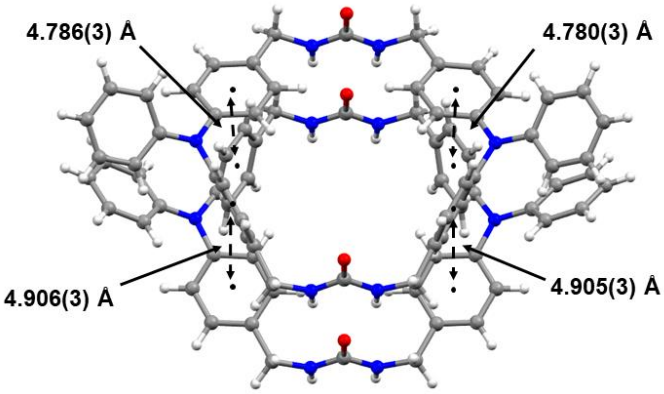

Figure S22. Crystal view of complex **1**·DMSO showing the edge-to-face π-stacking in-between macrocycles. Distances were measured from centroid to centroid of the phenyl rings. DMSO guests were removed for clarity.

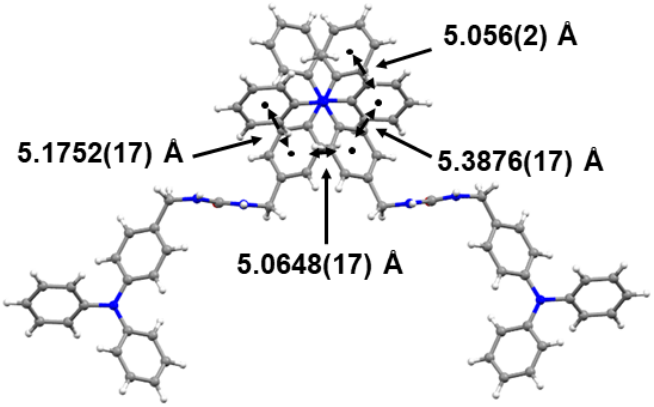

Figure S23. Crystal view of linear analog **2** showing the edge-to-face π-stacking in-between macrocycles. Distances were measured from centroid to centroid of the phenyl rings. Disorder in methylene urea bridge was removed for clarity.

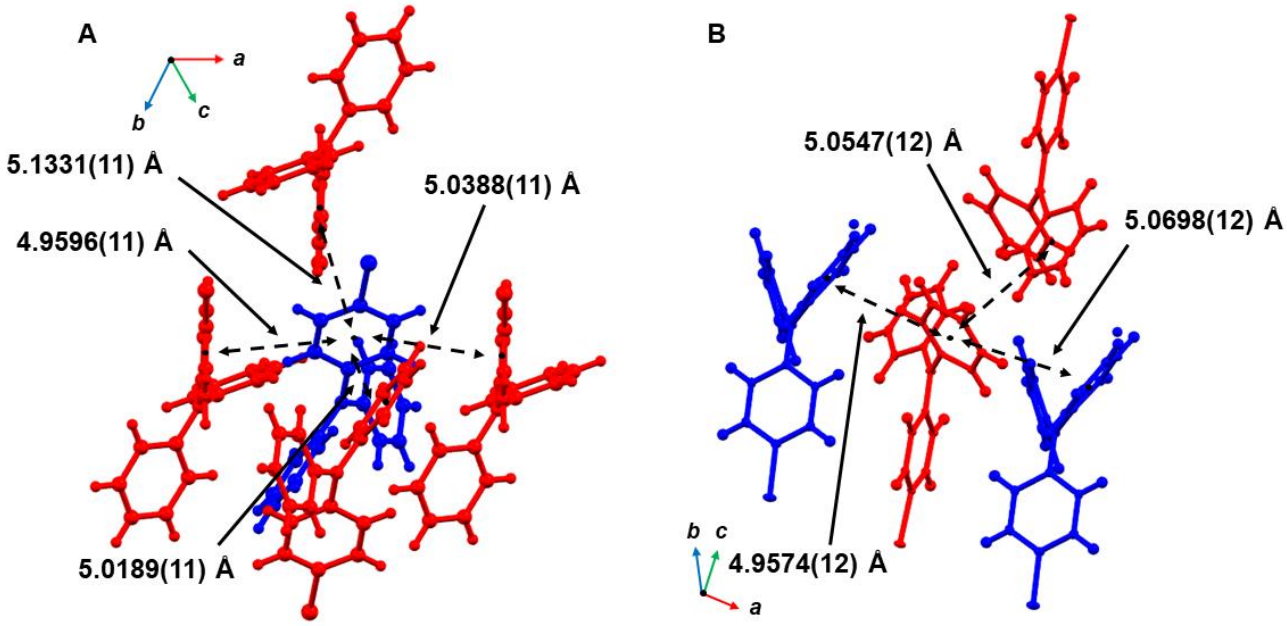

Figure S24. Crystal views of the triclinic polymorph of TPA **3a** showing the edge-to-face π-stacking in-between different TPA units. (A) and (B) show different views of this stacking. Distances were measured from centroid to centroid of the phenyl rings. Symmetry equivalent TPAs were colored either red or blue. Disorder was removed for clarity.

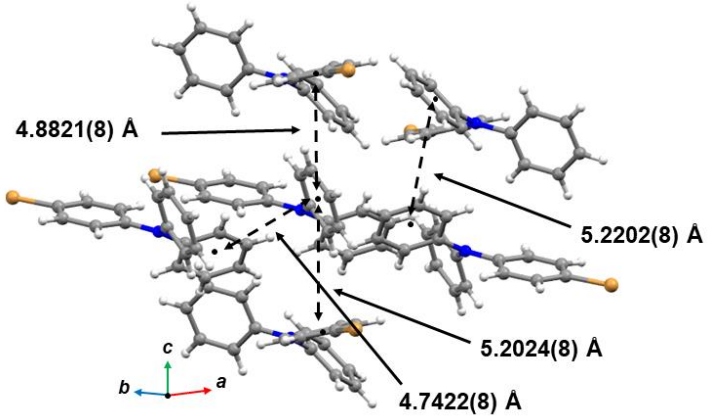

Figure S25. Crystal views of the monoclinic polymorph of TPA **3a** showing the edge-to-face π-stacking in-between different TPA units. Distances were measured from centroid to centroid of the phenyl rings.

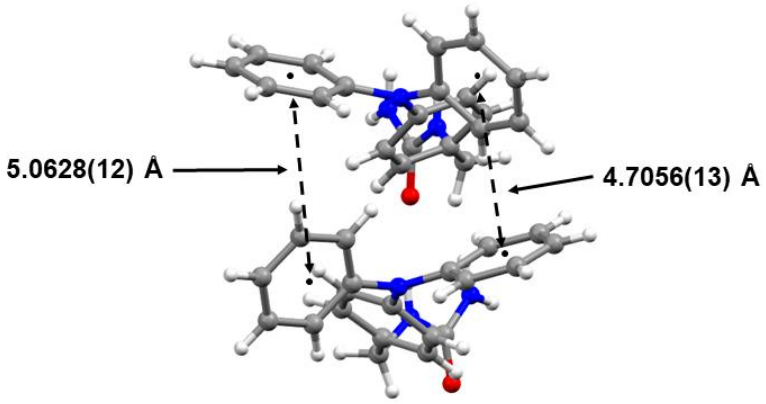

Figure S26. Crystal views of TPA **4** showing the edge-to-face π-stacking in-between different TPA units. Distances were measured from centroid to centroid of the phenyl rings.

Powder X-ray Diffraction (PXRD)

PXRD data was collected on a Rigaku D/Max-2100 powder X-ray diffractometer using Cu Kα radiation at room temperature. The step can covered an angular range of 5-50˚ 2Θ in steps of 0.02˚.

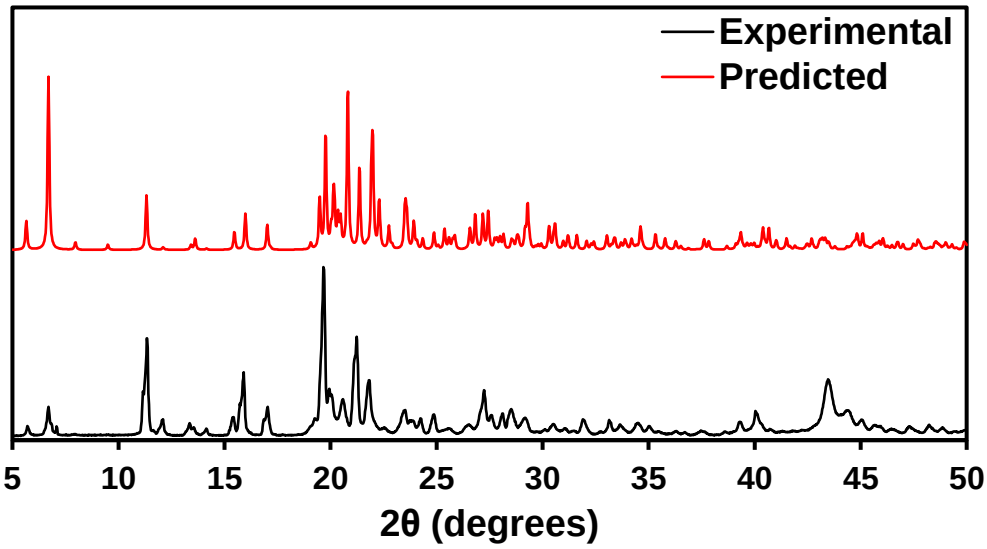

Figure S27. PXRD of the complex **1a**·DME.

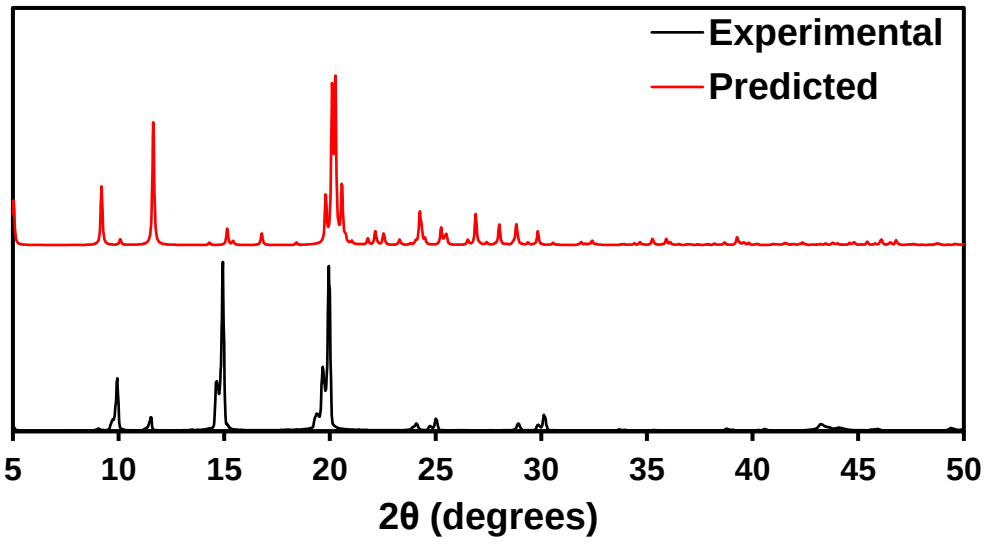

Figure S28. PXRD of linear analog **2**.

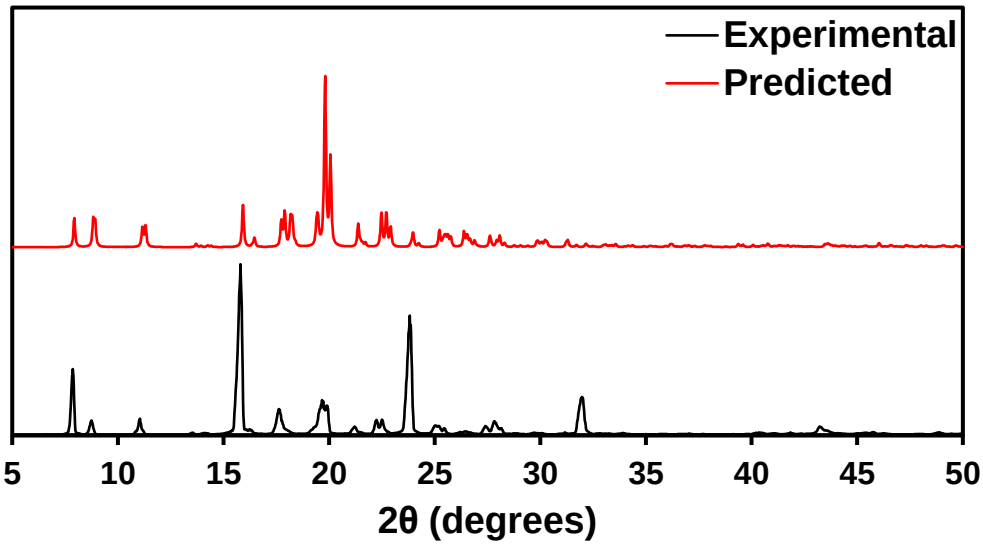

Figure S29. PXRD of TPA **3**.

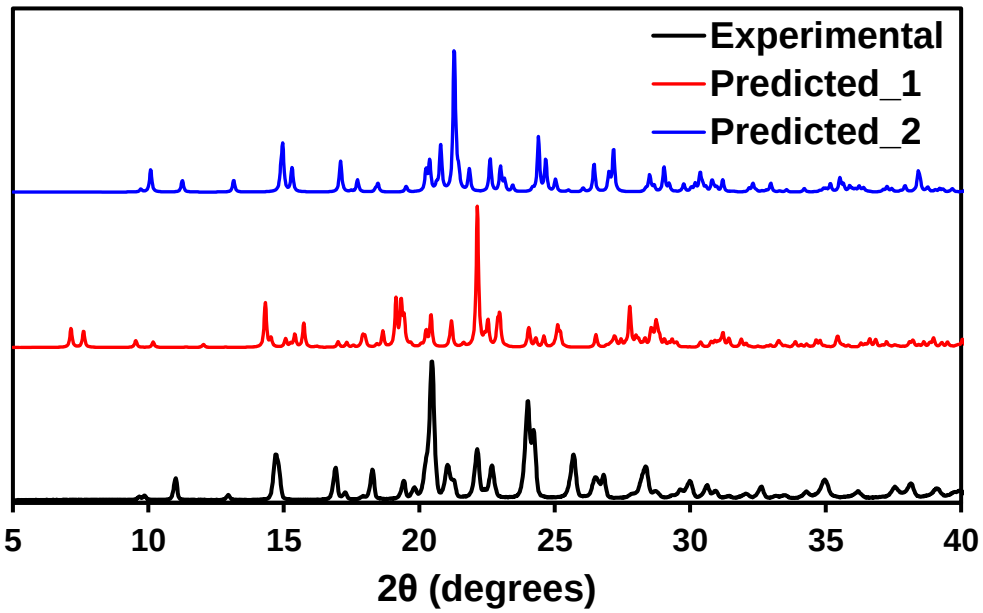

Figure S30. PXRD of TPA **3a**. Predicted_1 and Predicted_2 are the calculated patterns for the triclinic and monoclinic polymorphs, respectively.

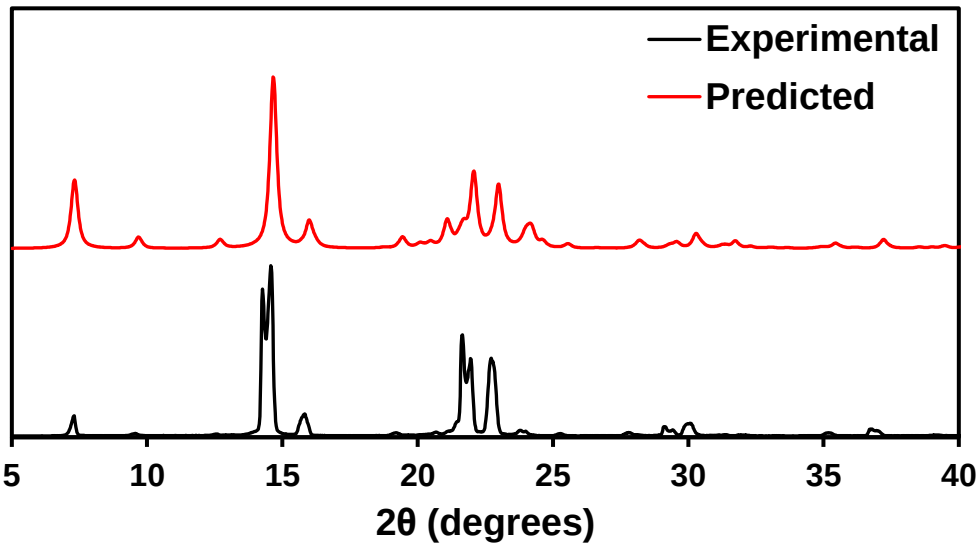

Figure S31. PXRD of TPA **4** with preferential orientation along the [100] direction and the full-width at a half-maximum of 0.3 2θ.

Thermal Gravimetric Analysis (TGA)

TGA was carried out using TA instruments SDT-Q600 simultaneous DTA/TGA at a rate of 4 ℃/min from 25-180 °C with a 5-minute isotherm before temperature increase and 15 minute isotherm afterwards.

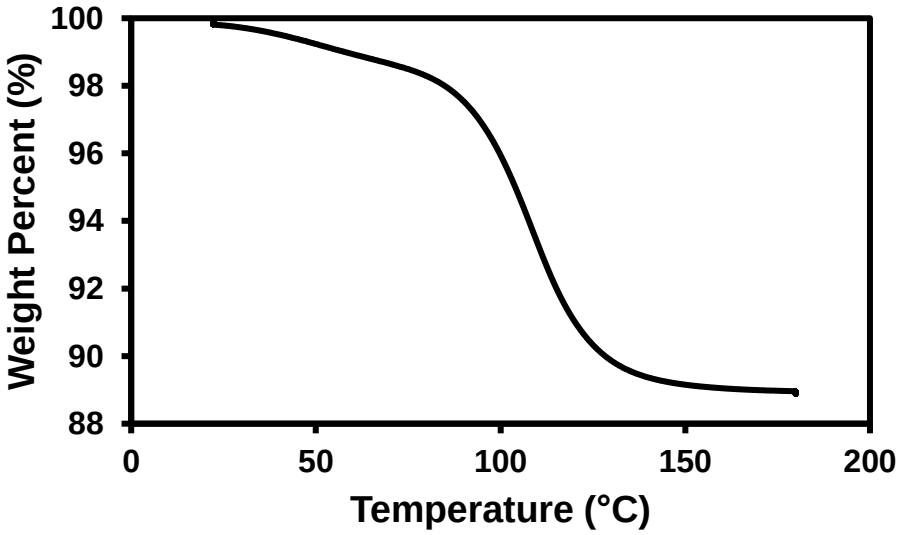

Figure S32. TGA graph showing a one-step desorption of DMSO from complex **1**·DMSO. Host-guest ratio was calculated to be 1:1.05.

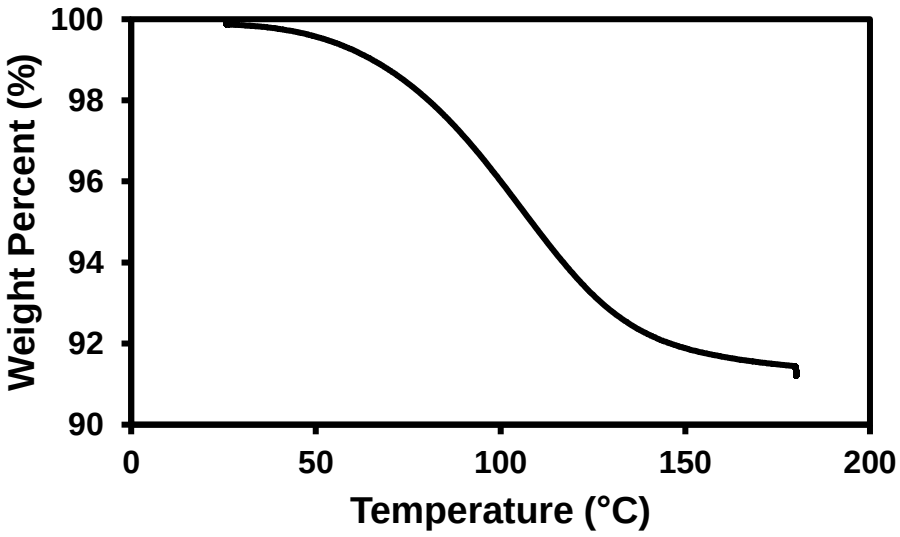

Figure S33. TGA graph showing a one-step desorption of C_6H_5Br from complex **1a**·C_6H_5Br after the radical regeneration studies. Host-guest ratio was calculated to be 1:0.50.

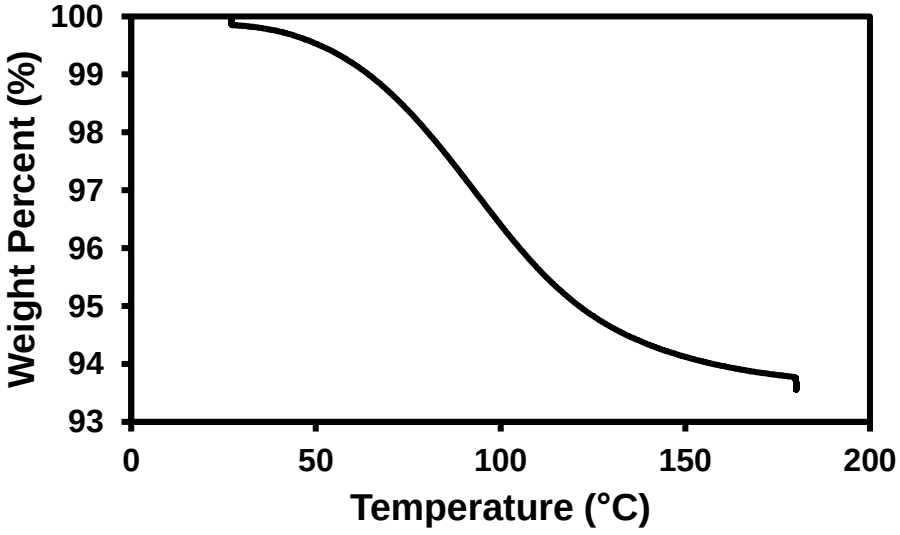

Figure S34. TGA graph showing a one-step desorption of C_6H_5Cl from complex **1a**·C_6H_5Cl after the radical regeneration studies. Host-guest ratio was calculated to be 1:0.51.

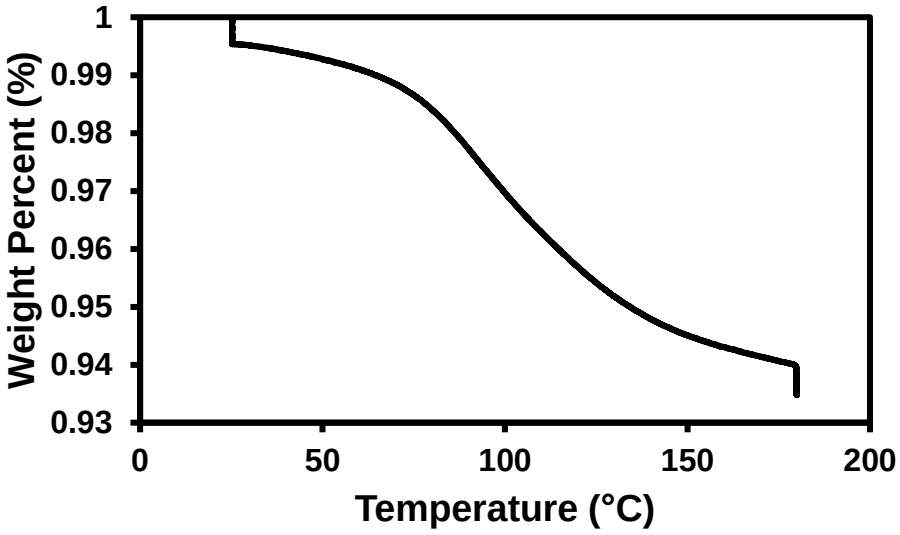

Figure S35. TGA graph showing a one-step desorption of DMF from complex **1a**·DMF after the radical regeneration studies. Host-guest ratio was calculated to be 1:0.78.

Diffuse Reflectance and Absorbance Measurements

UV/Vis data was collected on either a Perkin Elmer Lambda 35 UV/Vis spectrometer with UV Winlab software referenced to a TiO_2 reflection standard or a SoftMax M2 spectrometer (solid and solution, respectively). Spectra were recorded from either 330-600 nm (solid) or 270-550 nm (solution) at 1 nm steps. 10 μM concentrations were used for solution samples.

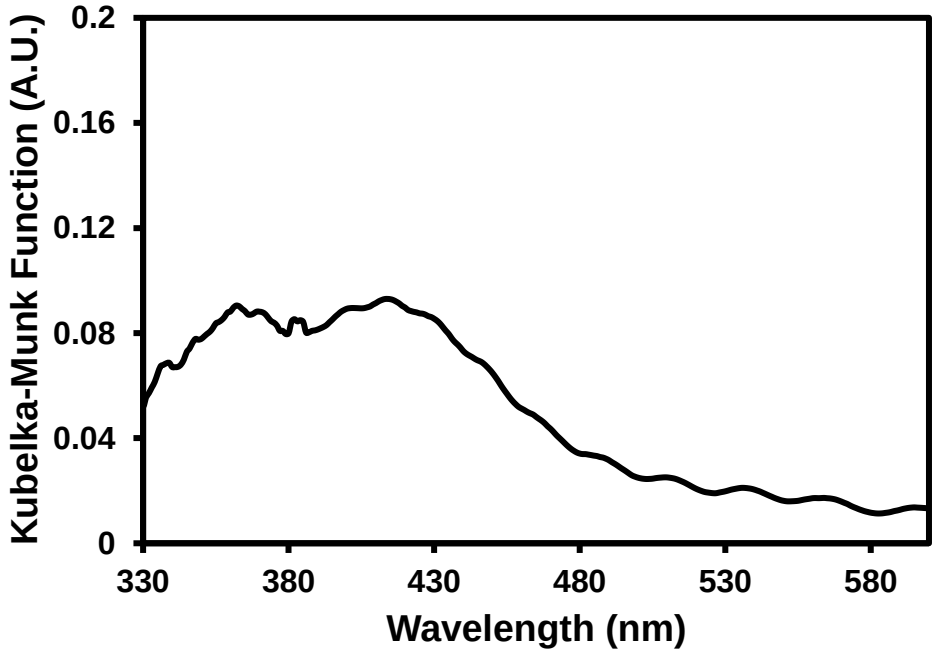

Figure S36. Diffuse reflection spectrum of activated **1** in the solid-state.

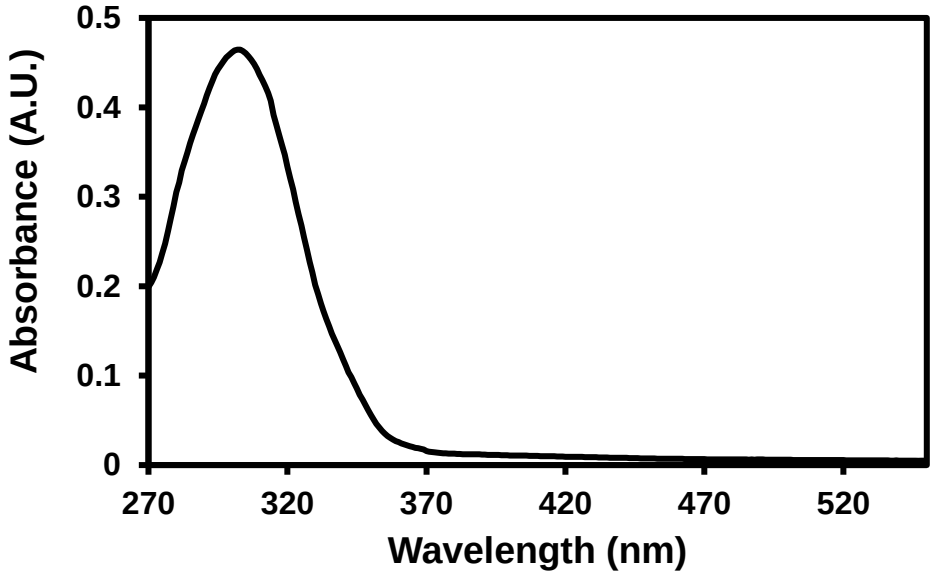

Figure S37. UV/Vis absorption spectrum of macrocycle **1a** in DMSO.

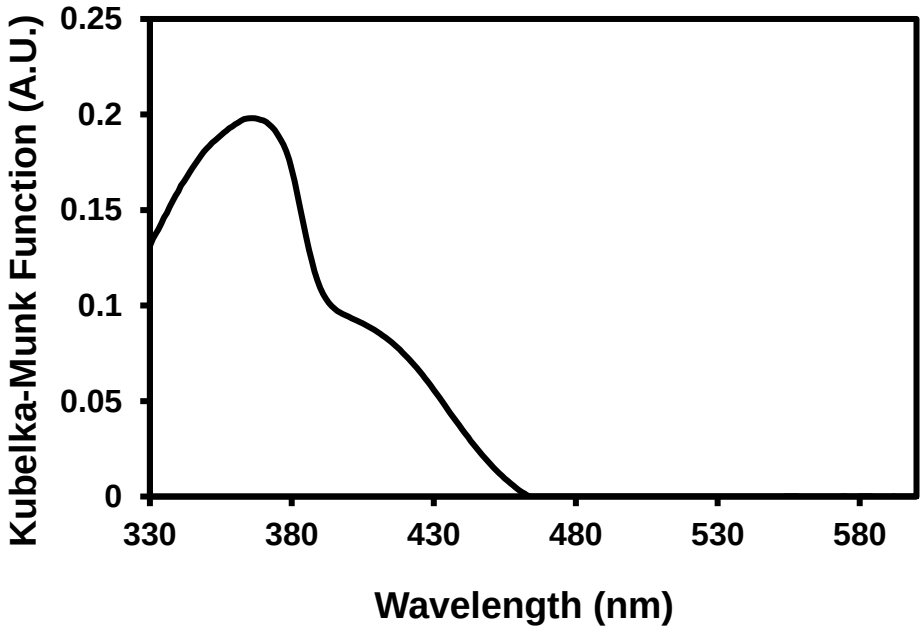

Figure S38. Diffuse reflection spectrum of activated **1a** in the solid-state.

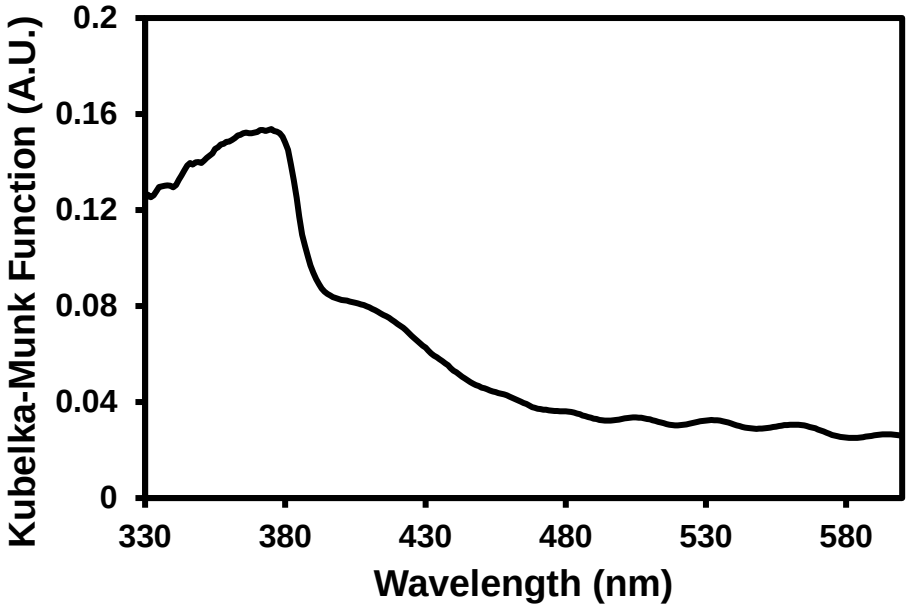

Figure S39. Diffuse reflection spectrum of complex **1a**·C_6H_6 in the solid-state.

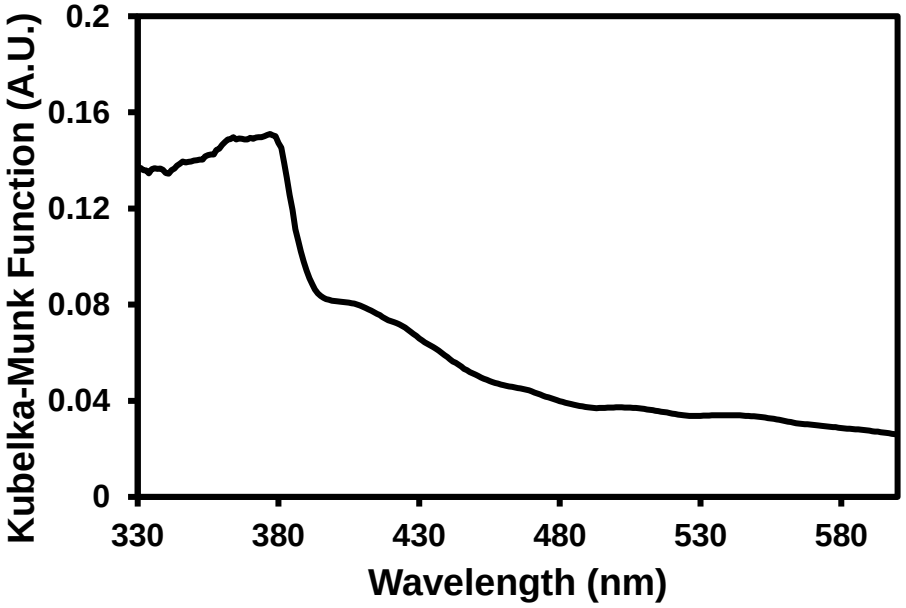

Figure S40. Diffuse reflection spectrum of complex **1a**·DME in the solid-state.

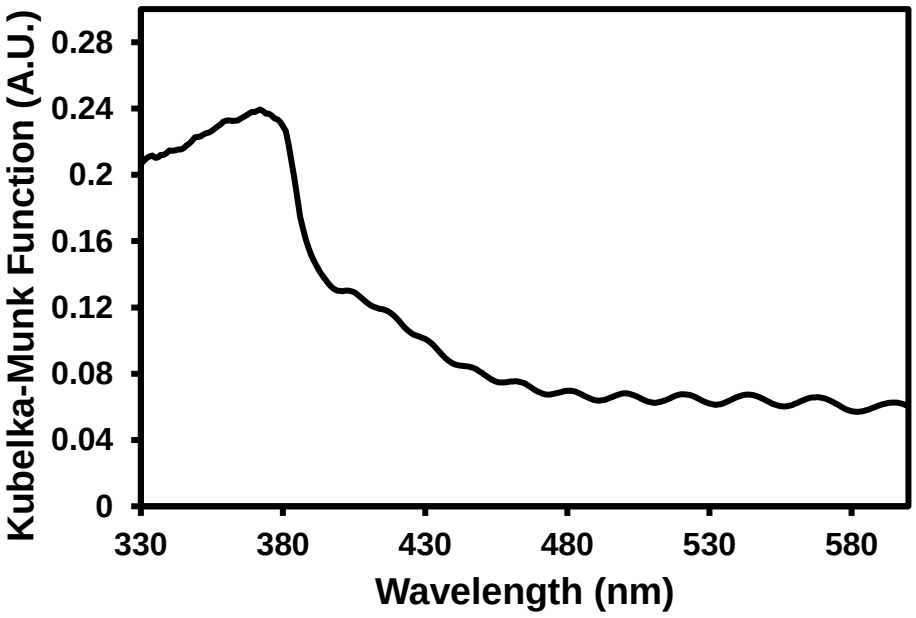

Figure S41. Diffuse reflection spectrum of complex **1a**·DMF in the solid-state.

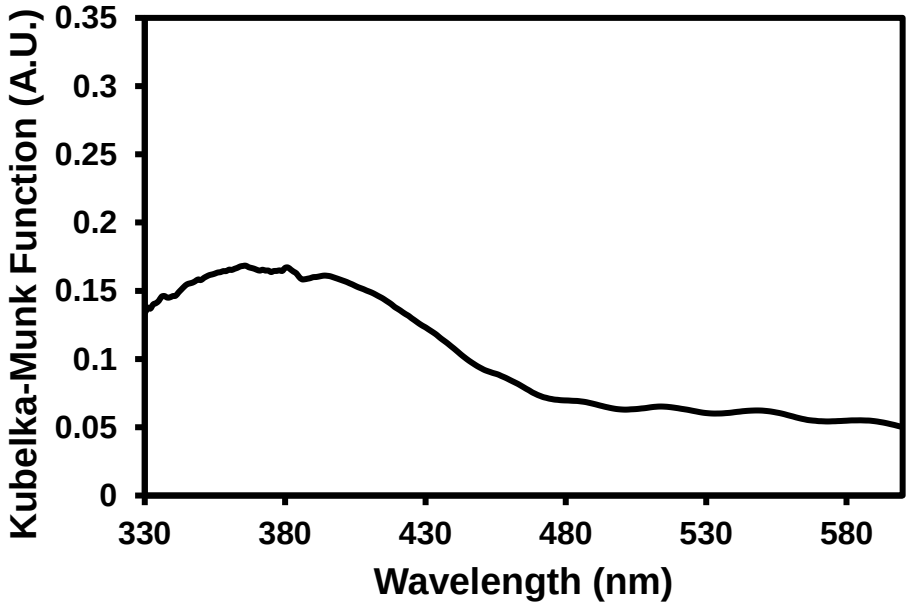

Figure S42. Diffuse reflection spectrum of linear analog **2** in the solid-state.

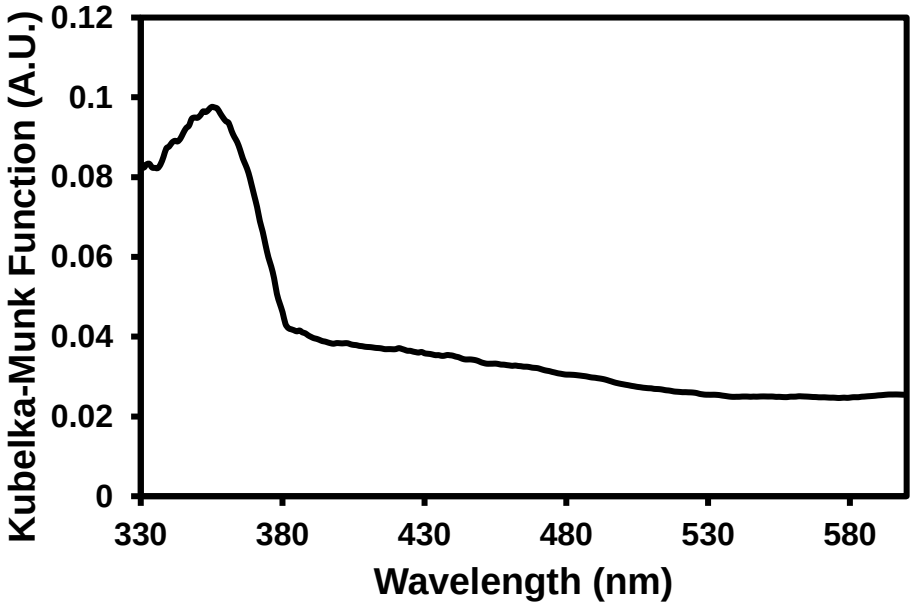

Figure S43. Diffuse reflection spectrum of TPA **3** in the solid-state.

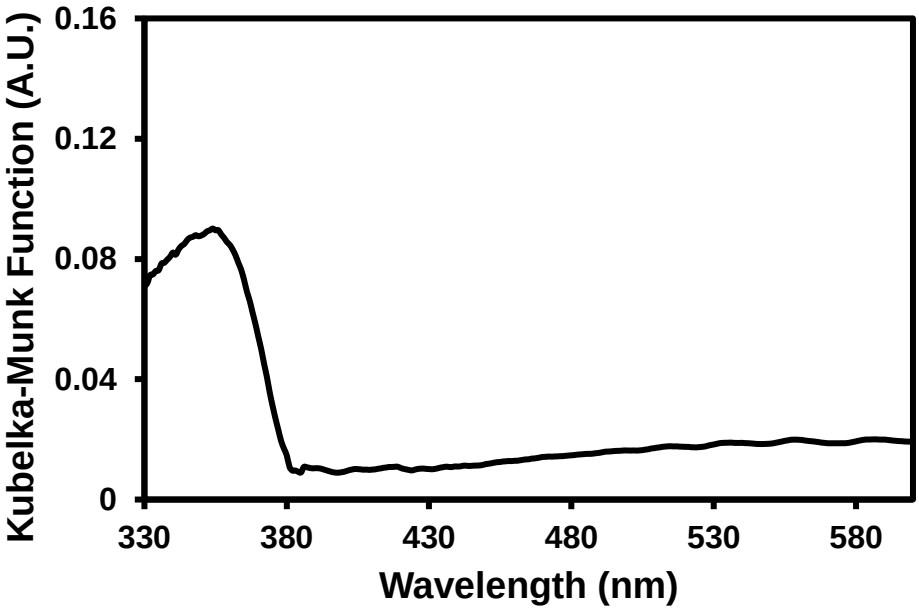

Figure S44. Diffuse reflection spectrum of TPA **3a** in the solid-state.

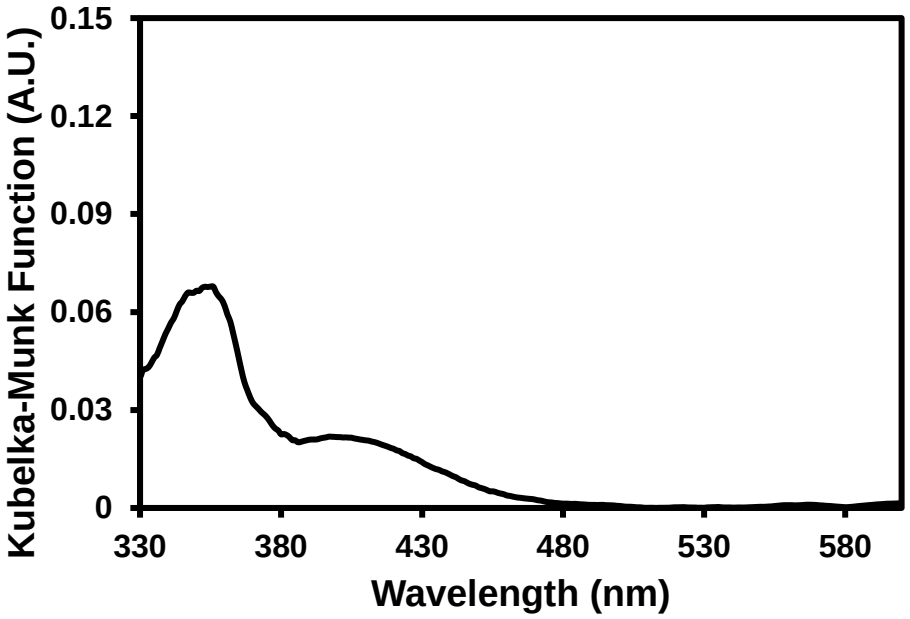

Figure S45. Diffuse reflection spectrum of TPA **4** in the solid-state.

Emission Measurements

Emission data was collected on an Edinburgh FS5 instrument equipped with a 150 W continuous wave xenon lamp source for excitation. Excitations were performed at the λ_{max} of absorbance. Spectra were gathered from 400-650 nm (solid) or 325-800 nm (solution) at 1 nm steps and are an average of three measurements. 10 µM concentrations were used for solution samples.

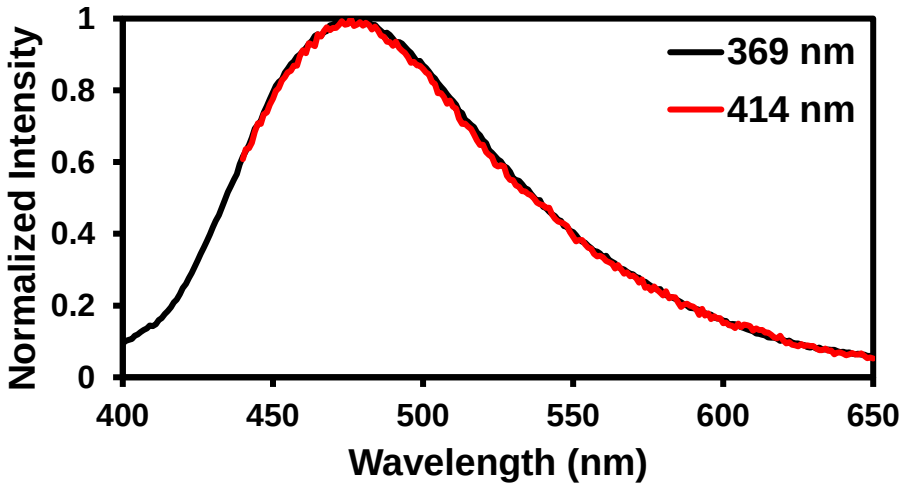

Figure S46. UV/Vis emission spectrum of activated **1** in the solid-state. Two different spectra were taken at each λ_{max} of absorption.

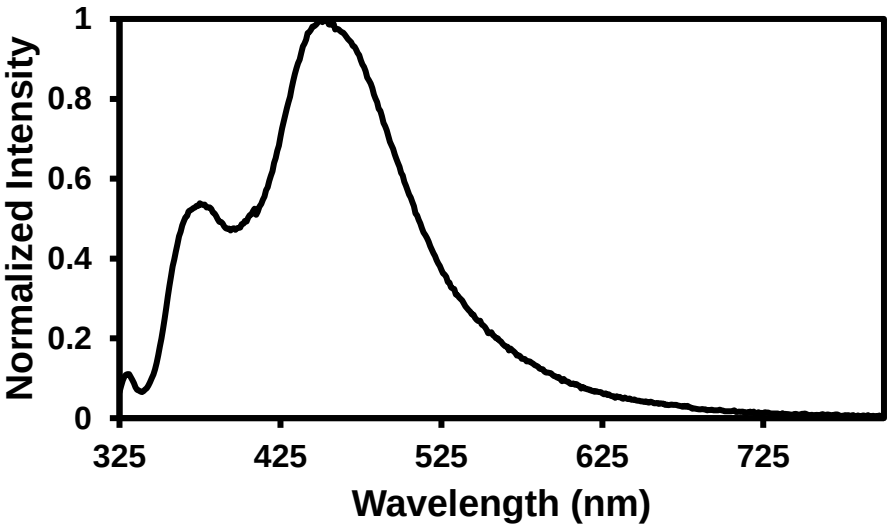

Figure S47. UV/Vis emission spectrum of macrocycle **1a** in DMSO.

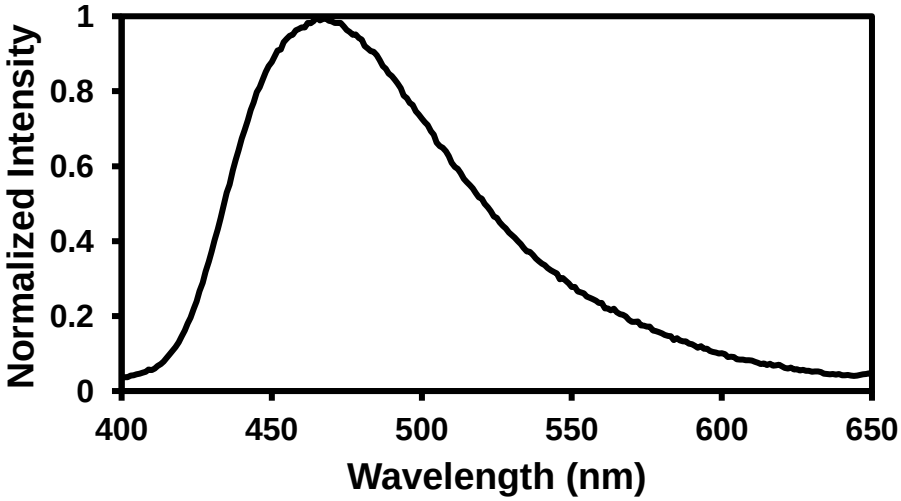

Figure S48. UV/Vis emission spectrum of activated **1a** in the solid-state.

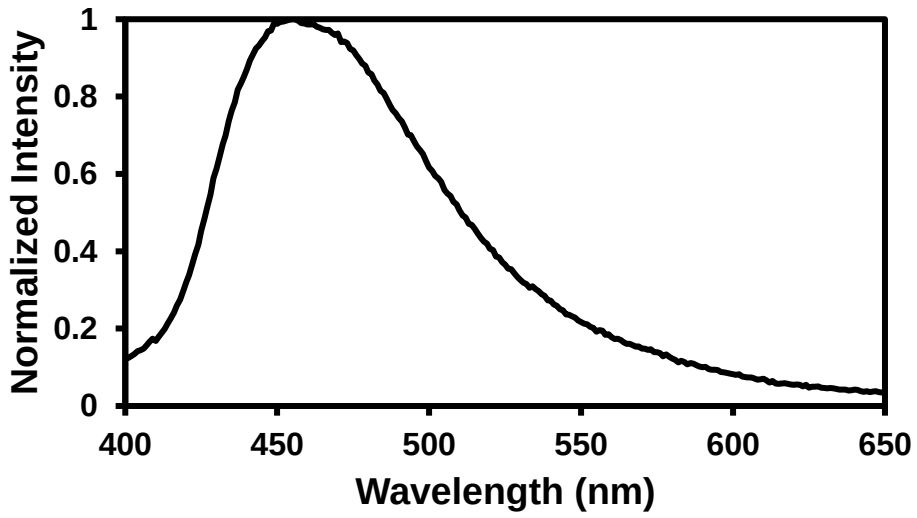

Figure S49. UV/Vis emission spectrum of complex **1a**·C_6H_6 in the solid-state.

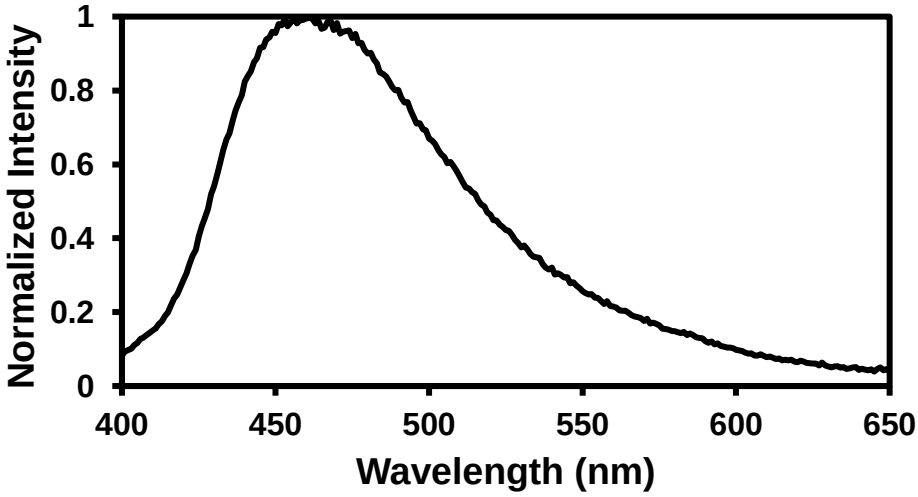

Figure S50. UV/Vis emission spectrum of complex **1a**·DME in the solid-state.

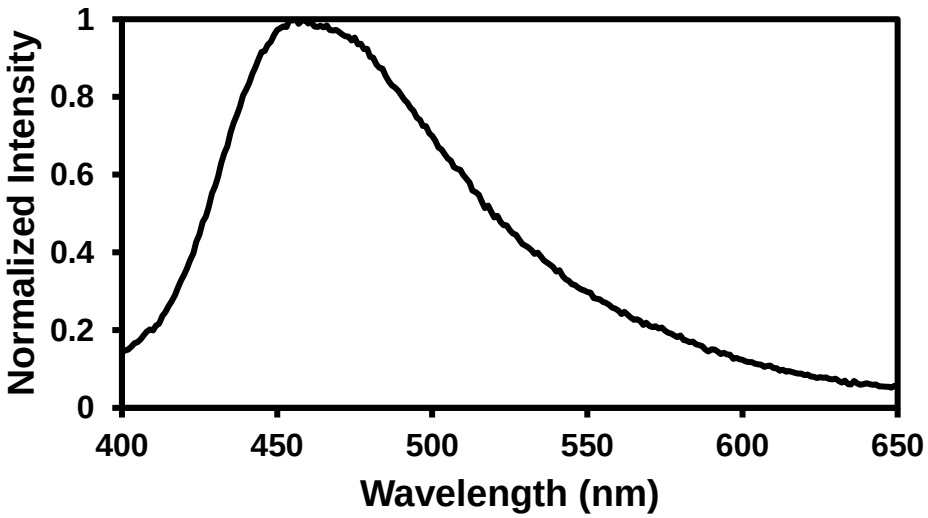

Figure S51. UV/Vis emission spectrum of complex **1a**·DMF in the solid-state.

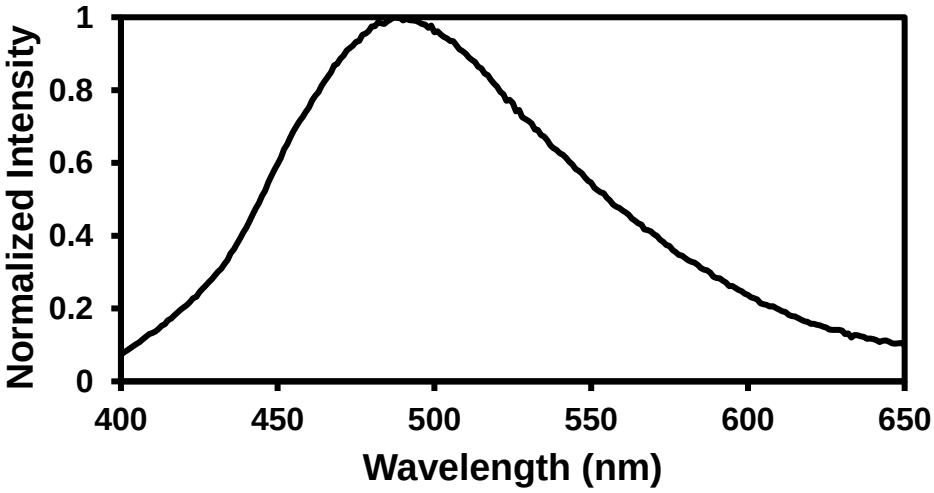

Figure S52. UV/Vis emission spectrum of linear analog **2** in the solid-state.

Lifetime Measurements

Photoluminescent lifetimes were measured using a Mini-τ lifetime spectrometer from Edinburgh Instruments equipped with either a 300 nm picosecond-pulsed-light-emitting diode (EPLED 300) or an EPLED 365. The lifetimes were recorded for the largest emission peak given in Table 1. Bandpass filters (325-385, 425-475, or 475-525 nm) were used to selectively measure the data for these peaks although this resulted in a high pre-excitation baseline in some cases. The lifetime decays for were fit according to Equation S1 as either a bi- or triexponential function where τ and *B* are the lifetime and amplitude, respectively. 10 μM concentrations were used for solution samples.

$$\mathrm{I(t)} = \int_{-\infty}^{t} \mathrm{IRF}(t') \sum_{\mathrm{i}=1}^{\mathrm{n}} B_{\mathrm{i}} e^{-\frac{t-t'}{\tau_i}} dt'$$

Equation S1. Fitting equation for fluorescence decay.

The amplitude-weighted average luminescent lifetimes τ_{av} were calculated using Equation S2. B_3 and τ_3 were only used for triexponential fits.

$$\langle \tau_{\mathrm{av}} \rangle = \frac{B_1\tau_1 + B_2\tau_2 + B_3\tau_3}{B_1 + B_2 + B_3}$$

Equation S2. Equation for amplitude-weighted average lifetime.

Table S4. Lifetimes for **1**, **1a** (and its complexes), **2**, and **2a**.

Compound	B_1	τ_1 (ns)	B_2	τ_2 (ns)	B_3	τ_3 (ns)	τ_{av} (ns)	X^2
1	0.0614	0.536	0.0437	2.144	0.0096	5.959	1.6	1.290
10 μM **1a** in DMSO	0.0754	1.435	0.0134	7.126			2.3	1.336
1a	0.0749	0.501	0.0301	1.785	0.0096	4.157	1.1	1.327
1a·C_6H_6	0.0644	0.381	0.0374	1.691	0.0150	3.619	1.2	1.275
1a·DME	0.0591	0.328	0.0343	1.790	0.0220	3.866	1.4	1.314
1a·DMF	0.0640	0.347	0.0385	1.773	0.0150	4.491	1.3	1.268
2	0.0652	0.469	0.0348	2.057	0.0093	7.046	1.5	1.164

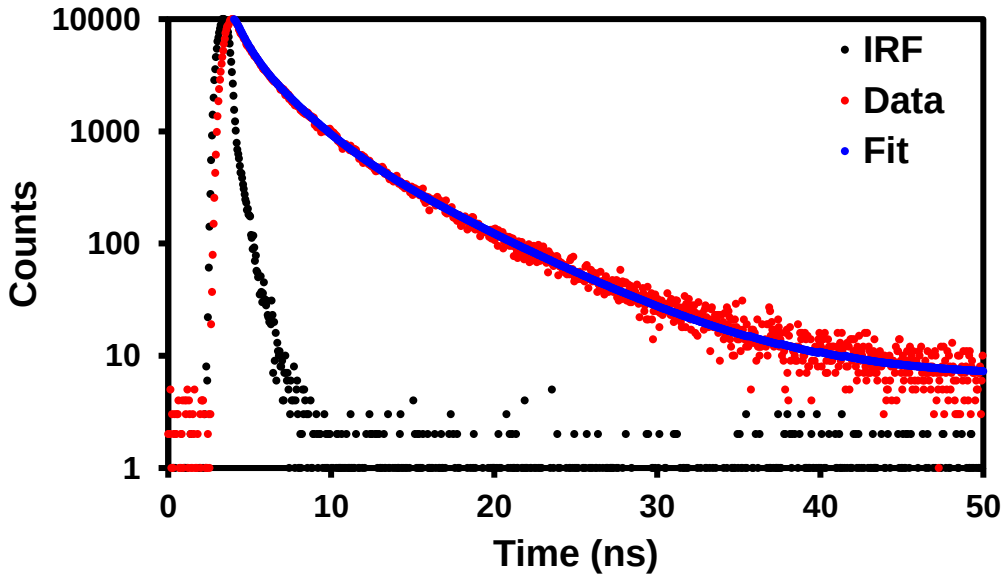

Figure S53. Lifetime data for activated **1** in the solid-state.

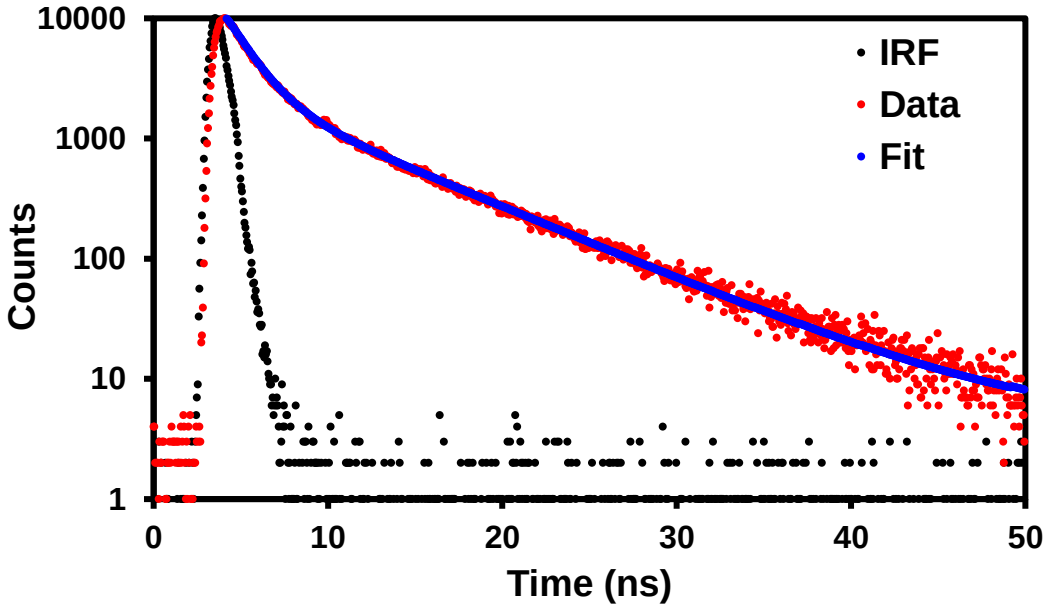

Figure S54. Lifetime data for macrocycle **1a** in DMSO.

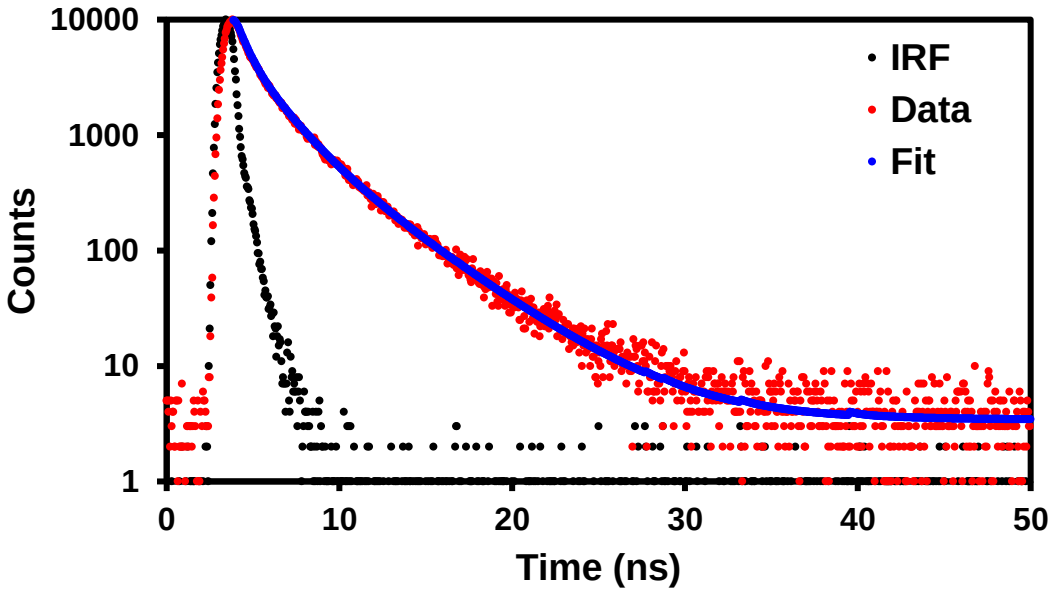

Figure S55. Lifetime data for activated **1a** in the solid-state.

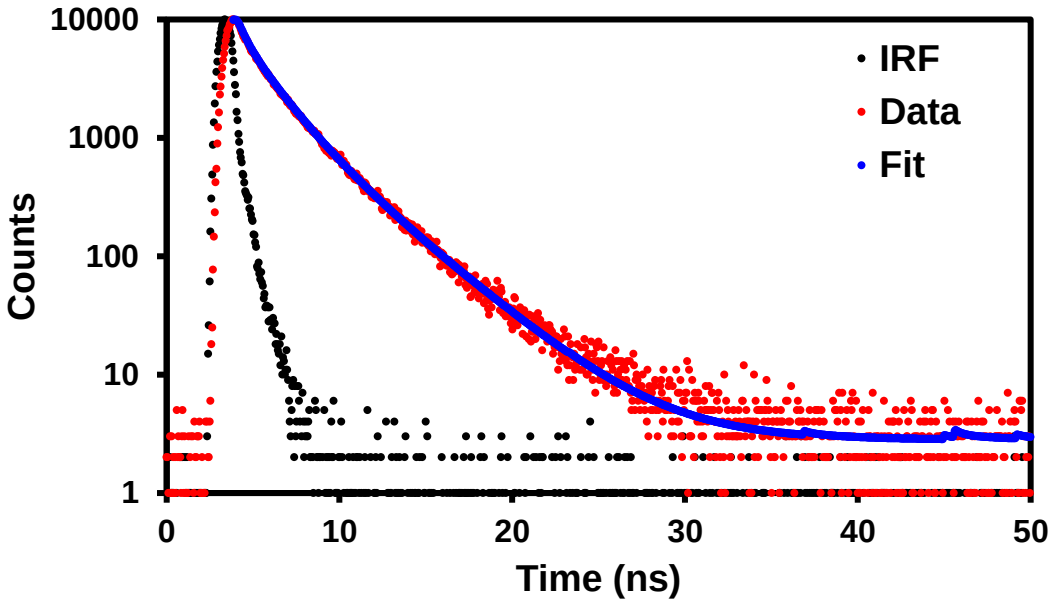

Figure S56. Lifetime data for complex **1a**·C_6H_6 in the solid-state.

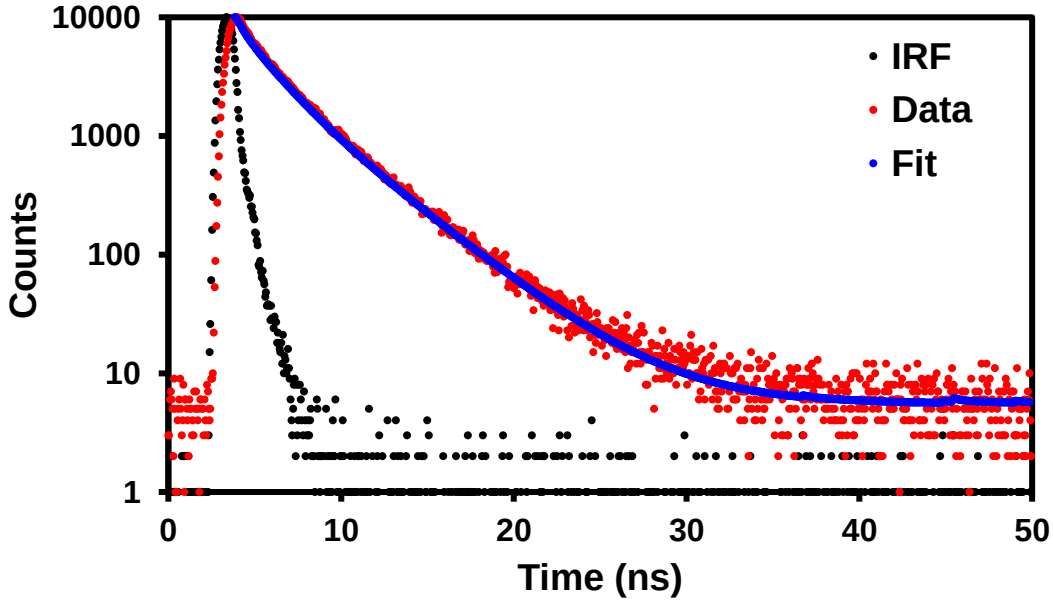

Figure S57. Lifetime data for complex **1a**·DME in the solid-state.

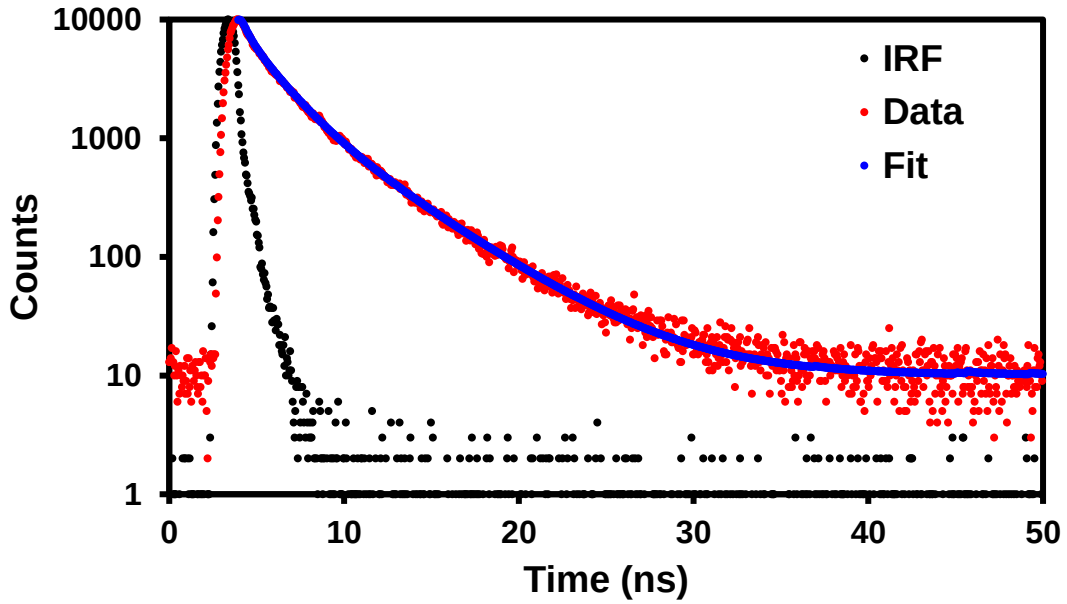

Figure S58. Lifetime data for complex **1a**·DMF in the solid-state.

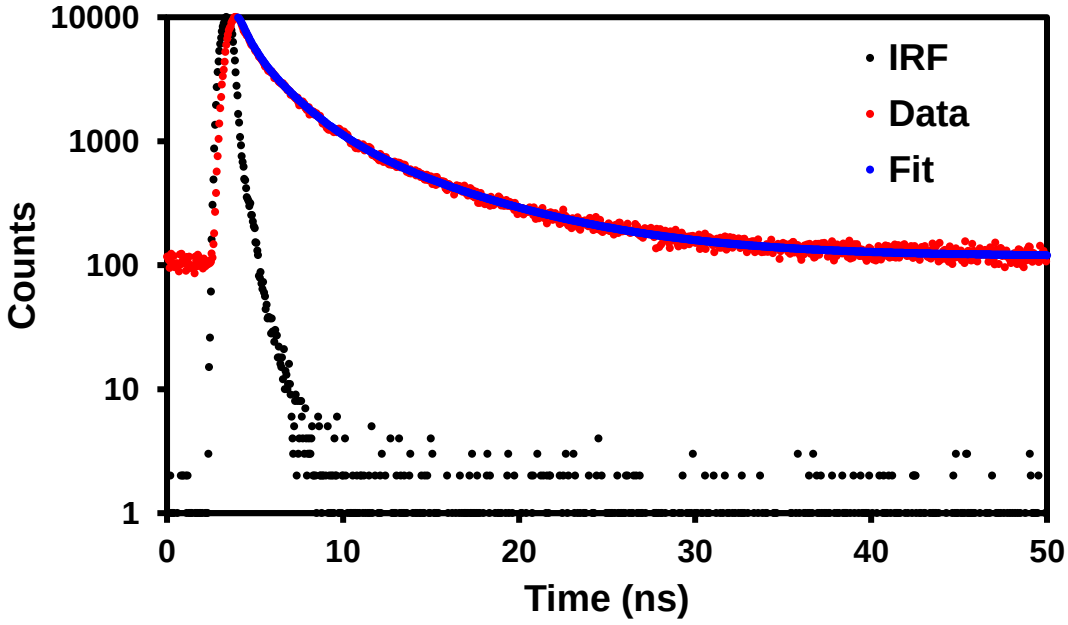

Figure S59. Lifetime data for linear analog **2** in the solid-state.

EPR Measurements

EPR measurements were carried out on a Bruker EMX plus equipped with a Bruker X-band microwave bridgehead and Xenon software (v 1.1b.66). All spectra were recorded at room temperature and a power of ~1.589 mW with a modulation amplitude of 2.0 G. The double integration to obtain peak areas was performed in the Xenon software. Samples were sealed under argon and UV-irradiated in Norell Suprasil Quartz EPR tubes. For most studies, an EPR spectra was taken pre and post UV irradiation. In a few cases, pre-UV spectra displayed a small signal, which maybe a result of pre-exposure to ambient light. The intensity of this signal varied from sample to sample. The post-UV spectra were taken directly after UV-irradiation as well as at specific time intervals (1 h to 3 weeks).

One difference from previous studies was the light source used for irradiation. Instead of using a medium pressure mercury arc lamp we used 365 nm LEDs. This was done because preliminary studies with the blank quartz tube, showed the formation of quartz impurities using the mercury lamp. The quartz tube itself was generating a small EPR signal with a *g*-value of 2.002. The 365 nm LEDs precluded this issue as no radical signal was detected in the EPR tube after irradiation. To investigate if we were still activating the same radical processes as before we irradiated **2a** with the 365 nm LEDs to ensure the same spectra would be obtained as previously seen with the mercury lamp. Indeed, a nearly identical spectra with the same *g*-value = 2.006 (Figure 9) was obtained. However, the sample did require a longer irradiation time to generate the same signal intensity as previously observed for the mercury lamp. This is likely due to the lower intensity of the LEDs versus the mercury lamp (15 W versus 450 W). Overall, this suggests we are activating the same radical generation process with the LEDs as with the medium pressure Hg lamp just at a slower rate.

To determine the number of radicals formed upon UV-irradiation, the overall area of the experimental EPR spectra were compared to a calibration curve performed using known concentrations

of a stable triphenylamine radical cation (Magic Blue). Because the EPR signal is a first-derivative absorption signal, the spectra were doubly integrated to obtain the area under the curve. First, to obtain the absorption curve and a second time to obtain the area under the absorption curve. In this calibration, the area of the EPR spectra for varying concentrations of 100 µL Magic Blue solutions in dichloromethane were recorded (Figure S68). Each Magic Blue molecule is considered to have one radical per molecule. This allows for a line of best fit to approximate the number of radicals in a given sample. In this work, concentrations were reported either as 1 in X number of molecules contain a radical or as an X percentage of molecules contain a radical. These numbers are inversely related. For example, 1 in 150 the molecules in activated **1a** contain a radical at its maximum radical concentration. This is the same amount as 0.69% of the molecules containing a radical. For reference, this is also the same number of radicals seen in 100 µL of a 0.83 mM solution of Magic Blue in a dichloromethane solution.

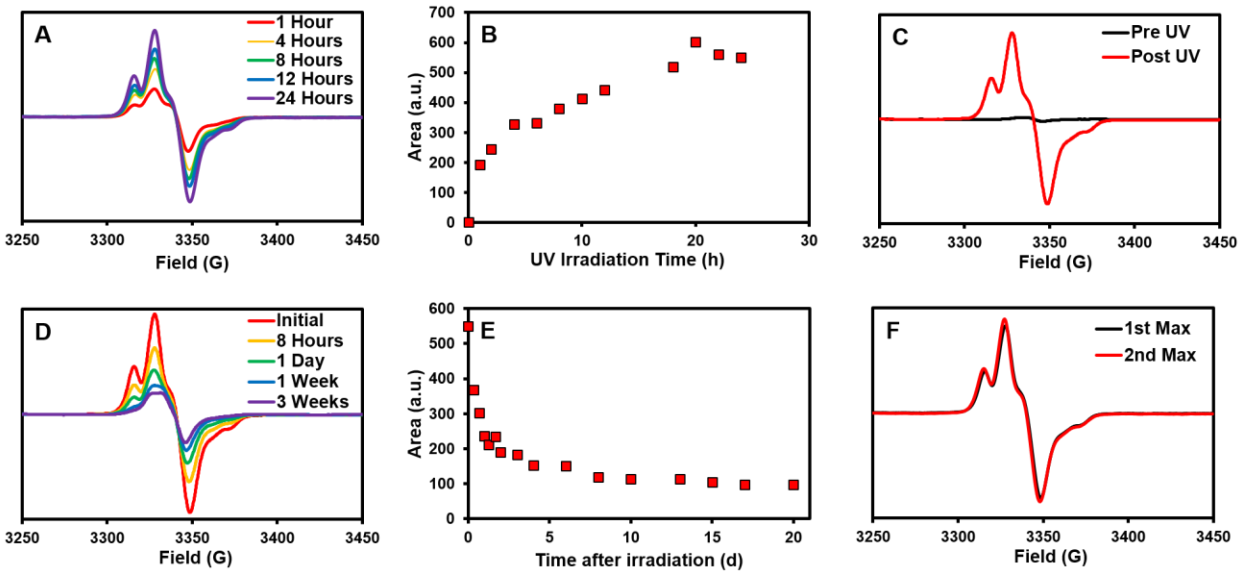

Figure S60. EPR data for activated **1a**. (A) EPR after incremental times of UV-irradiation. (B) Double integration over time of UV-irradiation. A maximum radical concentration of 0.69% was found for 9.8 mg of macrocycle by averaging the last four data points. (C) EPR signal pre and post UV irradiation. (D) Dark decay after initial UV-irradiation. (E) Double integration over time after initial UV-irradiation. (F) EPR signal after initial maximum radical concentration was reached (1st Max) versus when the maximum radical concentration was reached again (2nd Max) during the first cycle of radical regeneration (see Figure 8).

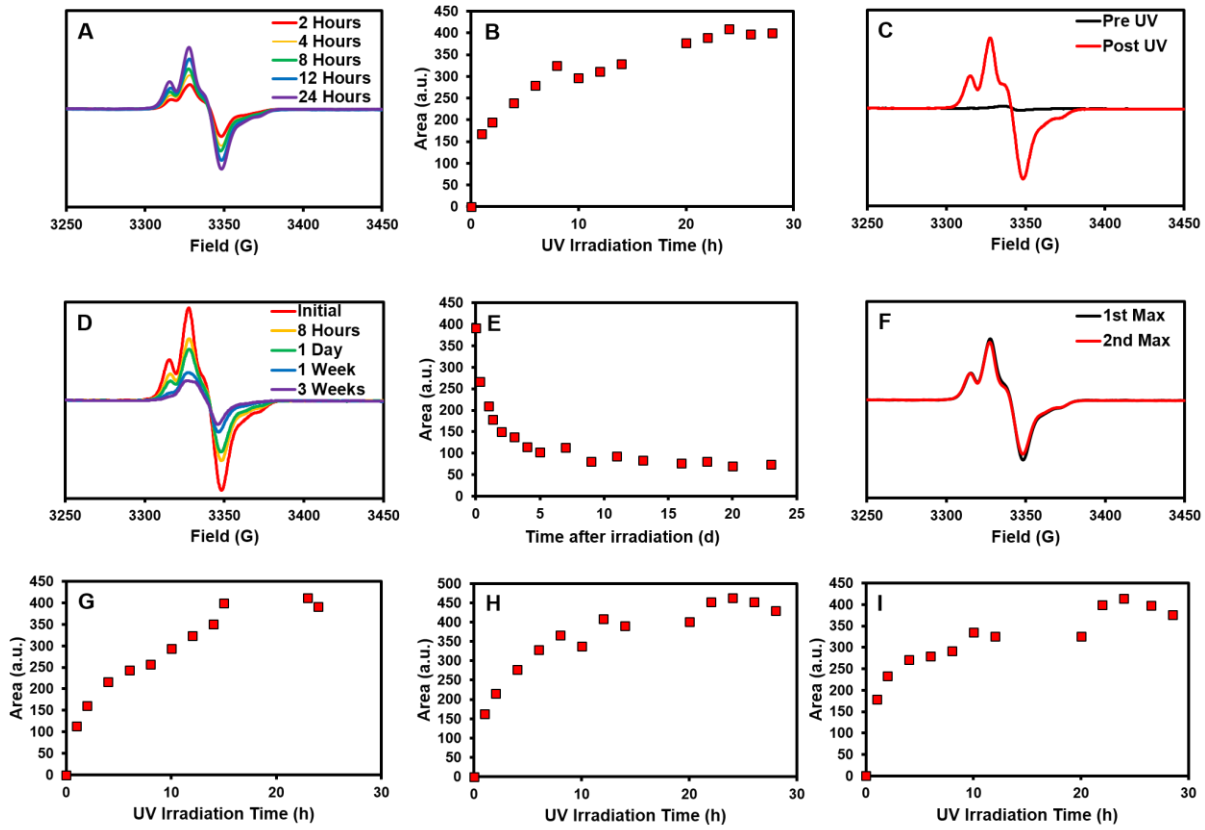

Figure S61. EPR data for complex **1a**·C_6H_6. (A) EPR after incremental times of UV-irradiation. (B) Double integration over time of UV-irradiation. A maximum radical concentration of 0.78% was found for 6.5 mg of macrocycle by averaging the last three data points. (C) EPR signal pre and post UV irradiation. (D) Dark decay after initial UV-irradiation. (E) Double integration over time after initial UV-irradiation. (F) EPR signal after initial maximum radical concentration was reached (1st Max) versus when the maximum radical concentration was reached again (2nd Max) during the first cycle of radical regeneration (see Figure 8). (G) A second trial of the double integration over time of UV-irradiation. A maximum radical concentration of 0.82% was found for 6.1 mg of macrocycle by averaging the last three data points. (H) A third trial of the double integration over time of UV-irradiation. A maximum radical concentration of 0.88% was found for 6.3 mg of macrocycle by averaging the last four data points. (I) A forth trial of the double integration over time of UV-irradiation. A maximum radical concentration of 0.93% was found for 5.3 mg of macrocycle by averaging the last four data points. An average maximum concentration of 0.85% was found over all four trials with a standard deviation of 0.06%.

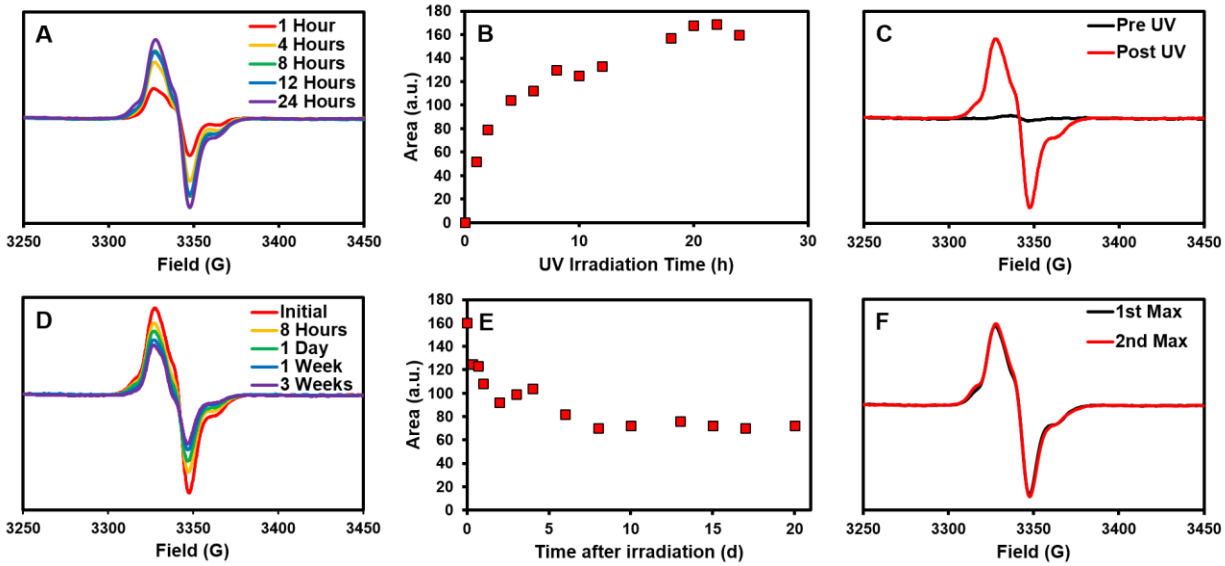

Figure S62. EPR data for complex **1a**·DME. (A) EPR after incremental times of UV-irradiation. (B) Double integration over time of UV-irradiation. A maximum radical concentration of 0.28% was found for 8.2 mg of macrocycle by averaging the last four data points. (C) EPR signal pre and post UV irradiation. (D) Dark decay after initial UV-irradiation. (E) Double integration over time after initial UV-irradiation. (F) EPR signal after initial maximum radical concentration was reached (1st Max) versus when the maximum radical concentration was reached again (2nd Max) during the first cycle of radical regeneration (see Figure 8).

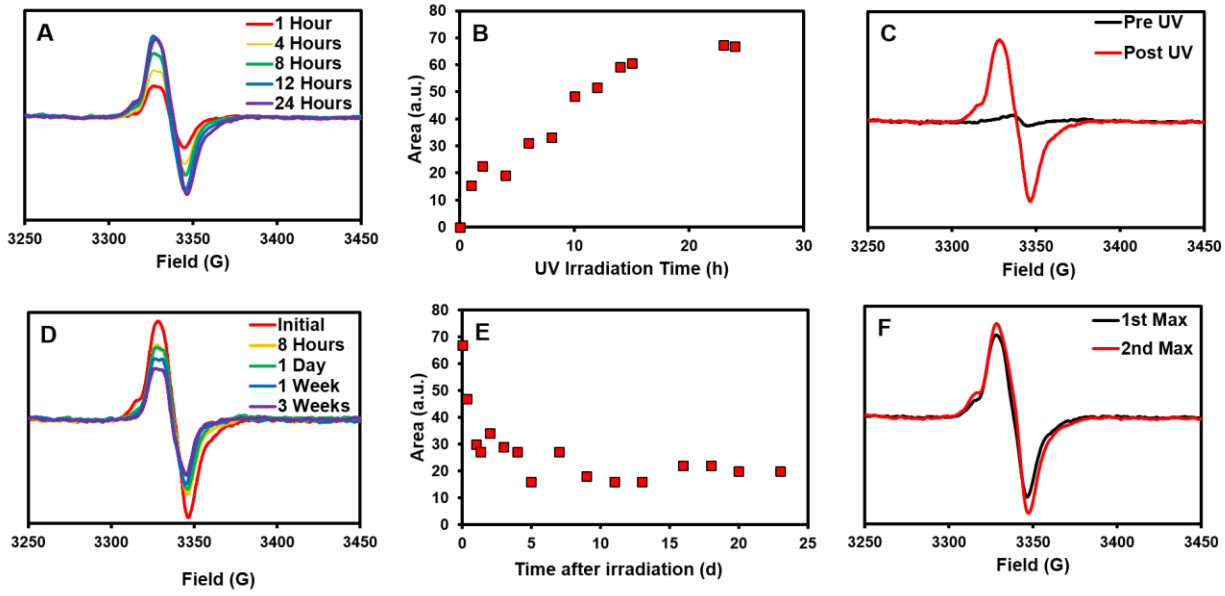

Figure S63. EPR data for complex **1a**·DMF. (A) EPR after incremental times of UV-irradiation. (B) Double integration over time of UV-irradiation. A maximum radical concentration of 0.15% was found for 8.1 mg of macrocycle by averaging the last two data points. (C) EPR signal pre and post UV irradiation. (D) Dark decay after initial UV-irradiation. (E) Double integration over time after initial UV-irradiation. (F) EPR signal after initial maximum radical concentration was reached (1st Max) versus when the maximum radical concentration was reached again (2nd Max) during the first cycle of radical regeneration (see Figure 8).

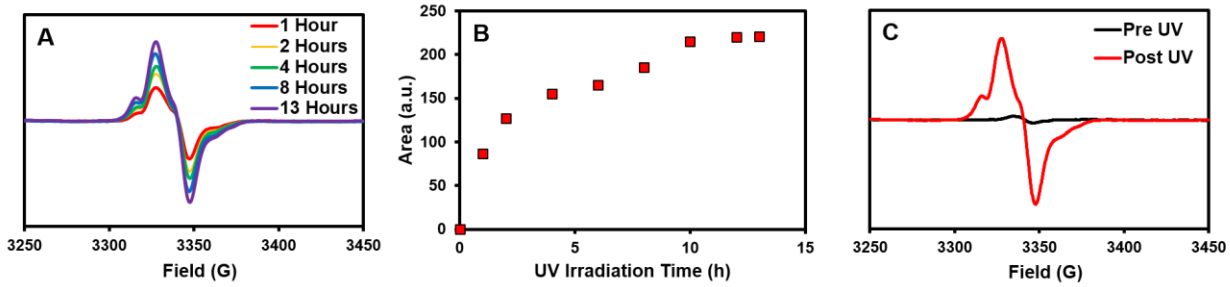

Figure S64. EPR data for complex **1a**·C_6H_5F. (A) EPR after incremental times of UV-irradiation. (B) Double integration over time of UV-irradiation. A maximum radical concentration of 0.45% was found for 6.6 mg of macrocycle by averaging the last two data points. (C) EPR signal pre and post UV irradiation.

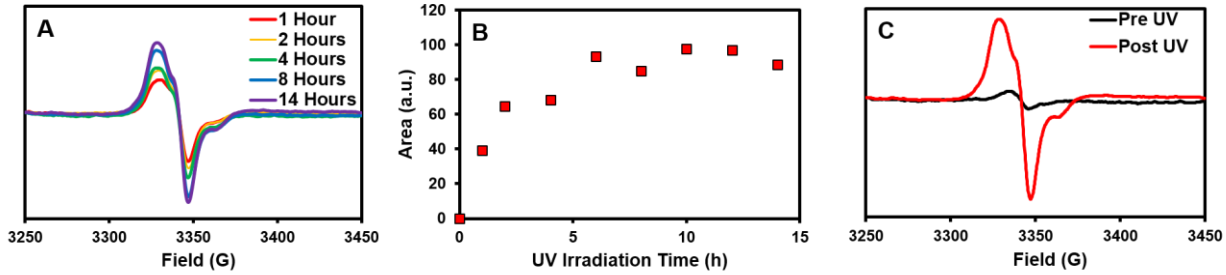

Figure S65. EPR data for complex **1a**·C_6H_5Cl. (A) EPR after incremental times of UV-irradiation. (B) Double integration over time of UV-irradiation. A maximum radical concentration of 0.24% was found for 6.2 mg of macrocycle by averaging the last five data points. (C) EPR signal pre and post UV irradiation.

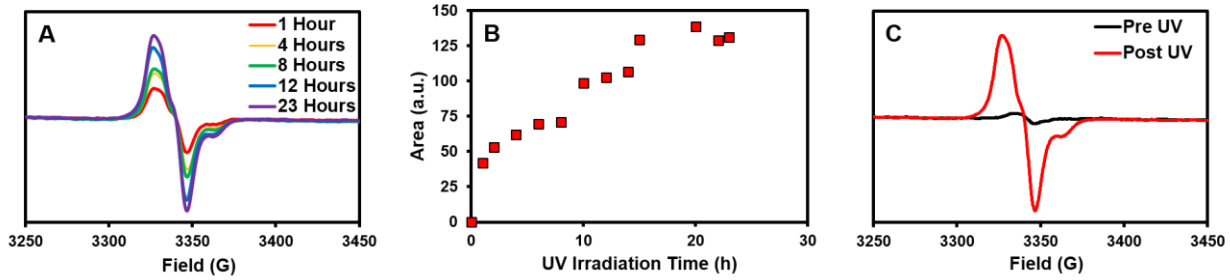

Figure S66. EPR data for complex **1a**·C_6H_5Br. (A) EPR after incremental times of UV-irradiation. (B) Double integration over time of UV-irradiation. A maximum radical concentration of 0.23% was found for 8.5 mg of macrocycle by averaging the last four data points. (C) EPR signal pre and post UV irradiation.

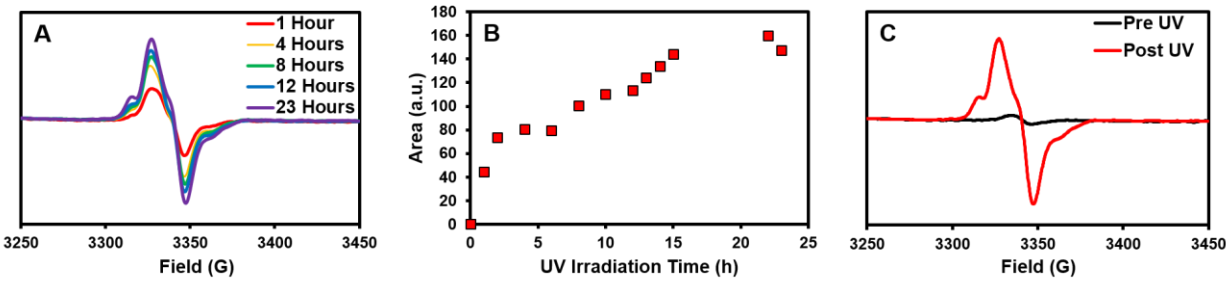

Figure S67. EPR data for complex **1a**·1,4-dioxanes. (A) EPR after incremental times of UV-irradiation. (B) Double integration over time of UV-irradiation. A maximum radical concentration of 0.38% was found for 5.6 mg of macrocycle by averaging the last three data points. (C) EPR signal pre and post UV irradiation.

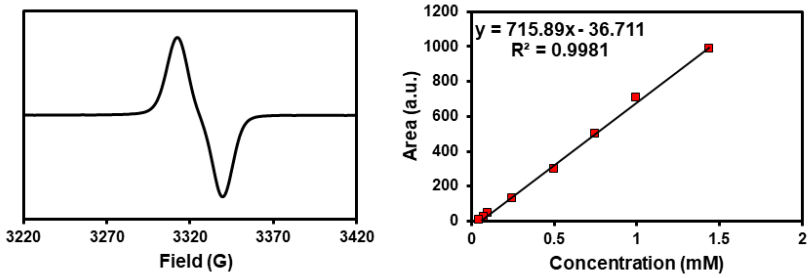

Figure S68. EPR data and radical concentration determination for Magic Blue. (A) EPR spectra for Magic Blue as a 1 mM solution in degassed dichloromethane. (B) Calibration curve for radical concentration determination. It should be noted that Magic Blue noticeably degrades after 4-6 weeks, so it must be used quickly once obtained.

NMR Spectra Pre and Post UV

NMR spectra were taken on a Bruker Avance III-HD 300 MHz spectrometer. Measurements were taken after radical regeneration studies were completed.

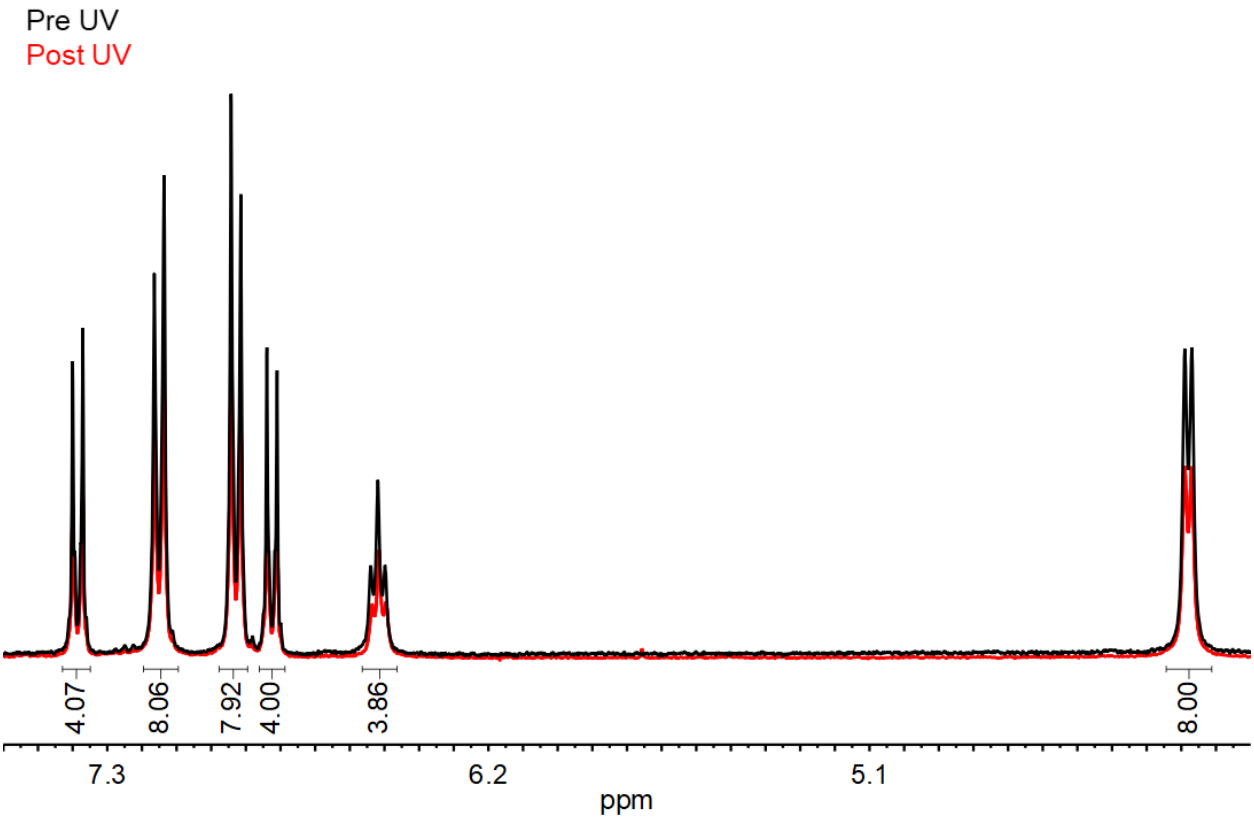

Figure S69. ^{1}H NMR of activated **1a** after radical regeneration studies (DMSO-d_6, 300 MHz). Sample was redissolved before measurement. No changes were observed for parent resonances of macrocycle **1a**. Peaks and integrals are for the redissolved sample (red). Black is for comparison represents a freshly synthesized sample of macrocycle **1a**.

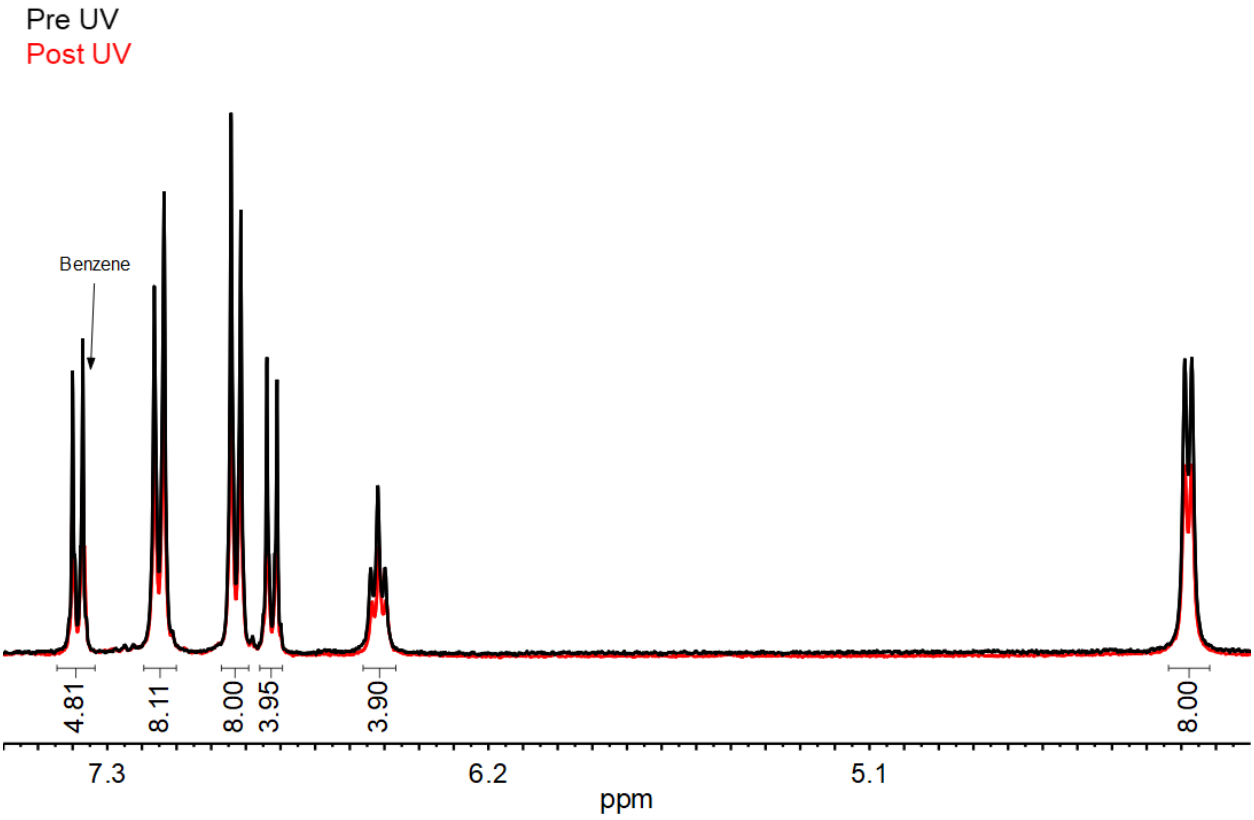

Figure S70. ^{1}H NMR of complex **1a**·C_6H_6 after radical regeneration studies (DMSO-d_6, 300 MHz). Sample was redissolved before measurement. No changes were observed for parent resonances of macrocycle **1a** except the benzene is now in the spectra (as it was the guest in complex **1a**·C_6H_6). Peaks and integrals are for the redissolved sample (red). Black is for comparison represents a freshly synthesized sample of macrocycle **1a**.

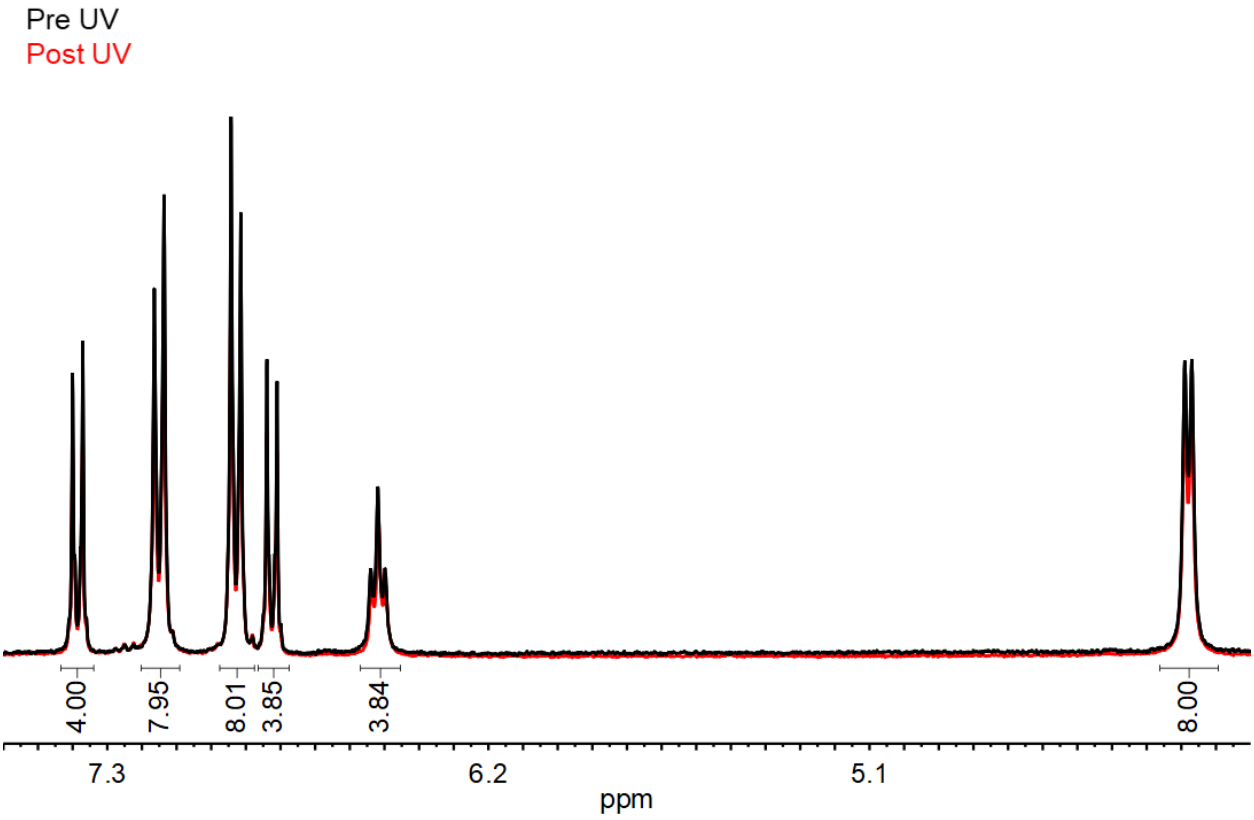

Figure S71. ^{1}H NMR of complex **1a**·DME after radical regeneration studies (DMSO-d_6, 300 MHz). Sample was redissolved before measurement. No changes were observed for parent resonances of macrocycle **1a**. Peaks and integrals are for the redissolved sample (red). Black is for comparison represents a freshly synthesized sample of macrocycle **1a**.

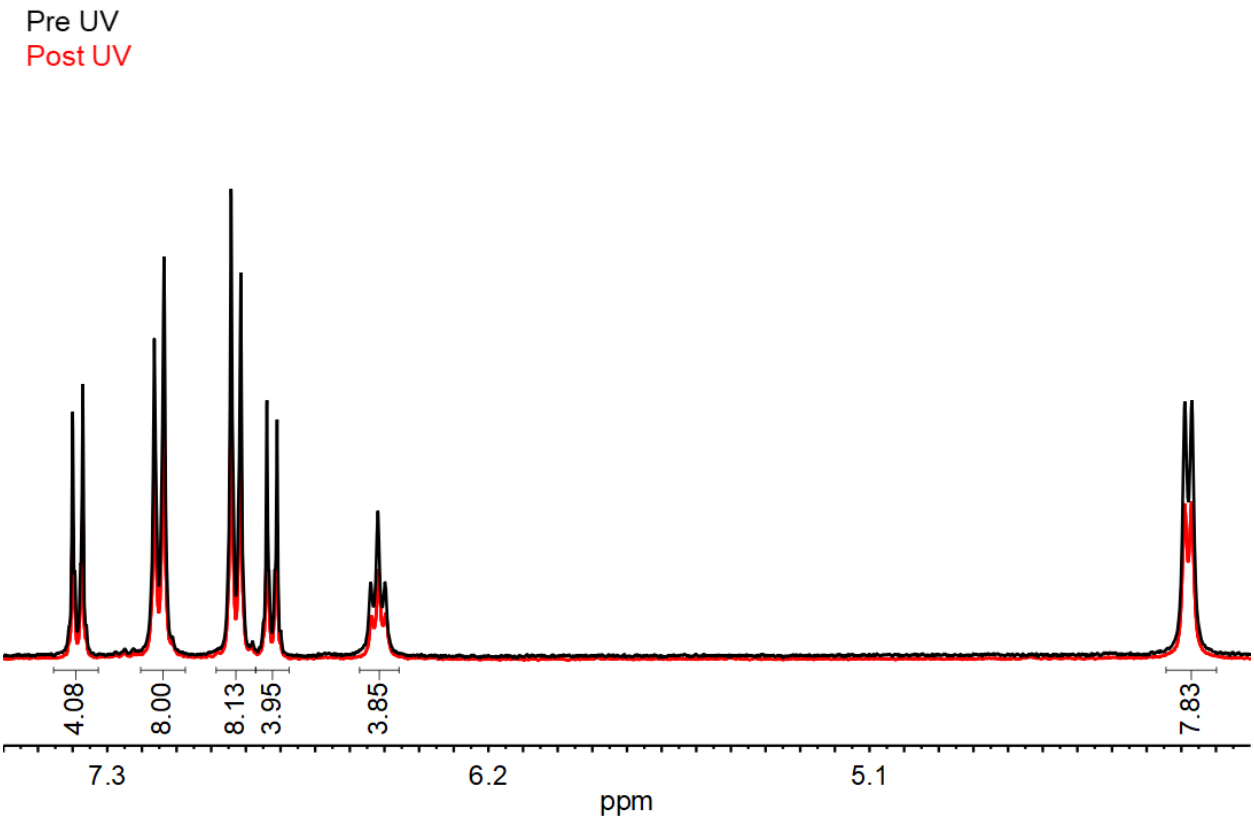

Figure S72. ^{1}H NMR of complex **1a**·DMF after photophysical studies (DMSO-d_6, 300 MHz). Sample was redissolved before measurement. No changes were observed for parent resonances of macrocycle **1a**. Peaks and integrals are for the redissolved sample (red). Black is for comparison represents a freshly synthesized sample of macrocycle **1a**.

Solid-state NMR

^{13}C CP MAS NMR were performed at 298 K using a wide-bore Avance III HD 17.6 T spectrometer (Bruker Biospin) at the Advanced Magnetic Resonance Imaging and Spectroscopy (AMRIS) Facility in Gainesville, Florida.

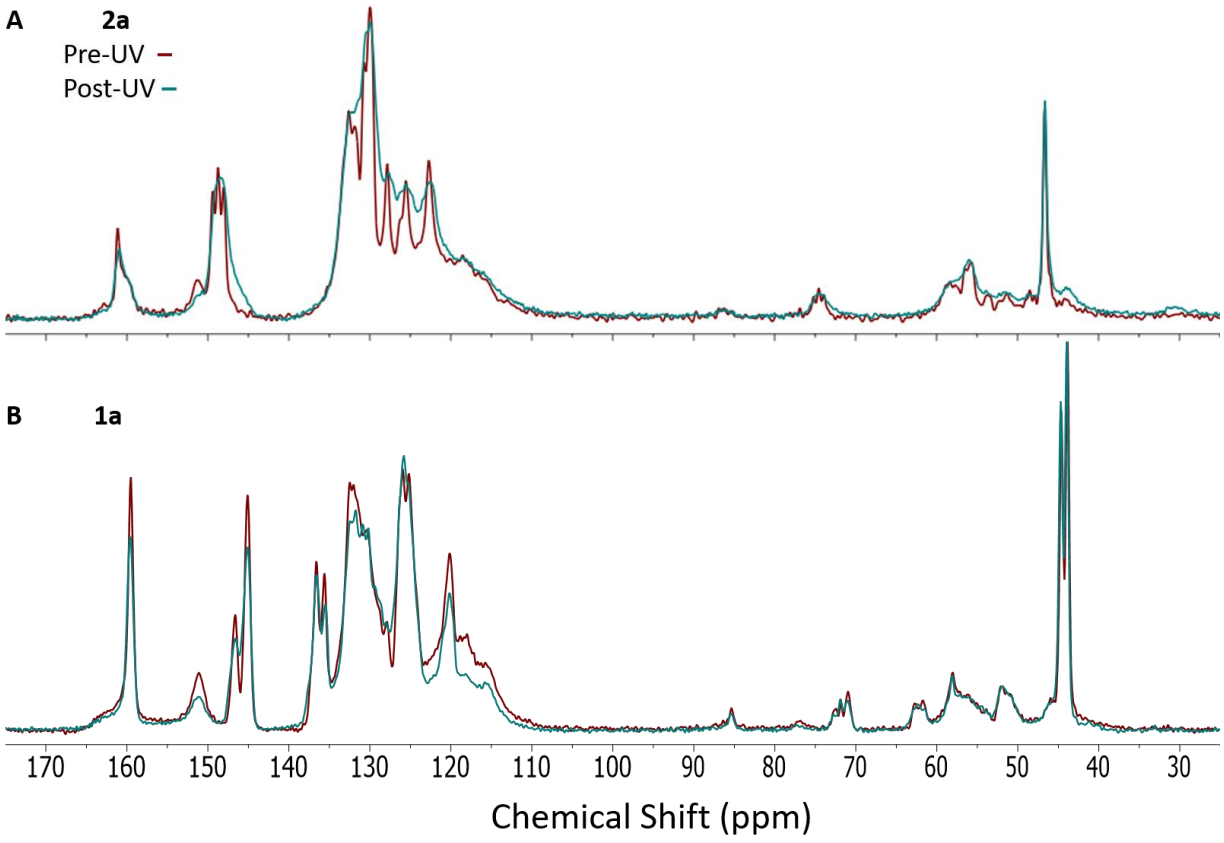

Figure S73. Room temperature carbon-13 CP-MAS NMR spectra of the pre and post-UV irradiated (8 hours irradiation) of the linear analog **2a** (a) and activated host **1a** (b) acquired at 17.6 T at a spinning speed of 14 kHz and a recycle delay of 3 s.

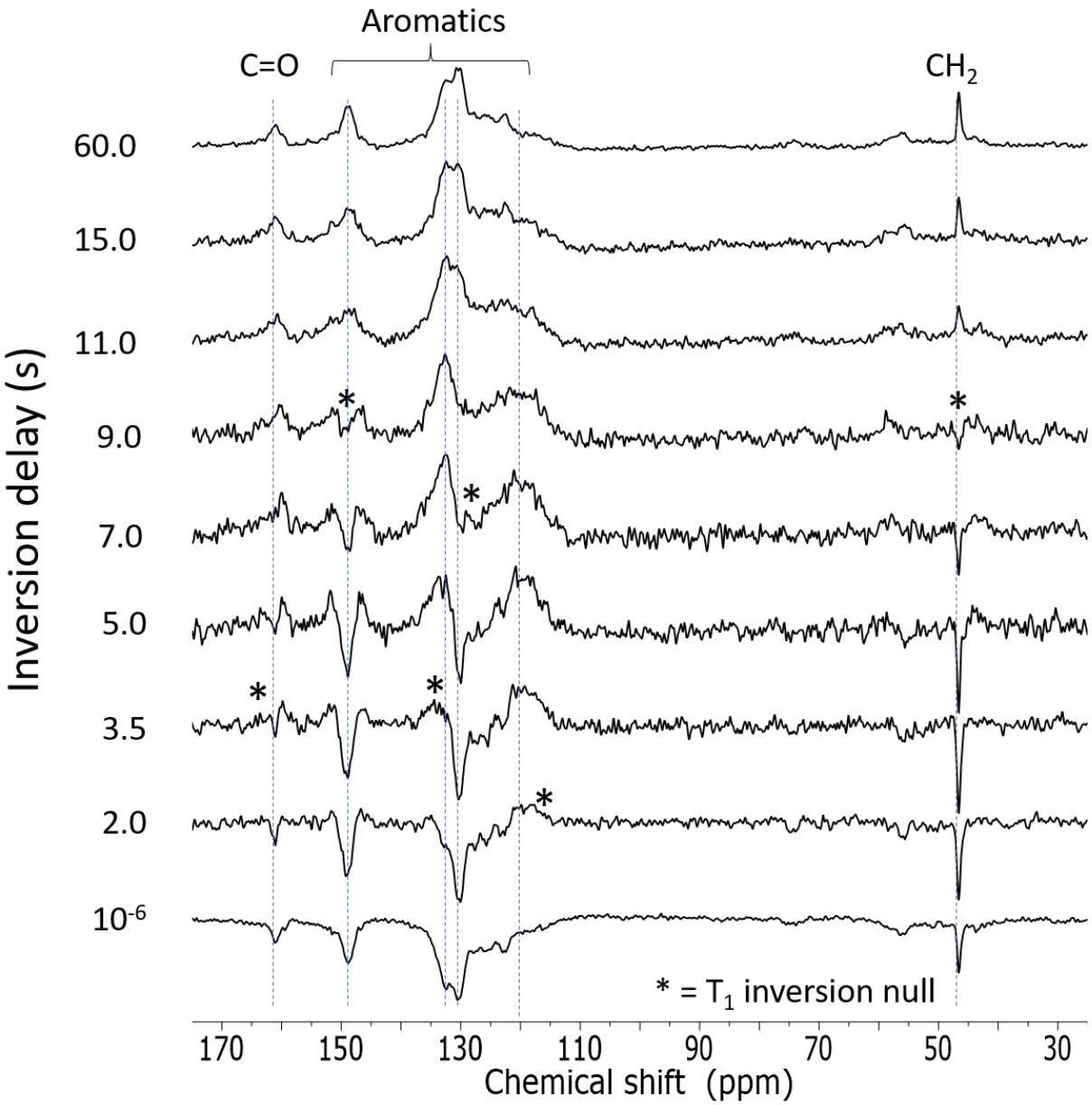

Figure S74. Room temperature carbon-13 detected proton T_1 inversion-recovery CP-MAS spectra for varying relaxation delay, acquired at 17.6 T at a spinning speed of 14 kHz.

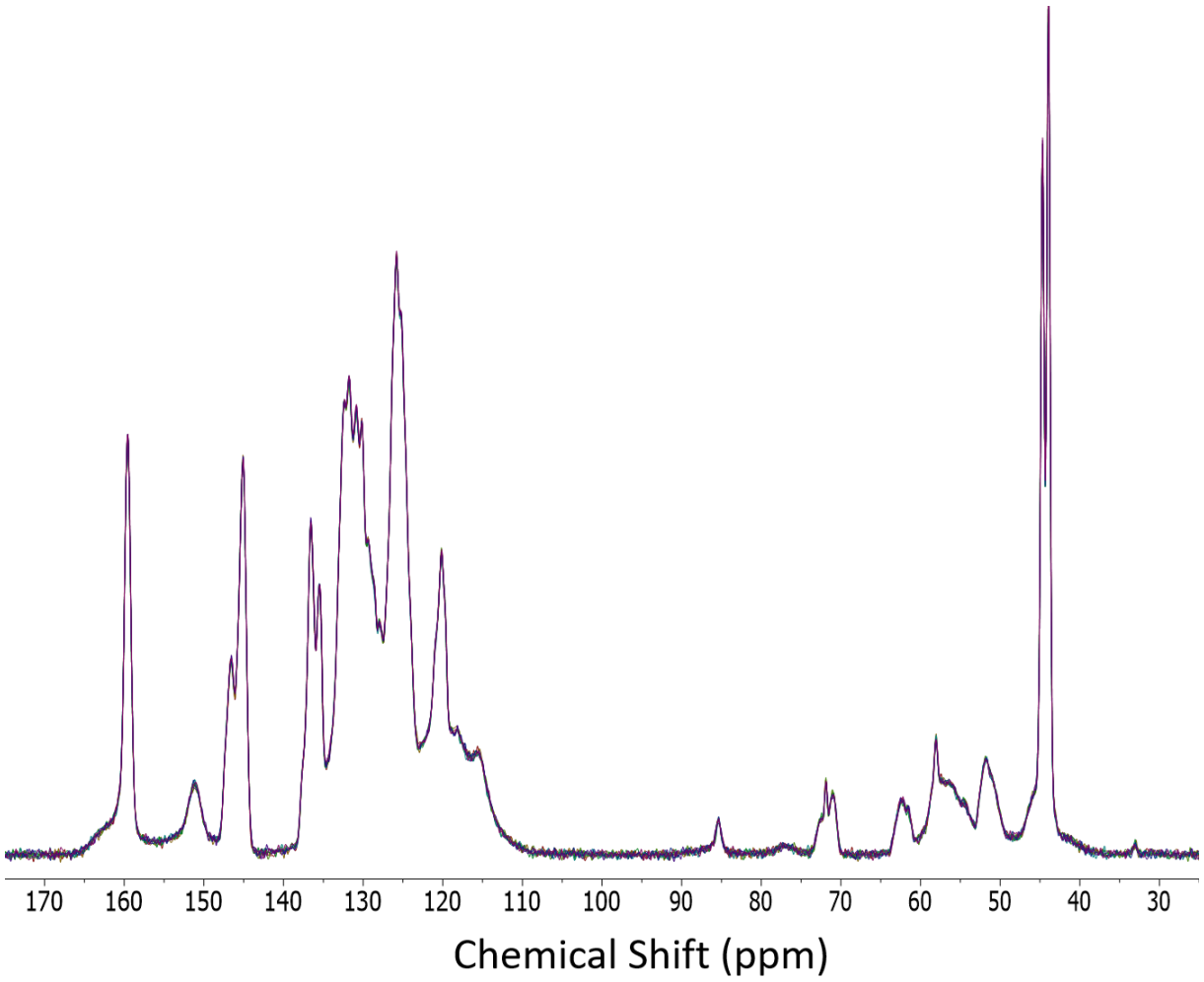

Figure S75. Overlay of the room temperature carbon-13 CP-MAS spectra of the post-UV irradiated activated host **1a** acquired at intervals of 106 minutes over the course of approximately 16 hours. The spectra are all identical, indicating the stability of the photoinduced radical on the timescale of the experiment.

Cyclic Voltammetry

Measurements were carried out in dichloromethane using a WaveDriver 20 Bipotentiostat combined with Aftermath software. Solutions contained 1 mM solute and 100 mM $((n\text{-Bu})_4N)^+(PF_6)^-$ as the electrolyte. Measurements were performed in an H cell equipped with a SCE reference, platinum wire counter, and glassy carbon working electrodes. Measurements were conducted at a potential rate of 100 mV/s.

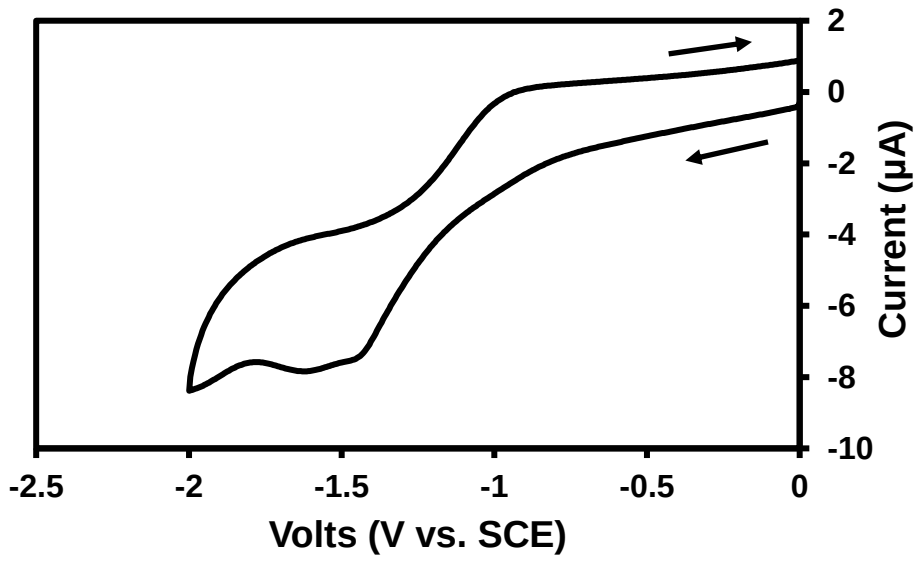

Figure S76. Reductive cyclic voltammetry for linear analog **2**.

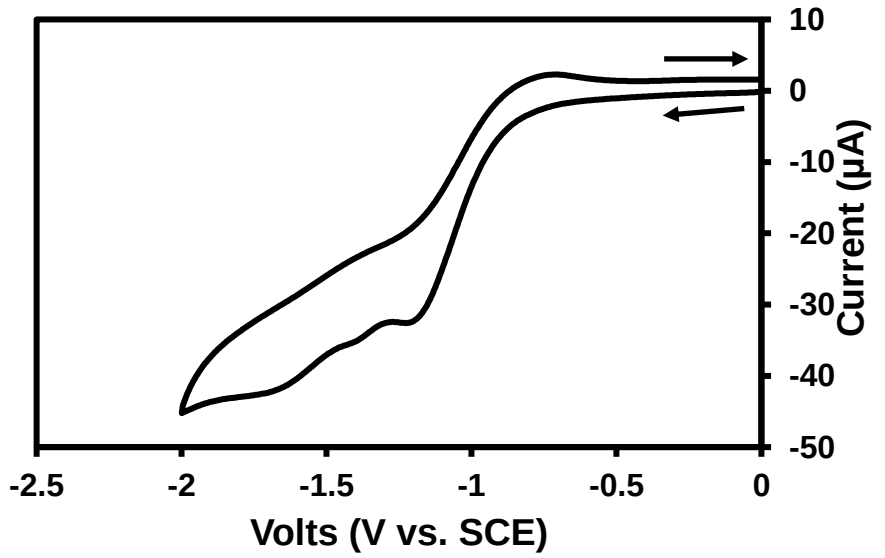

Figure S77. Reductive cyclic voltammetry for linear analog **2a**.

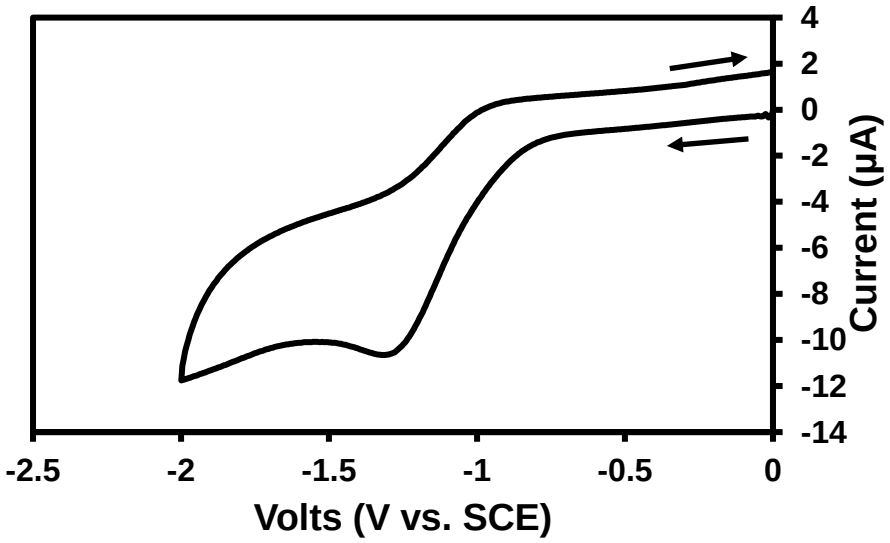

Figure S78. Reductive cyclic voltammetry for TPA **3**.

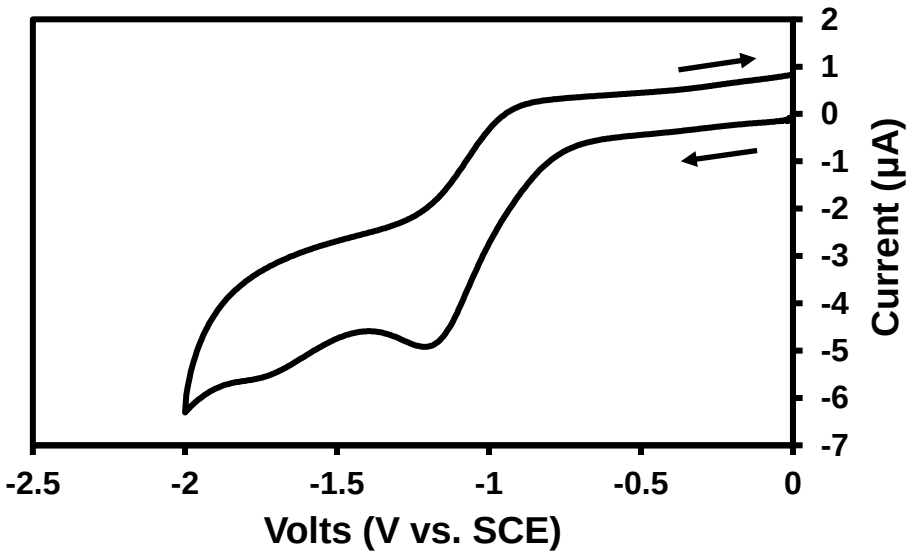

Figure S79. Reductive cyclic voltammetry for TPA **3a**.

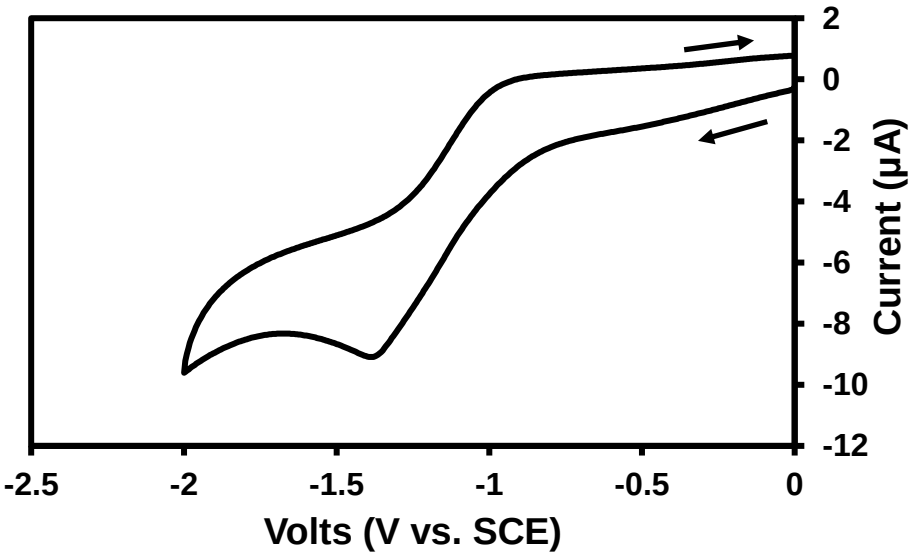

Figure S80. Reductive cyclic voltammetry for TPA **4**.

References

1. Ji, L.; Yuan, M.-S.; Liu, Z.-Q.; Shen, Y.-X.; Chen, H.-F. Switching High Two-Photon Efficiency: From 3,8,13-Substituted Triindole Derivatives to Their 2,7,12-Isomers. *Org. Lett.* **2010**, *12*, 5192-5195.

2. Li, Z.; Dong, Q.; Xu, B.; Li, H.; Wen, S.; Pei, J.; Yao, S.; Lu, H.; Li, P.; Tian, W. New Amorphous Small Molecules-Synthesis, Characterization and their Application in Bulk Heterojunction Solar Cells. *Sol. Energy Mater. Sol. Cells* **2011**, *95*, 2272-2280.

3. Wang, Y.-X.; Leung, M.-K. 4,4',4''-Tris(acetoxymethylene)triphenylamine: An Efficient Photoacid Promoted Chemical Crosslinker for Poly(vinylcarbazole) and Its Applications for Photolithographic Hole-Transport Materials. *Macromolecules* **2011**, *44*, 8771-8779.

4. Chen, L.; Qian, G.; Jin, X.; Cui, Y.; Gao, J.; Wang, Z.; Wang, M. Inorganic−Organic Hybrid Nonlinear Optical Films Containing Bulky Alkoxysilane Dyes. *J. Phys. Chem. B* **2007**, *111*, 3115-3121.

5. Sindt, A. J.; Smith, M. D.; Berens, S.; Vasenkov, S.; Bowers, C. R.; Shimizu, L. S. Single-Crystal-to-Single-Crystal Guest Exchange in Columnar Assembled Brominated Triphenylamine Bis-Urea Macrocycles. *Chem. Commun.* **2019**, *55*, 5619-5622.

6. Paul, G. K.; Mwaura, J.; Argun, A. A.; Taranekar, P.; Reynolds, J. R. Cross-Linked Hyperbranched Arylamine Polymers as Hole-Transporting Materials for Polymer LEDs. *Macromolecules* **2006**, *39*, 7789-7792.

7. Tian, H.; Yang, X.; Chen, R.; Zhang, R.; Hagfeldt, A.; Sun, L. Effect of Different Dye Baths and Dye-Structures on the Performance of Dye-Sensitized Solar Cells Based on Triphenylamine Dyes. *J. Phys. Chem. C* **2008**, *112*, 11023-11033.

8. Sindt, A. J.; DeHaven, B. A.; McEachern, D. F.; Dissanayake, D. M. M. M.; Smith, M. D.; Vannucci, A. K.; Shimizu, L. S. UV-Irradiation of Self-Assembled Triphenylamines Affords Persistent and Regenerable Radicals. *Chem. Sci.* **2019**, *10*, 2670-2677.

9. Li, Q.-Q.; Zhong, A.-S.; Liu, H.-J.; Peng, M.; Liu, J.; Pei, Z.-G.; Huang, Z.-L.; Qin, J.-G.; Li, Z. Two-photon absorption in V-type chromophores with electron-rich heterocyclevinylene bridges. *Sci. China Chem.* **2011**, *54*, 625-630.

10. Dubinina, G. G.; Price, R. S.; Abboud, K. A.; Wicks, G.; Wnuk, P.; Stepanenko, Y.; Drobizhev, M.; Rebane, A.; Schanze, K. S. Phenylene Vinylene Platinum(II) Acetylides with Prodigious Two-Photon Absorption. *J. Am. Chem. Soc.* **2012**, *134*, 19346-19349.

11. APEX III Version 2016.5-0 and SAINT+ Version 8.37A. 2016, Bruker AXS, Inc., Madison, Wisconsin, USA.

12. Krause, L.; Herbst-Irmer, R.; Sheldrick, G. M.; Stalke, D. Comparison of Silver and Molybdenum Microfocus X-Ray Sources for Single-Crystal Structure Determination. *J. Appl. Crystallogr.* **2015**, *48*, 3–10.

13. Sheldrick, G. M. SHELXT – Integrated Space-Group and Crystal-Structure Determination. *Acta Crystallogr. A* 2015, *71*, 3–8.

14. Sheldrick, G. M. Crystal Structure Refinement with SHELXL. *Acta Crystallogr. C* **2015**, *71*, 3-8.

15. Dolomanov, O. V.; Bourhis, L. J.; Gildea, R. J.; Howard, J. A. K.; Puschmann, H. OLEX2: A Complete Structure Solution, Refinement and Analysis Program. *J. Appl. Crystallogr.* **2009**, *42*, 339–341.

16. APEX III Version 2016.9-0 and SAINT+ Version 8.37A, TWINABS Version 2012/1, Cell_Now Version 2008/4. 2016, Bruker AXS, Inc., Madison, Wisconsin, USA.

17. APEX III Version 2018.1-0 and SAINT+ Version 8.38A. 2016, Bruker AXS, Inc., Madison, Wisconsin, USA.